Research Article

A MIMO-Enabled Free Space Optical Link under Log-Normal Fading/Gamma-Gamma Channel: Exploring an Optimal Modulation Scheme

Haroun Errachid Adardour [1,2] **Samir Kameche,** [2] **and Mehtab Singh** [3,4]

[1]*Department of Electronics, Faculty of Technology, University Hassiba Benbouali-Chlef, Ouled Fares, Algeria*
[2]*STIC Laboratory, Department of Telecommunications, Faculty of Technology, University Abou Bekr Balkaid-Tlemcen, Post Box 230, Pole Chetouane, Tlemcen 13000, Algeria*
[3]*Department of Electronics and Communication Engineering, University Institute of Engineering, Chandigarh University, Mohali, Punjab, India*
[4]*Department of Electronics Technology, Guru Nanak Dev University, Amritsar, India*

Correspondence should be addressed to Mehtab Singh; mehtabece.rsh@gndu.ac.in

The technology of free-space optical communication (FSOC) systems has some distinctive merits compared to other technologies. Its use is extremely beneficial to meet the exigencies of optical telecommunications and wireless networks (OTWNs). However, since the OTWNs transport a lot of data, the choice of a reliable modulation scheme is highly crucial. To this end, the focus of this paper is an in-depth study of a Point-to-Point Optical Link (P2P-OL) system under a FSOC-Multiple-Input Multiple-Output (MIMO) channel using an optimal modulation scheme. Furthermore, atmospheric turbulence (AT) effects over the FSOC-MIMO channel are incorporated in the proposed system to obtain substantial results. The performance analysis test of the proposed high-rate P2P-OL system is validated under the case that the channel decreases significantly when the AT gets strong regimes. Finally, the proposed system uses an optimal Non-Return to Zero Pulse Generator-Mach-Zehnder Modulator ((NRZPG-MZM)) scheme, which displays acceptable performance levels in a dust-fog meteorological environment under a LNF FSOC-9×9 channel with the attenuation value of 59.66 dB/km (i.e., max OSNR = 24.9 dB, min BER = $1e-09$, and max Q-factor = 6), whereas with the same environment under a G-G FSOC-9×9 channel, the attenuation value is 58.55 dB/km (i.e., max OSNR = 24.67 dB, min BER = $1e-09$, and max Q-factor = 6).

1. Introduction and Motivation

Today's realistic workspaces require extraordinary bandwidth and connectivity performance levels to distribute data to exploit and provide a resource advantage. The land, air, maritime, and space areas have common bandwidth and connectivity requirements [1–3]. However, wireless communication has an inherent challenge associated with its dependence on radio frequency (or RF); its nature makes it very vulnerable due to weather conditions. In highly congested workspaces, RF communication has a very inefficient bandwidth and weak connectivity. To improve connectivity and use bandwidth efficiently, the fiber-optic (or FO) systems offer high-bandwidth digital links throughout the major part of the world. Nevertheless, in certain cases, the installation of a FO cable is not feasible or practical. Free Space optical communication (or FSOC) presents an alternative to FO and RF wireless communication systems. The FSOC can provide high-speed connectivity to link land, air, and maritime platforms. In the present paper, we will focus on FSOC technology [4–9].

Numerous research studies on the FSOC technology have been investigated and proposed to improve data transmission performances in optical telecommunications

and wireless networks (OTWNs). Sahoo [10] has investigated the error performances of an inter-symbol interference (or ISI) compensating modulation scheme named Return to Zero Coded Gaussian Minimum Shift Keying (or RZ-GMSK) sampled phase. According to the author, the error performance of RZ-GMSK over a log-normal turbulence fading channel has been compared and validated with other proposed modulation schemes, such as pulse position modulation (or PPM) [11] and pulse position modulation-minimum shift keying (or PPM-MSK) [12]. From the obtained numerical results in [10], the author has reported that the RZ-GMSK sampled phase modulation scheme outperforms other schemes, especially in adverse weather conditions and for high-speed data transmission. Finally, the authors have proposed their work for the optical wireless back-haul network application under a FSOC channel. In [13], the authors have investigated and reported performance of a hybrid FSOC/FO link as an alternative approach to the traditional FSO link under various weather conditions. From the obtained numerical results in [13], the authors have found that the hybrid FSO/FO link shows slight improvement as compared with the traditional FSO link throughout the range of FSO investigated from 0.2 km to 2 km. The communication distance of the hybrid link has been improved to 40 km. They have also noted that the system's performance is improved by using a dual FSO channel as compared to employing a single FSO channel. Finally, the authors have concluded that the obtained results indicate strong agreement with Kim's model, particularly at a high input power of 160 mW.

In [14], the authors report that wireless communication under a FSOC channel has attracted more interest based on the high data rates achievable, license-free bandwidth, secured links, and simplicity of deployment. For the work presented in [14], the authors proposed an analysis of the performances of the FSOC terrestrial links by taking into account the internal characteristics of the system exploiting 850 and 1310 nm transmission wavelengths. From the obtained numerical results in [14], the authors observed that the performances of the suggested system are optimized considering and varying different input powers, modulation formats, data rates, link ranges, beam divergence, and detector types. In addition, they have also detected that a higher value of the Q-factor can be obtained in different modulation schemes at a wavelength of 1310 nm as compared to an 850 nm wavelength. Finally, the authors have reported that the system has achieved its maximum transmission range at 1.7 km with data rates up to 10 Gbps. The optimum value of beam divergence for a better quality of the received optical signal over the maximum possible transmission range has been obtained at 2 mrad.

In [15], the authors have studied the impact of several internal factors on the FSOC-based system under the effects of diffractive optical elements and rain mitigation. The results report that NRZ with an APD detector performs better than RZ with a PIN detector. In another paper [16], the authors have proposed the design of a wavelength division multiplexing (or WDM) system under a multibeam FSOC channel. The authors have successfully studied and evaluated

TABLE 1: Attenuation values for different weather types [13–25].

Weather	Attenuation values (dB/km)
Clear	0.2
Little fog	4.2850
Light rain	6.2702
Moderate fog	15.555
Heavy rain	19.2795
Dust fog	34
Dense fog	84.904

in detail the effects of atmospheric and geometric nonlinearities in moderate atmospheric turbulence on the proposed design. The authors' goal in employing the multibeam FSOC channel is to reduce the attenuations caused by atmospheric and geometric nonlinearities. From the obtained numerical results in [16], the authors have found that the multibeam FSOC channel at 30 Gbps in the proposed system provides improved performances compared to the case where the single-beam FSOC channel at 30 Gbps is used in the same system, with a maximum FSOC connection length of 3500 m.

For enhancing the spectral efficiency (or SE) and the FSO system performance, two interesting contributions have been made by the authors of the papers [17, 18]. In [17], the authors have proposed a transmission modulation adaptive technique for FSOC links under a gamma-gamma (or G-G) turbulence channels. However, the proposed technique by the authors allows an efficient use of the FSOC channel capacity to improve the SE by adjusting the order of the phase-shift keying (or PSK) scheme, considering the conditions of the G-G turbulence channel located in the FSOC link environment as well as the required bit error rate (or BER). In addition, they have addressed the problems of channel degradation due to the turbulence and pointing errors (or PE) effects through the modification and integration of the SIMO (or single-input multiple-output) technique into the channel with maximum ratio combining (or MRC). As a result, they have concluded that the suggested adaptive technique can enhance the SE more than five times compared to the nonadaptive technique under a target BER threshold which is 10^{-3} with a signal-to-noise ratio (or SNR) value equal to 27 and 42 dB in the case of G-G turbulence channel without and with PE, respectively. Also, the same SE enhancement is obtained with SNR equals to 30 dB but when using the FSOC-1x4 (i.e., FSOC-SIMO) scheme with MRC and PE, and with the same optical transmission power. In paper [18], the authors have studied and analyzed the pointing error impacts on the performances of a FSO system which employs the multipulse pulse position modulation (or MP-PPM) technique under a G-G turbulence channel. In addition, they have corrected the degradation in their proposed system with the employment of the SIMO technique in the channel with MRC diversity. As a result, they concluded that the optimization of the receiving beam waist resulted in a significant improvement in the proposed system's performance. As an example, to obtain low PE and ASER (average symbol error rate) values, the estimated optimum value of the beam waist radius is 0.5 and 2 m with
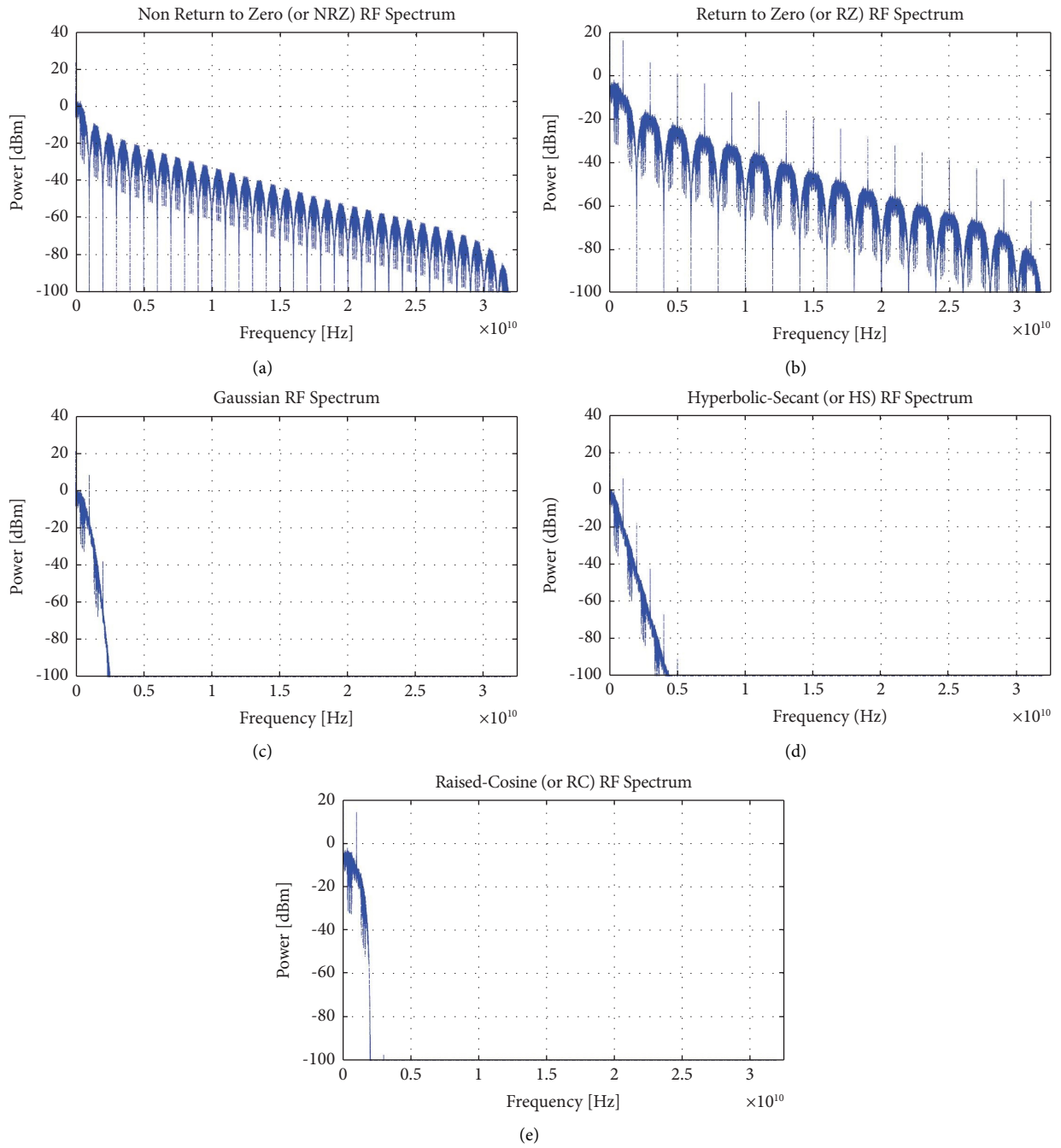
Figure 1: Power (dBm) vs. frequency (Hz), for EPG formats. (a) Nonreturn to zero (NRZ) RF spectrum. (b) Return to zero (RZ) RF spectrum. (c) Gaussian RF spectrum. (d) Hyperbolic-secant (HS) RF spectrum. (e) Raised-cosine (RC) RF spectrum.
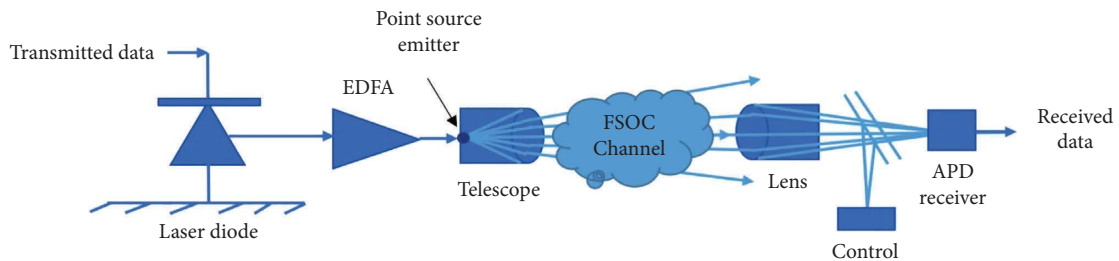

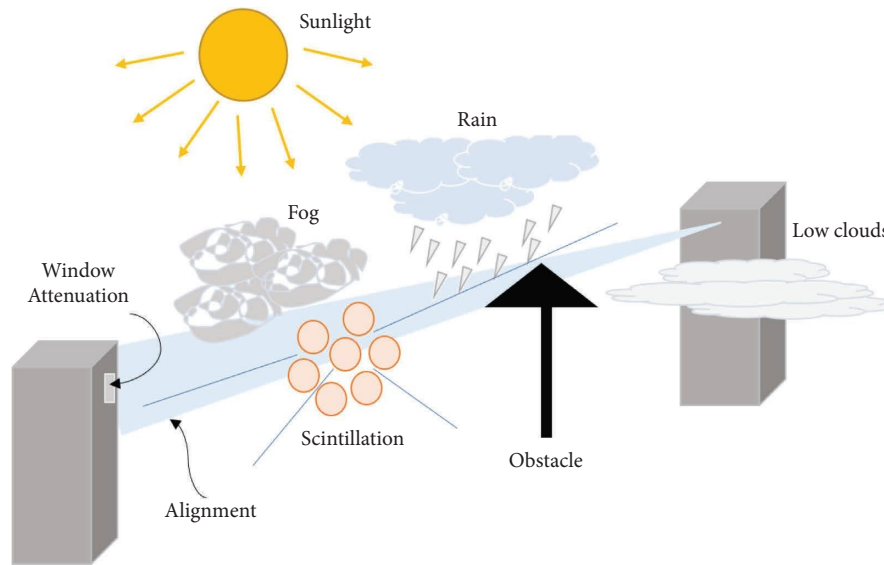Figure 2: Outdoor long-haul FSOC system configuration [26, 27].

FIGURE 3: Various physical conditions and weather effects on FSOC link [31, 32].
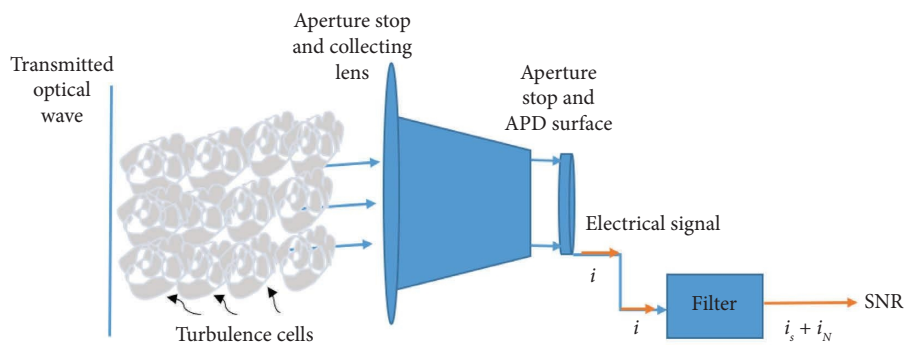

FIGURE 4: Direct detection of the FSOC system [48–50].

normalized jitter values of 1 and 5, respectively. In addition, they also recorded that with fixed transmit power at optimal beam waist values, high gains in system performance are achieved. For instance, with a transmission power of 20 dBm and a range of 3 km, ASER values of 10^{-08} and 10^{-03} have been achieved for the same normalized jitter values of 1 and 5, respectively. However, they also mentioned that these values can be improved considerably when the FSOC-1×4 (i.e., FSOC-SIMO) scheme with the MRC technique is applied, and finally, they demonstrated that the outage probability of the proposed system when employing the SIMO technique with MRC can be enhanced by a factor of three compared to the use of the SISO technique.

In [19], the authors proposed an excellent contribution in the enhancement of WDM performances for FSOC systems through the use of three modulation schemes, such as a digital pulse-position modulation (or DPPM), M-ary pulse-position modulation (M-ary PPM), and on–off keying (OOK). In addition, they hypothesized that on their proposed system, cross-channel crosstalk (CCC), atmospheric turbulence (AT), pointing error (PE), and amplified spontaneous emission (ASE) noise are included. However, the authors [19] report

that the WDM/DPPM-FSOC system suffers from CCC, AT, PE, and ASE noise, which are responsible for the reduction of the link efficiency and system performances. As a solution, the authors [19] recommended addressing those problems through the implementation of M-ary PPM in order to attenuate the effects of AT and enhance the receiver sensitivity. Furthermore, they developed a combination approach between the N-hybrid diversity of spatial modulation (or N-SM) technique and the M-ary-PPM technique for improving the BER performances and the effectiveness for WDM/SM/M-ary PPM-FSOC system. Finally, the authors demonstrated that the proposed WDM/SM/M-ary PPM-FSOC system presents a significant enhancement in terms of receiver sensitivity and power penalty when compared to the WDM/OOK-NRZ-FSOC system.

The authors in [19] reported a very strong contribution in the FSO literature [20], which focuses on the improved performances of the average SE employing aperture averaging (or AA) and spatial coherence diversity (or SCD) based on the modified PPM (or MPPM) technique for the FSOC-MISO channel. However, the investigation of average SE is performed for the FSOC-MISO channel with the use of
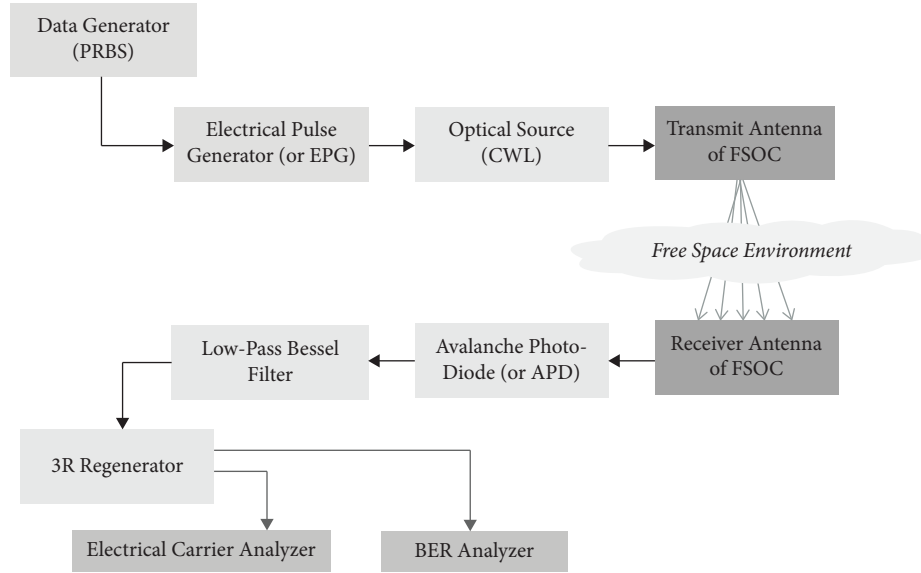
FIGURE 5: Configuration of a simple high-speed P2P-OL under a FSOC-SISO channel using DOM without PE.

TABLE 2: Simulation parameters ([7, 53] and proposed).

Operating parameters	Values
Bit rate	1 Gbps
Power of CW laser	30 dBm
Wavelength of CW laser	1552.5244 nm
Attenuation	Variable
Geometrical loss	Yes
Transmitter aperture diameter	5 cm
Receiver aperture diameter	25 cm
Transmitter optics efficiency	1
Receiver optics efficiency	1
Transmitter azimuth pointing error angle	Variable
Receiver azimuth pointing error angle	0 μrad
Beam divergence	1.5 mrad
Additional losses	3 dB
Filter type	Low-pass bessel filter, order 4
APD sensitivity	1 A/W
APD gain	100
APD dark current	10 nA
APD load resistance	50 Ω
APD temperature	298 K
APD responsivity	1 A/W
Electron charge	1.6×10^{-19}°C
Planck constant	6.625×10^{-34}

MPPM, spatial pulse-position modulation (or SPPM), and SCD. After this investigation, they proposed a new modulation as a hybrid MPPM/SPPM technique to enhance average SE performances. As a result, they have concluded that reducing AT effects and scintillation under a FSOC-MISO channel is achieved by using the AA technique. Furthermore, they also illustrated that the average SE performance can be enhanced by using SCD in a coherent FSOC-MISO system, and finally, SCD in a coherent FSOC-MISO system

significantly outperforms both OOK and MPPM techniques even in the presence of PE under strong AT.

There are studies that have demonstrated that the RF system is complementary to the FSOC system. Consequently, the employment of the hybrid RF/FSOC system is a preferred way to enhance the performance of the FSOC system in inappropriate channel conditions [21–24].

After extensive research into the works related to the FSO technology, this paper deals with the design and evaluation of a point-to-point optical link (or P2P-OL) under a FSOC channel exploiting an optimal modulation scheme under different weather conditions (see Table 1) which has not been discussed in the literature so far. The key motivation behind this work is to evaluate the impact of the electrical pulse generator (EPG) format on the proposed systems, which are NRZ pulse generator (NRZPG), RZ pulse generator (RZPG), Gaussian pulse generator (GPG), hyperbolic-secant pulse generator (HSPG), and raised cosine pulse generator (or RCPG). Figure 1 illustrates the distribution of the total power of the transmitted data versus the frequency for different EPG formats. It is quite clear that each format has a specific distribution of its power; from observation, one can see that the GPG, HSPG, and RCPG formats, which are used in optical satellite transmissions, have the advantage of producing signals whose spectra are well localized in frequencies (every format has a power that is concentrated in a small spectral range).

To achieve and accomplish our work objective, we rely on the following parts:

In the first part, we investigate the P2P-OL system under free-space optical communication-single-input and single-output (FSOC-SISO) channel performance and availability in varying weather conditions based on the attenuation variation with using the direct optical modulation (or DOM) for different EPG formats. To evaluate the performances of the proposed system, we have tested it under two different
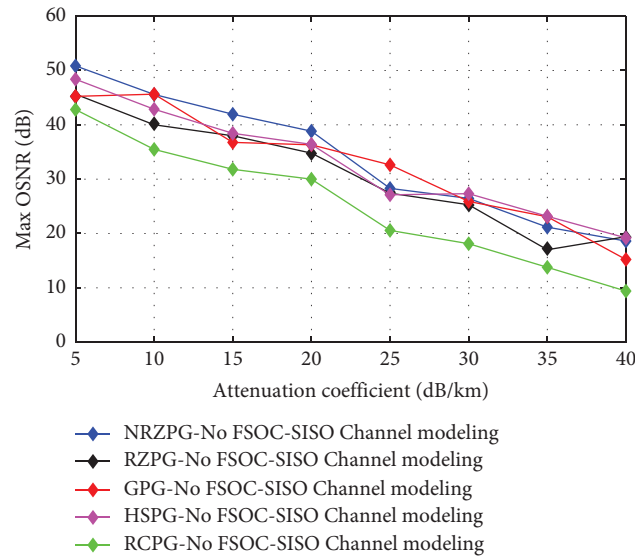
FIGURE 6: Max OSNR (dB) vs. attenuation coefficient (dB/km): using DOM for EPG formats, without PE.
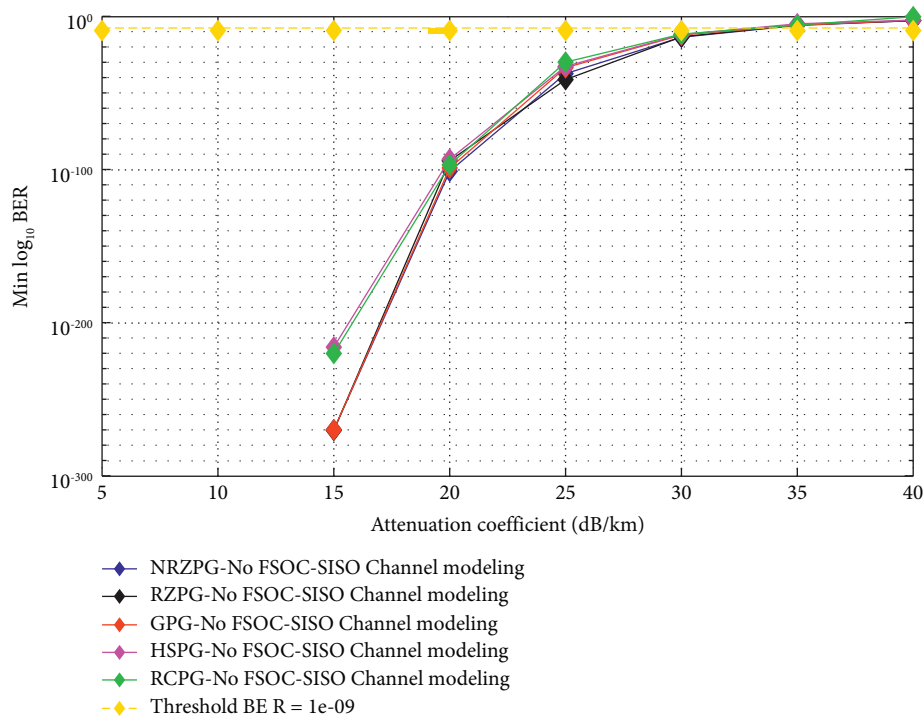

FIGURE 7: Min BER vs. attenuation coefficient (dB/km) using DOM for EPG formats, without PE.

channels, such as log-normal fading FSOC channel and gamma-gamma FSOC channel without pointing errors (or PE). In the second part, we improve the previous proposed system through the use of an optical amplifier, the EDFA (erbium-doped fiber amplifier). For more information on the EDFA, refer to the following sections. However, in the third part, we use the same improved system that was evaluated in the second part, but we exploit the external optical modulation (EOM) for different EPG formats under a log-normal fading FSOC channel and a gamma-gamma FSOC channel without PE. In the final part, we investigate the performances of the proposed system under a free-space optical communication-multiple-input and multiple-output (or FSOC-MIMO) channel based on the highest quality EOM and EPG techniques, where we also demonstrate the effect of beam forming gain over a FSOC-MIMO channel (also under a log-normal fading FSOC channel and a gamma-gamma FSOC channel, without and with PE) in which we present their advantages and disadvantages. To finish this part, we have exploited the maximum capacity of
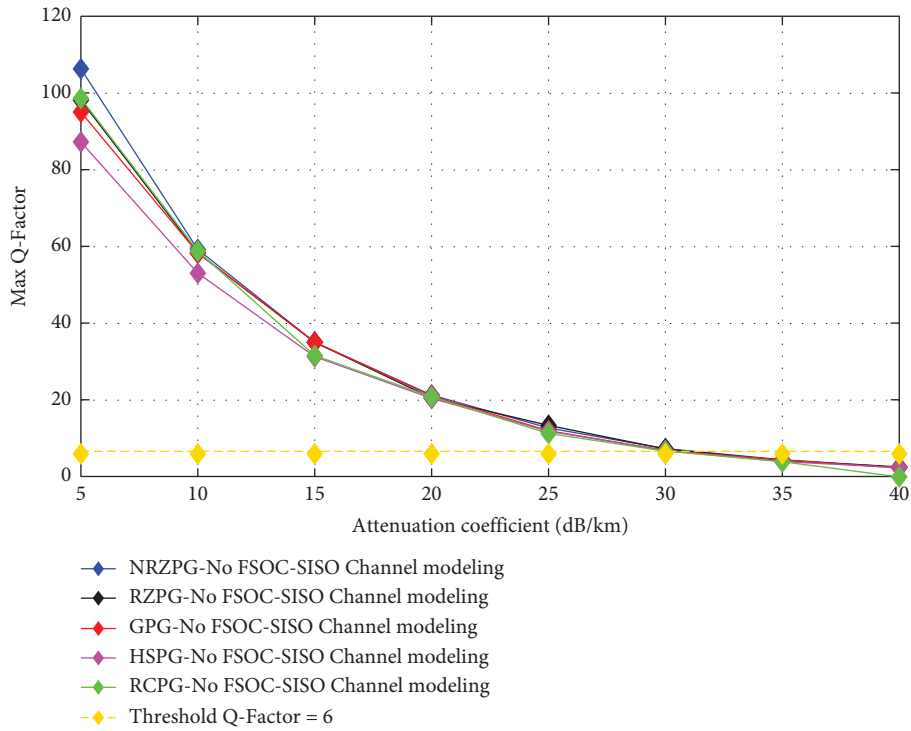
FIGURE 8: Max Q-factor vs. attenuation coefficient (dB/km) using DOM for EPG formats, without PE.

TABLE 3: Acceptable performances of min BER, max Q-factor, and max OSNR vs. attenuation coefficient (dB/km) using DOM for EPG formats without PE.

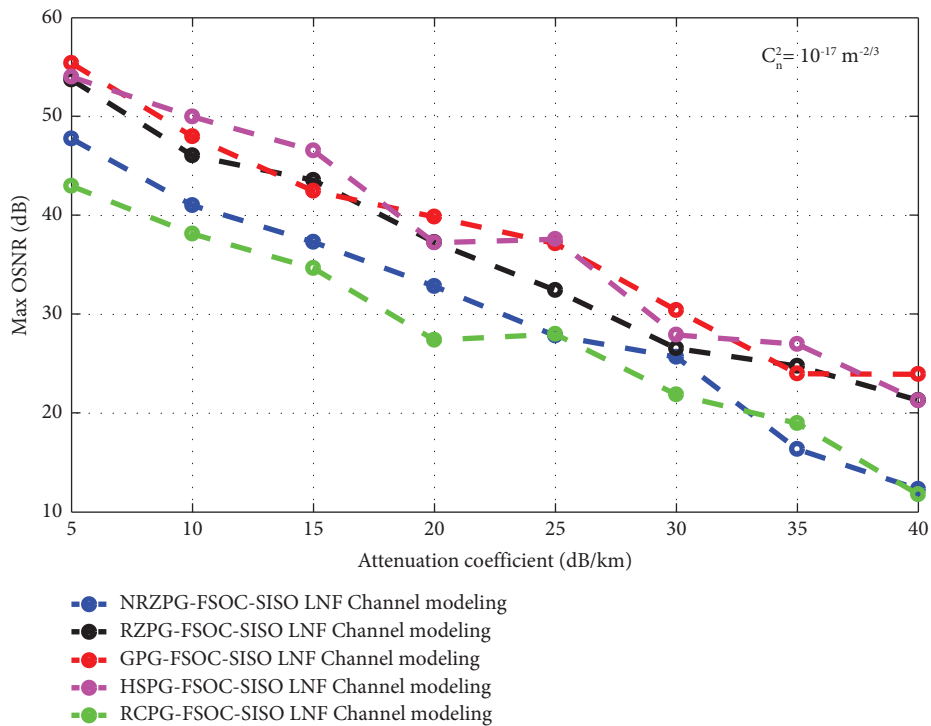| Attenuation (dB/km)	32.83 (NRZPG) $\Longrightarrow$	32.63 (RZPG) $\Longrightarrow$	32.30 (GPG) $\Longrightarrow$	31.97 (RCPG) $\Longrightarrow$	31.87 (HSPG) $\Longrightarrow$
Min BER	$1.000e-09$	$1.000e-09$	$1.000e-09$	$1.000e-9$	$1.000e-09$
Max Q-factor	6	6	6	6	6
Max OSNR (dB)	23.46	20.94	24.60	16.41	25.77

FIGURE 9: Max OSNR (dB) vs. attenuation coefficient (dB/km) with weak AT using DOM for EPG formats under various LNF FSOC-SISO channel states without PE.
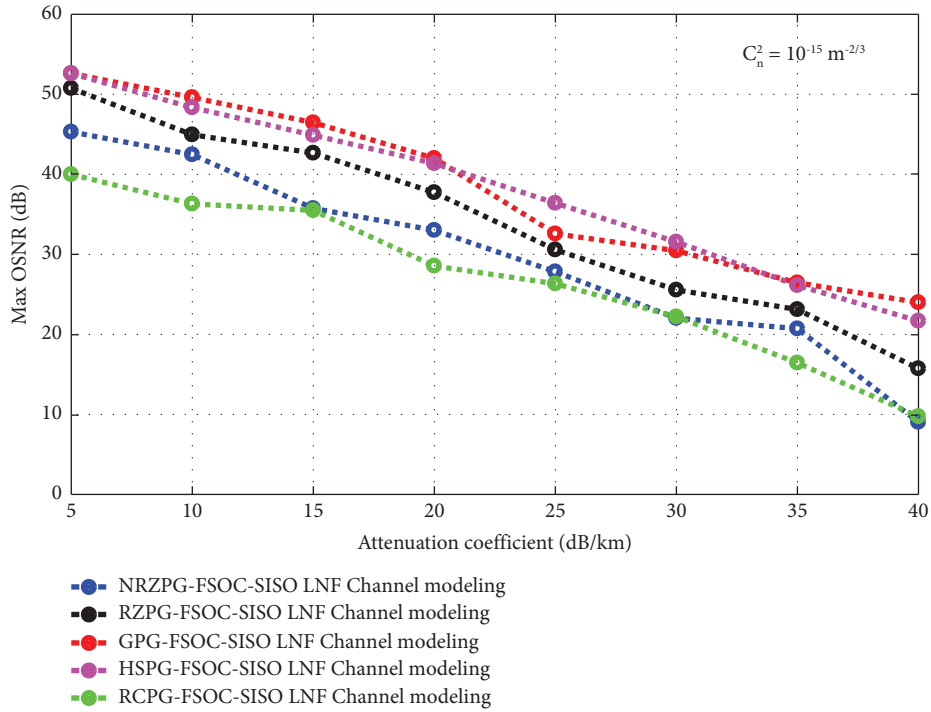
FIGURE 10: Max OSNR (dB) vs. attenuation coefficient (dB/km) with moderate AT using DOM for EPG formats under various LNF FSOC-SISO channel states without PE.
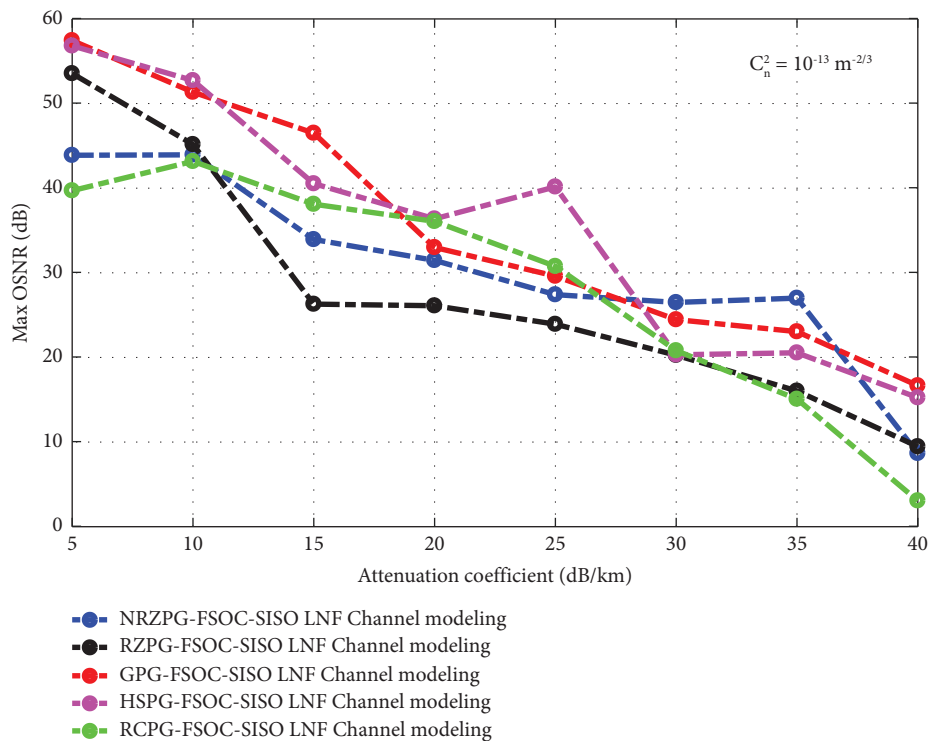

FIGURE 11: Max OSNR (dB) vs. attenuation coefficient (dB/km) with strong AT using DOM for EPG formats under various LNF FSOC-SISO channel states without PE.
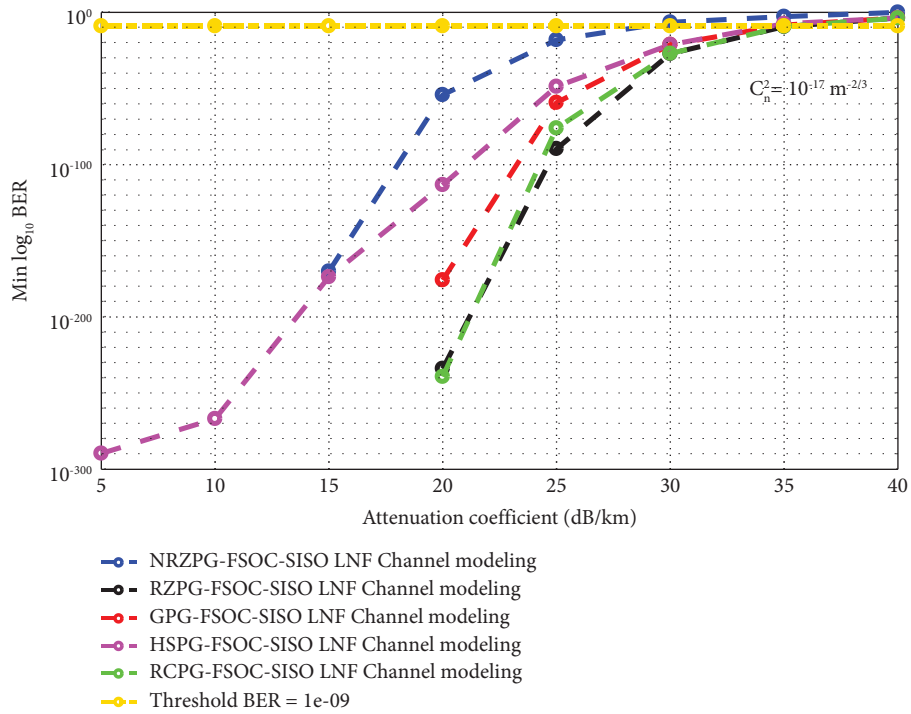
FIGURE 12: Min BER vs. attenuation coefficient (dB/km) with weak AT using DOM for EPG formats under various LNF FSOC-SISO channel states, without PE.

FIGURE 13: Min BER vs. attenuation coefficient (dB/km) with moderate AT using DOM for EPG formats under various LNF FSOC-SISO channel states without PE.

FIGURE 14: Min BER vs. attenuation coefficient (dB/km) with strong AT using DOM for EPG formats under various LNF FSOC-SISO channel states without PE.

FIGURE 15: Max Q-factor vs. attenuation coefficient (dB/km) with weak AT using DOM for EPG formats under various LNF FSOC-SISO channel states without PE.
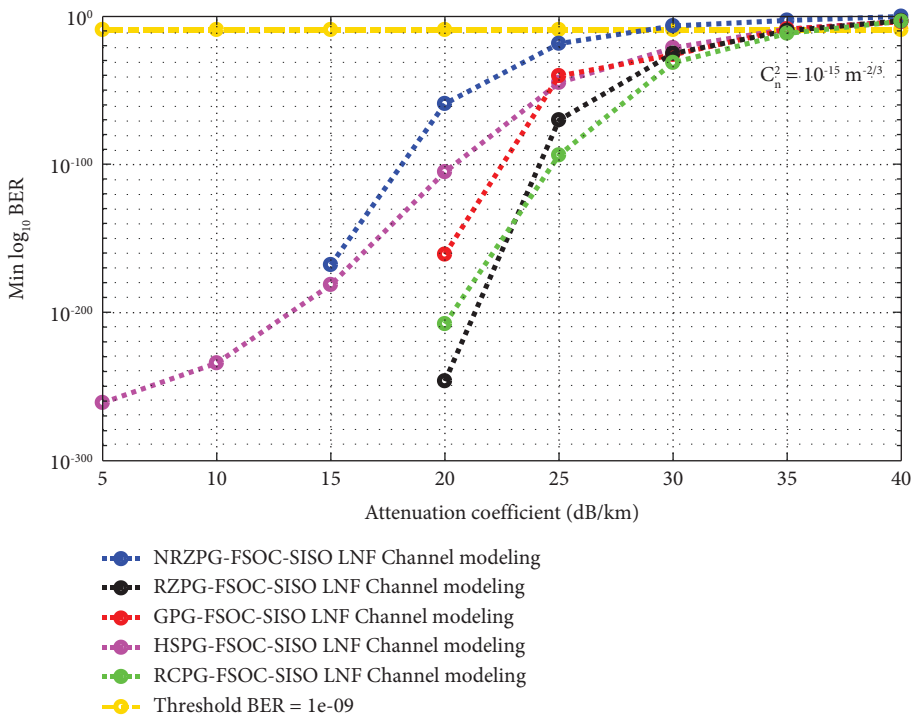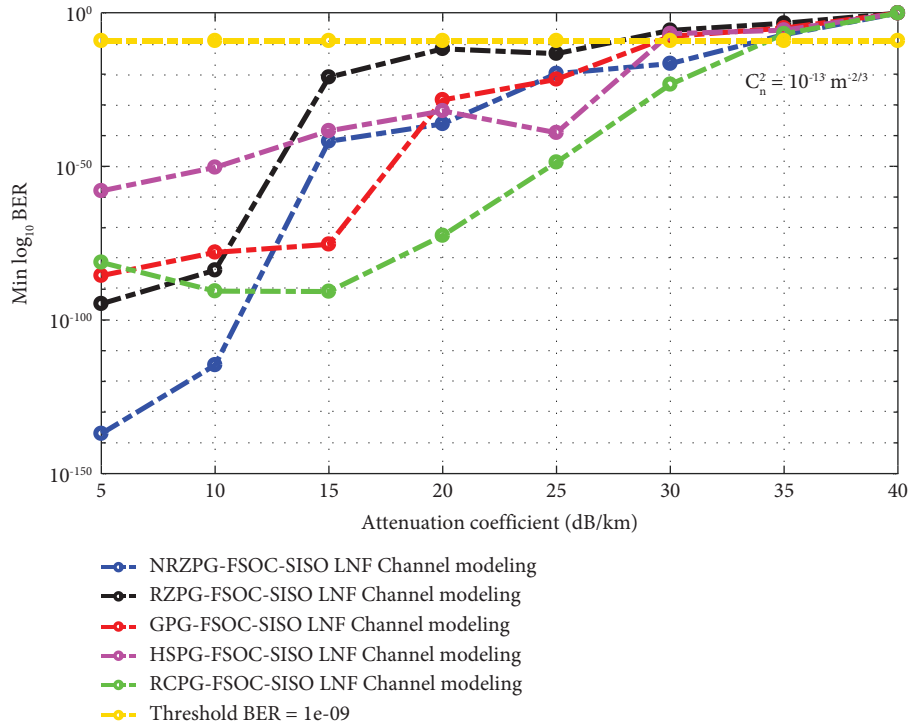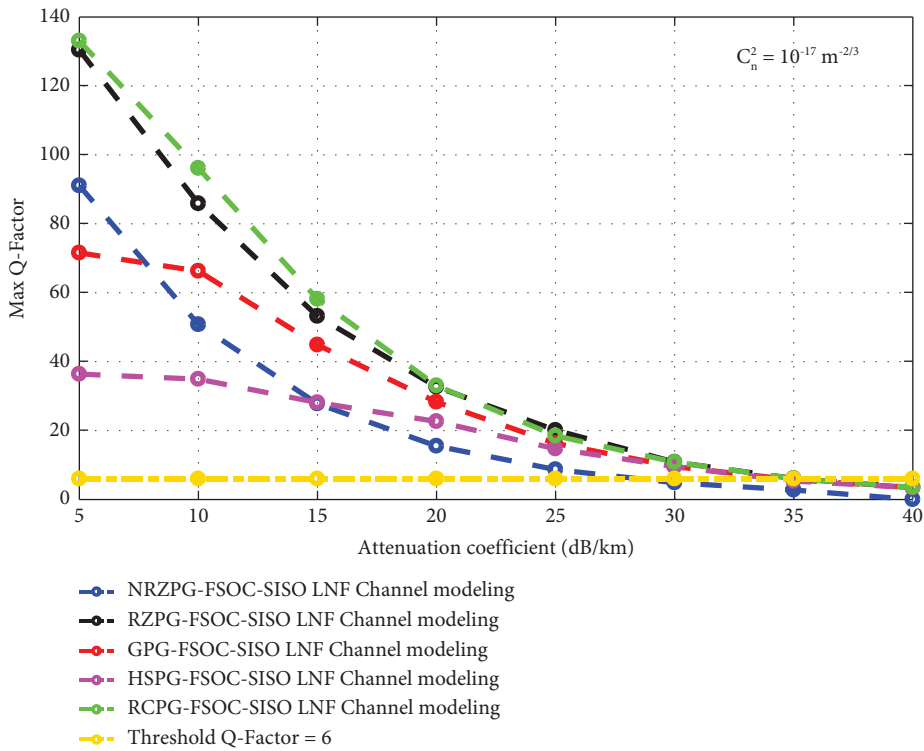
Figure 16: Max Q-factor vs. attenuation coefficient (dB/km) with moderate AT using DOM for EPG formats under various LNF FSOC-SISO channel states without PE.
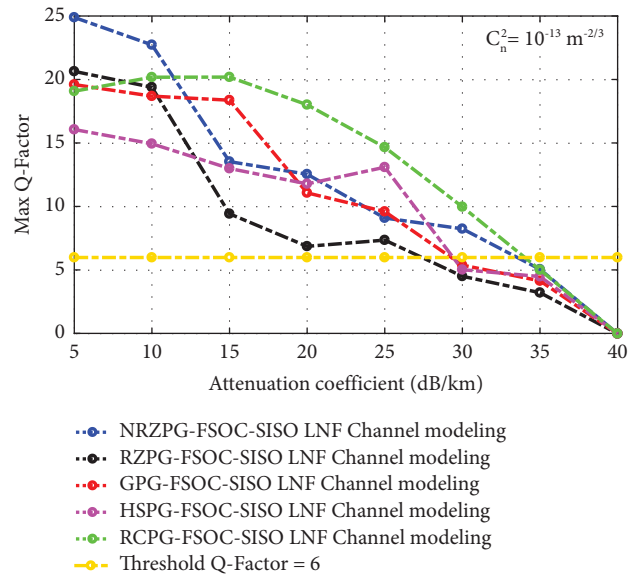
Figure 17: Max Q-factor vs. attenuation coefficient (dB/km) with strong AT using DOM for EPG formats under various LNF FSOC-SISO channel states without PE.

Table 4: Acceptable performances of min BER, max Q-factor, and max OSNR vs. attenuation coefficient (dB/km) using DOM for EPG formats under LNF FSOC-SISO channel with $C_n^2 = 10^{-13}$ m$^{-2/3}$, without PE.

Attenuation (dB/km)	34.23 (RCPG) $\Longrightarrow$	33.92 (NRZPG) $\Longrightarrow$	29.64 (HSPG) $\Longrightarrow$	29.48 (GPG) $\Longrightarrow$	27.76 (RZPG) $\Longrightarrow$
Min BER	$1.000e-09$	$1.000e-09$	$1.000e-09$	$1.000e-9$	$1.000e-09$
Max Q-factor	6	6	6	6	6
Max OSNR (dB)	15.96	26.9	21.75	25	21.91

FIGURE 18: Max OSNR (dB) vs. attenuation coefficient (dB/km) with weak AT using DOM for EPG formats under various G-G FSOC-SISO channel states without PE.
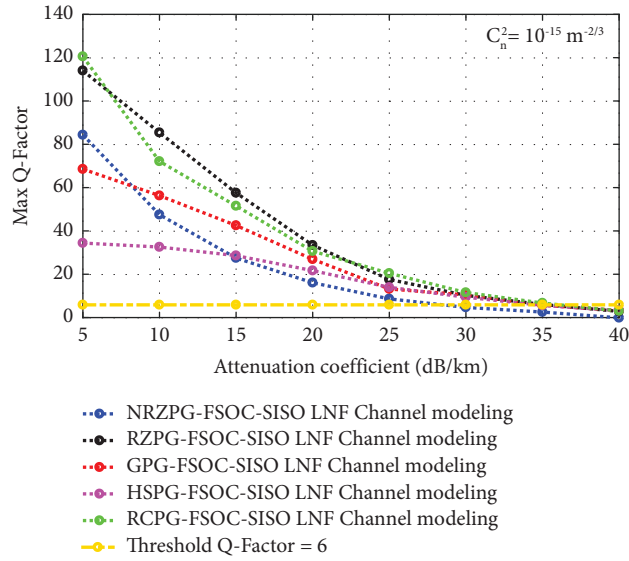

FIGURE 19: Max OSNR (dB) vs. attenuation coefficient (dB/km) with moderate AT using DOM for EPG formats under various G-G FSOC-SISO channel states without PE.
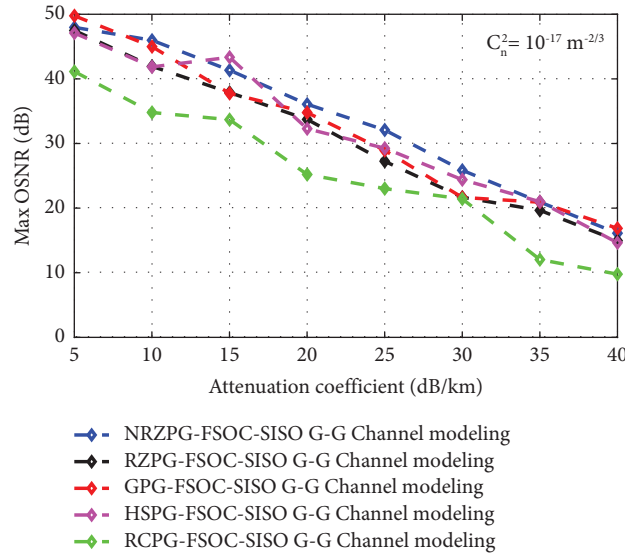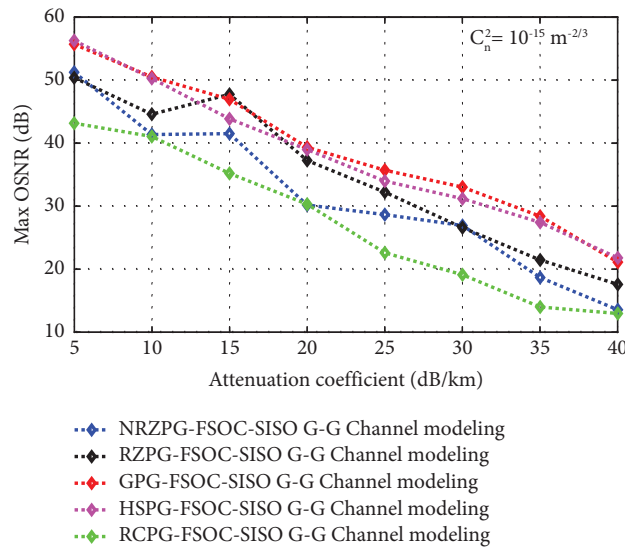
the FSOC-MIMO channel by using WDM technology for 16 users, where we have estimated the transmission capacity (or TC) for each of the 16 users and the overall transmission capacity (or OTC) of the proposed system.

The rest of this paper is organized as follows. Section 2 introduces the configuration of the outdoor long-haul FSOC system. Section 3 presents the meteorological characteristics which can deteriorate the FSOC system's performance. Section 4 provides an analysis for calculating the electrical signal-to-noise ratio (ESNR) and the bit error rate (BER). Section 5 describes the basic FSOC system suggested in this paper. Section 6 discusses the simulation results and depicts the graphical analysis. Finally, Section 7 gives a summary of the key findings of this study.

2. Outdoor Long-Haul FSOC System

In an outdoor long-haul FSOC system, the optical transceivers (OTx/ORx: optical transmitter/optical receiver) are communicating wirelessly over the air via P2P line-of-sight (or LOS) FSOC links, as illustrated in Figure 2. The emitter (or OTx part), however, typically employs semiconductor lasers with large bandwidth and high-power output, such as CW laser (i.e., it generates a continuous wave optical signal), and the receiver (ORx part) employs a trans-impedance combined bootstrap design, such as PINs photodiodes (or positive-intrinsic-negative photodiodes) or APDs (avalanche photodiodes) of various dimensions. To modulate the optical signals, intensity modulation and direct detection based on OOK (or

FIGURE 20: Max OSNR (dB) vs. attenuation coefficient (dB/km) with strong AT using DOM for EPG formats under various G-G FSOC-SISO channel states, without PE.

FIGURE 21: Min BER vs. attenuation coefficient (dB/km) with weak AT: using DOM for EPG formats under various G-G FSOC-SISO channel states without PE.

on off Keying) are broadly applied. In this paper, we focus on the application of other modulation formats [26–30].

The beam signal strength of a P2P-LOS FSOC link is affected by the atmospheric losses and interference throughout the propagation path, including free-space losses, free-air absorption, scattering, refraction, atmospheric turbulence (also referred to as scintillation), and interference from ambient light, which is stray light beside the exploited light beam reaching the ORx part. In Figure 3, different effects of physical and weather-related conditions occurring on the FSOC link are illustrated. In addition, there has been evidence from the field tests in major cities of the world that prove the atmospheric attenuation of these over-mentioned factors is persistently weak. Therefore, these factors may be collectively modeled as a constant parameter compared to the turbulence within

FIGURE 22: Min BER vs. attenuation coefficient (dB/km) with moderate AT using DOM for EPG formats under various G-G FSOC-SISO channel states without PE.
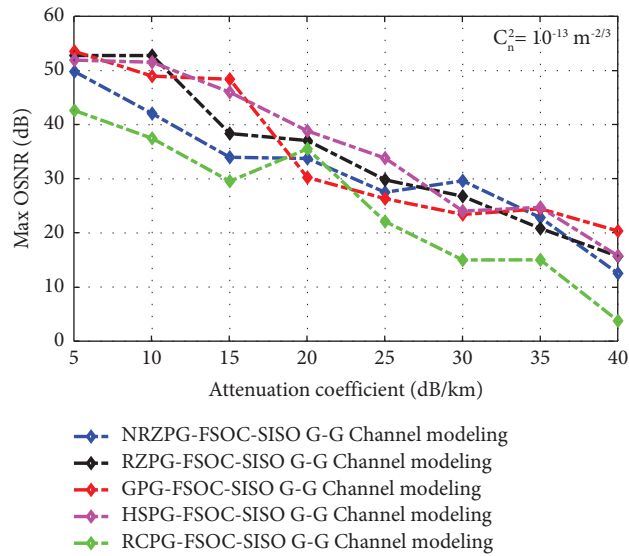

FIGURE 23: Min BER vs. attenuation coefficient (dB/km) with strong AT using DOM for EPG formats under various G-G FSOC-SISO channel states without PE.
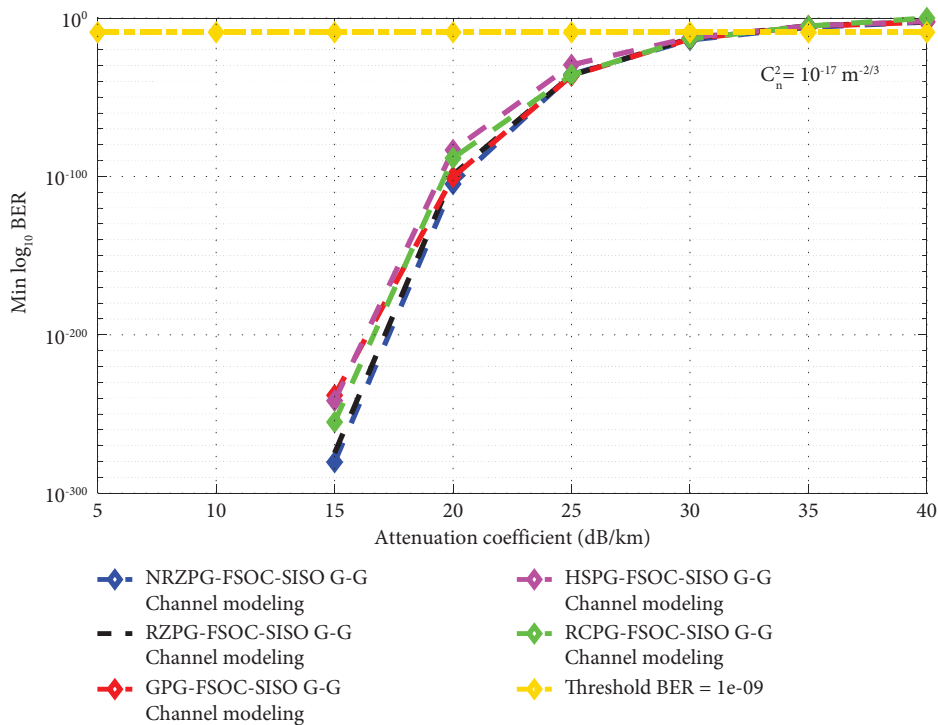
FIGURE 24: Max Q-factor vs. attenuation coefficient (dB/km) with weak AT using DOM for EPG formats under various G-G FSOC-SISO channel states without PE.
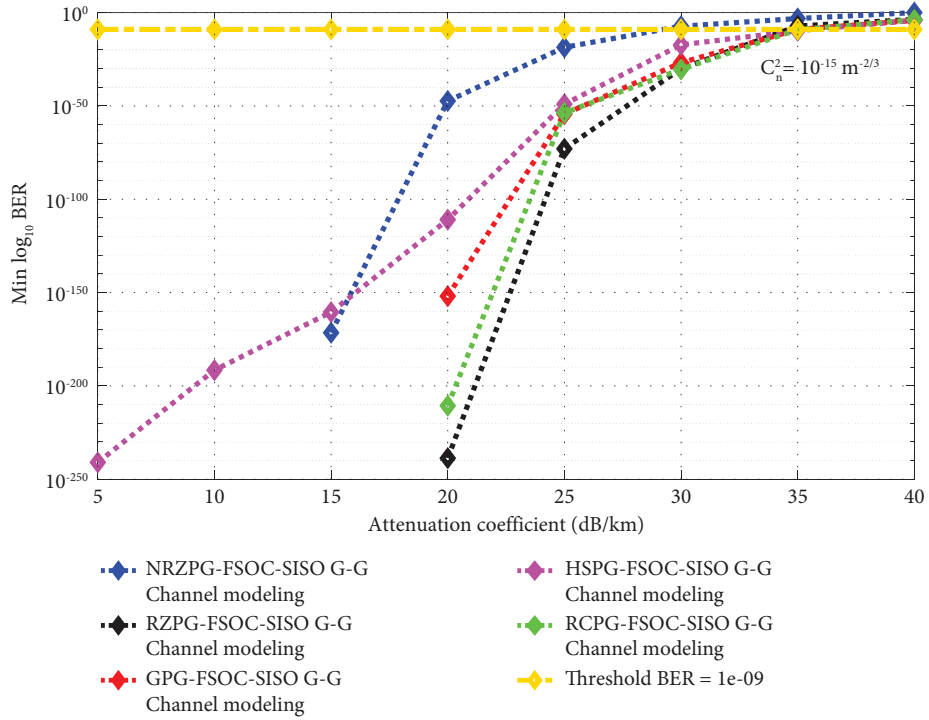

FIGURE 25: Max Q-factor vs. attenuation coefficient (dB/km) with moderate AT using DOM for EPG formats under various G-G FSOC-SISO channel states without PE.
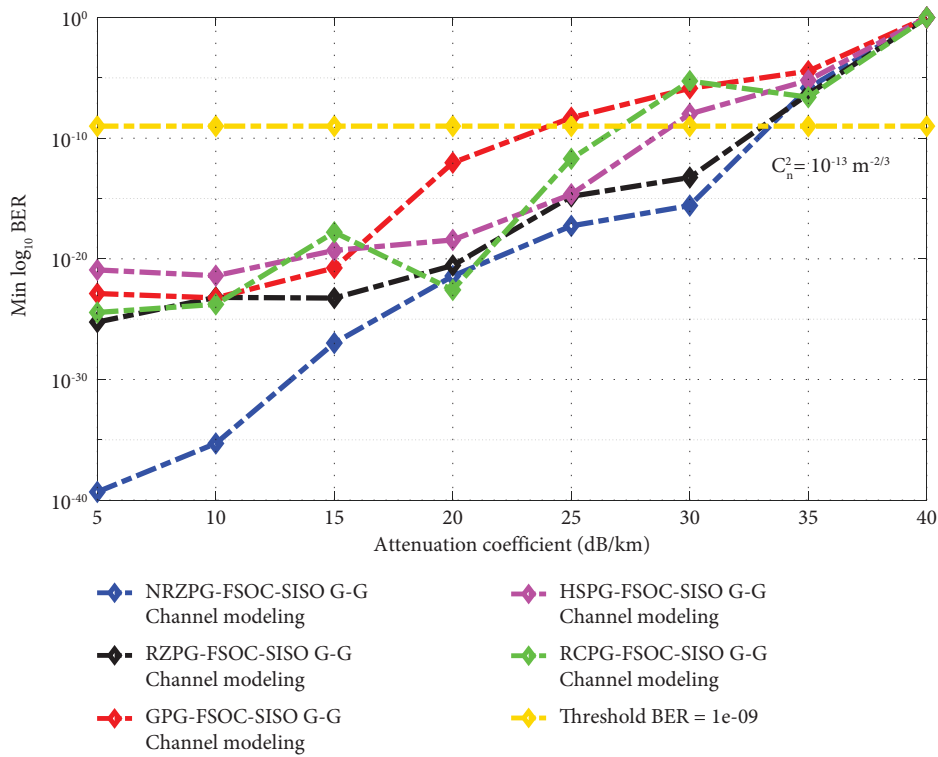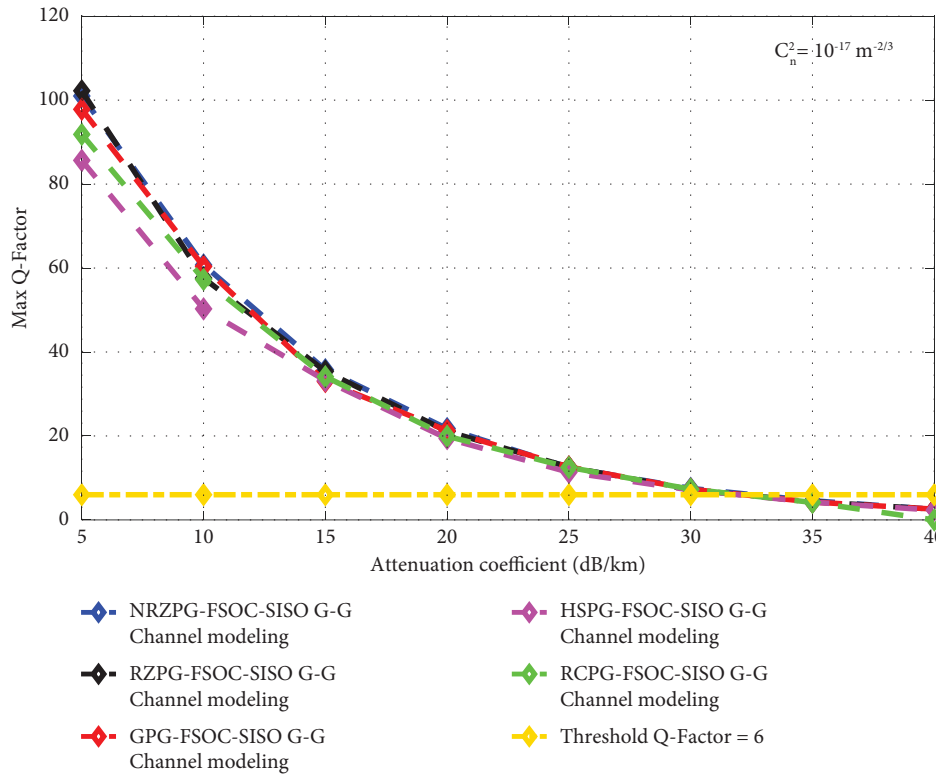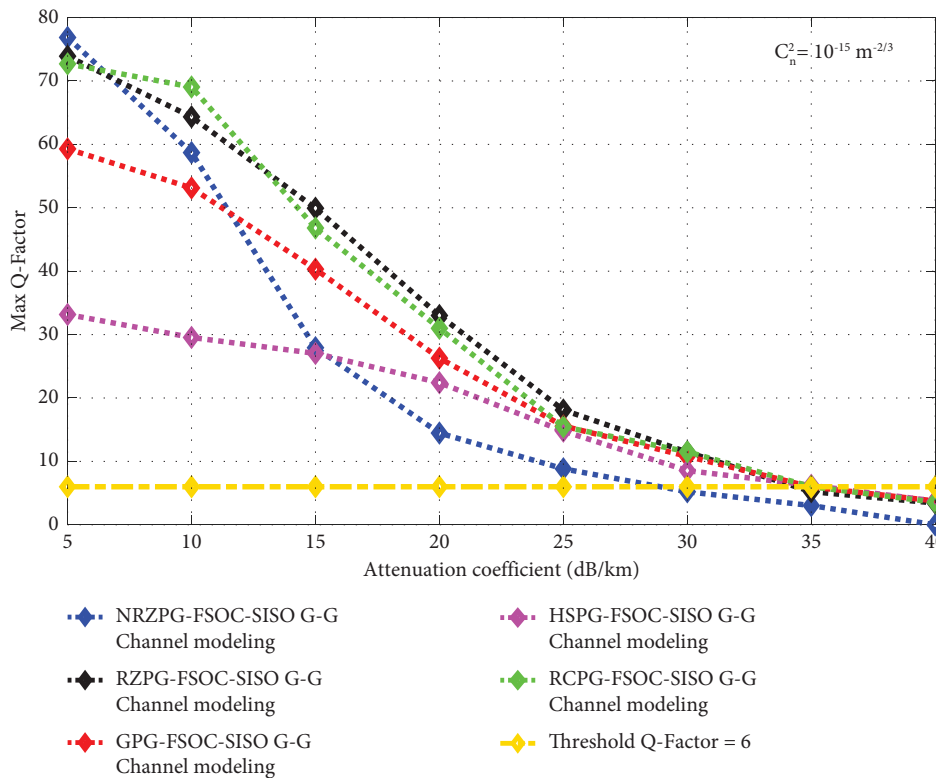
a mathematical model. However, the main weakness of the outdoor long-haul FSOC system is atmospheric turbulence, which arises as a result of refractive index variation related to inhomogeneities in temperature and pressure fluctuations and ultimately induces random amplitude fluctuations associated with the transmitted optical signals over the FSOC channel. As is well known, atmospheric turbulence is physically represented by the Kolmogorov theory [26–30].

2.1. Log-Normal Turbulence Model.
For carrying out the FSOC channel fading, the FSOC channel needs to be modeled with a log-normal distribution, as the log-normal model is widely applied to model the fading effect, especially under low-moderate, high-moderate, and high-turbulence conditions. To do that, we employ the log-normal statistical channel model, which can be described as follows [26, 27, 31–35]:

$$y_{\text{ORx}} = s \cdot z_{\text{OTx}} + b_{\text{AWGN}}, \tag{1}$$

where

$$s = \eta \cdot I. \tag{2}$$

In equations (1) and (2), y_{ORx} is the received signal from the destination node (ORx); s is the instantaneous intensity gain; $z_{\text{OTx}} \in \{0, 1\}$ is the OOK modulated signal transmitted from the source node (OTx); $b_{\text{AWGN}} \sim \text{N}(0, N_0/2)$ represents the additive white Gaussian noise (AWGN), which is mainly generated by the superposition of the circuit noise and the thermal noise in the electronics; η is the effective photo-current conversion ratio of the ORx; and I is the light intensity (normalized), which is caused by the AT, where

$$\eta = \gamma \cdot \frac{e \cdot \lambda}{h \cdot c}, \tag{3}$$

and

$$I = e^{(2 \cdot x)}. \tag{4}$$

In equations (3) and (4), γ represents the quantum efficiency of the photo receiver at the ORx; e is the electron charge; λ is the signal wavelength; c represents the light's speed; and h is Plank's constant. $x \sim \text{N}(0, \sigma_x^2)$ follows the Gaussian distribution with a zero-mean and a variance value equal to σ_x^2. Hence, I has a log-normal distribution with a mean value equal to $e^{2 \cdot \sigma_x^2}$ and a variance value equal to $e^{4 \cdot \sigma_x^2} \cdot (e^{4 \cdot \sigma_x^2} - 1)$, and probability density function (or PDF) is formulated as follows [26, 27, 31–35]:

$$F_I(x) = \left(\frac{1}{2 \cdot x \cdot \sigma_x \cdot \sqrt{2 \cdot \pi}} \right) \cdot e^{-\left((\ln(x))^2 / 8 \cdot \sigma_x^2 \right)}, \tag{5}$$

where σ_x^2 represents the normalized intensity fluctuation variance or scintillation index. For plane waves, the scintillation index is represented by the following Rytov variance:

$$\sigma_x^2 = \sigma_R^2. \tag{6}$$

In equation (6), the σ_R^2 refers to the Rytov variance which is calculated from $1.23 \cdot C_n^2 \cdot k^{1.17} \cdot L^{1.83}$, k denotes the wave number, L is the link distance, and C_n^2 in (m$^{-2/3}$) corresponds to the strength of the atmospheric turbulence or, simply, the strength of fluctuations in the refractive index of the environment. In fact, the C_n^2 numerical values, 10^{-13} m$^{-2/3}$, 10^{-15} m$^{-2/3}$, and 10^{-17} m$^{-2/3}$, are considered to indicate strong, moderate, and weak turbulence, respectively. The refractive index structure parameter (C_n^2) represents the critical parameter which characterizes the AT effects on the optical signal that is propagated over the FSOC channel [17–20, 26, 27, 31–38].

Finally, to configure the log-normal fading (or LNF) FSOC channel, we use the MATLAB component (it is located to the component library: MATLAB library) and integrate it into the suggested system. Alternatively, the LNF channel predefined in the FSO channel library can be used.

2.2. Gamma-Gamma Turbulence Model.
For carrying out the gamma-gamma (or G-G) channel fading for the FSOC link, the FSOC channel needs to be modeled with a gamma-gamma distribution. To do that, we employ the G-G statistical channel model, which can be described as follows [17–20, 26, 27, 31–38]:

$$y_{\text{ORx}}{}' = s{}' \cdot z_{\text{OTx}} + b_{\text{AWGN}}, \tag{7}$$

where

$$s{}' = \eta \cdot II. \tag{8}$$

In equations (7) and (8), $y_{\text{ORx}}{}'$ is the received signal from the destination node (or ORx) under a G-G FSOC channel, $s{}'$ is the instantaneous intensity gain under a G-G FSOC channel, II represents the intensity fluctuation of the optical signal during its propagation in space, which is caused by scintillation effects, and z_{OTx}, b_{AWGN}, and η are defined in the previous subsection.

It is well known, however, that the gamma-gamma model has a low to high turbulence regimes where the PDF of its intensity II is the product of two gamma random variables which indicate high and low turbulence fluctuations. The two random variables are indicated by X_G and Y_G. The received intensity I stands for II = $X_G \cdot Y_G$. The PDF of II is given by

$$F(\text{II}) = \frac{2(\alpha \cdot \beta)^{(\alpha+\beta/2)}}{\Gamma(\alpha) \cdot \Gamma(\beta)} \cdot \text{II}^{((\alpha+\beta/2)-1)} \cdot K_{\alpha-\beta}\left(2(\alpha \cdot \beta \cdot \text{II})^{0.5}\right), \text{II} > 0. \tag{9}$$

In equation (9), the parameters α and β are related to the small-scale and large-scale turbulence effects, respectively, and as are set in equations (9) and (10). $\Gamma(\cdot)$ and $K_{\alpha-\beta}(\cdot)$ are the gamma function and the Bessel function of the second order $(\alpha - \beta)$, respectively. The resulting scintillation index (or SI) is the II fluctuations which are linked to the parameters α and β, as $SI = 1/\alpha + 1/\beta + 1/\alpha \cdot \beta$

(α and β are suitable for the beam of a plane wave at the optical receiver).

$$\alpha = \left[e^{\left(0.49 \cdot \sigma_R^2 / \left(1 + 1.11 \cdot \sigma_R^{2.4}\right)^{1.17}\right)} - 1 \right]^{-1}. \tag{10}$$

Also,

$$\beta = \left[e^{\left(0.51 \cdot \sigma_R^2 / \left(1 + 0.69 \cdot \sigma_R^{2.4}\right)^{0.83}\right)} - 1 \right]^{-1}. \tag{11}$$

In equations (10) and (11), σ_R^2 is defined in the previous subsection [17–20, 26, 27, 31–39].

Finally, to configure the G-G FSOC channel, we use the MATLAB component (it is located in the component library: MATLAB library) and integrate it into the suggested system. Alternatively, the G-G channel predefined in the FSO channel library can be used.

3. Meteorological Characteristics against the FSOC System Performances

When it comes to meteorological conditions such as the presence of atmospheric turbulence, haze, rain, and fog, the optical wave which propagates between the installed optical antennas (OTx part and ORx part) in a FSOC system may be strongly influenced by these conditions. Therefore, there are various statistical meteorological models to be considered for a correct estimation of the FSOC link performance for any installed system. Nevertheless, the visibility between the installed optical antennas (OTx part and ORx part) for the FSOC system is the main parameter required to predict the atmospheric fluctuations caused by several meteorological conditions. As a result, the telecommunications engineer or researcher can know the binding margin of any proposed model under various meteorological situations. For that, one can measure various atmospheric data successfully using different sensors and electronic devices with the best accuracy [39–47].

When reference is made to the subject of visibility or visual range in meteorological terms, it can always be defined as the maximum range that can be seen clearly and be determined by the light and weather conditions. As a result of this, the FSOC model performance between two separate nodes in a specific region can be predicted by the measured visibility data. So based on the visibility, the effectiveness of the FSOC model is established. The visibility performance for a full FSOC system is strongly affected by 3 key variables, namely, the level of source coherence, the linking range between the source and the detector, and the detector position with regard to the source. Visibility may be lowered when particle concentration and size exceed the standard level of visibility. Finally, as per Koschmieder's law, visibility is technically the distance over which the propagating light loses two percent of the original power [39–47].

Atmospheric attenuation (or AA_{tt}) refers to the unexpected attenuation which affects the FSOC link's performance. In addition, it results in the additive effect of the absorption and scattering of infrared light and laser photons from its path by aerosols and gas molecules which are present in the atmosphere. One can compute it from the scattering coefficient. Due to the exploited laser beam wavelength being within the atmospheric weak absorption spectra, the absorption effects at the total attenuation coefficient are regarded as very weak. Consequently, the total attenuation coefficient is primarily affected through scattering effects. The scattering type is defined by the atmospheric particle size at each transmission laser wavelength. When one wishes to calculate the AA_{tt} coefficient, one uses the Beer–Lambert exponential law which is shown mathematically as the following formula [39–47]:

$$\alpha_{AA_{tt}} = e^{\left(-\varphi_{sca} \cdot L\right)}, \tag{12}$$

and

$$\varphi_{sca} = \left(\frac{3.91}{V}\right) \cdot \left(\frac{\lambda}{550 \, nm}\right)^{-q}. \tag{13}$$

In equations (12) and (13), $\alpha_{AA_{tt}}$ denotes the atmospheric attenuation (or AA_{tt}), φ_{sca} represents the scattering coefficient, L denotes the link distance in (km), V represents the visible range of the original optical signal in (km), λ is the operating wavelength of the original optical signal in (nm), and q is the size distribution parameter of the scattering particles. The AA_{tt} in (dB) is easily calculated by the following formula:

$$\alpha_{AA_{tt}}[dB] = -10 \cdot \log\left(\alpha_{AA_{tt}}\right). \tag{14}$$

However, in the literature, the effects of scattering can be predicted for all proposed FSOC systems by various statistical models; we can mention in the next subsections two models, namely, Kruse's and Kim's [39–47].

3.1. Kruse's Model. The Kruse's model enables the size distribution parameter "q" to assume different values depending on the different meteorological conditions. For moderate and high visibility, the formula (9) for the size distribution of scattering particles is derived as follows [41, 42, 47]:

$$q = \begin{cases} 1.6 \longrightarrow & V > 50 \, km, \\ 1.3 \longrightarrow & 6 \, km \le V \le 50 \, km, \\ 0.585 \cdot V^{(1/3)} \longrightarrow & V < 6 \, km. \end{cases} \tag{15}$$

3.2. Kim's Model. The Kim's model for haze attenuation is regarded as an extended version of the Kruse's model which is applied to obtain better accuracy at low visibility. For low, moderate, and high visibility, the formula (10) for the size distribution of scattering particles is derived as follows [41, 42, 47]:

$$q = \begin{cases} 1.6 & \longrightarrow \quad V > 50 \, \text{km}, \\ 1.3 & \longrightarrow \quad 6 \, \text{km} < V < 50 \, \text{km}, \\ 0.16 \cdot V + 0.34 & \longrightarrow \quad 1 \, \text{km} < V < 6 \, \text{km}, \\ V - 0.5 & \longrightarrow \quad 0.5 \, \text{km} < V < 1 \, \text{km}, \\ 0 & \longrightarrow \quad V < 0.5 \, \text{km}. \end{cases} \quad (16)$$

4. ESNR and BER Analyses

As a standard FSOC system with direct detection, the data is intensity modulated on the optical field of a beam and transmitted to the receiver through the atmospheric channel. The receiving lens at the FSOC channel, which collects part of the transmitted optical field, which is subsequently pointed at a photodetector surface (here, APD is used), as shown in Figure 4. However, the current flow from the filter output, driven by the incident optical signal [48–50], is

$$i = i_s + i_N, \quad (17)$$

where i_s represents the signal current and i_N signifies the detector noise current. Both the current signal and the mean square random noise current are determined [48–50] as follows:

$$i_s = \frac{\eta \cdot e \cdot P_r(H)}{h \cdot f}, \quad (18)$$

and

$$\overline{i_N^2} = 2 \cdot e \cdot B \cdot i_s. \quad (19)$$

Equations (18) and (19) are put into equation (20) and then the electrical signal-to-noise ratio (or ESNR) for the direct detection FSOC system is derived as follows:

$$\text{ESNR} = \frac{i_s^2}{\overline{i_N^2}}, \quad (20)$$

$$\text{ESNR} = \frac{\eta \cdot P_r(H)}{2 \cdot B \cdot h \cdot f}. \quad (21)$$

In equation (21), the parameters η and h are defined in the previous subsection, f refers the optical frequency, and B denotes the bandwidth of filter and $P_r(H)$ is the received signal power at the ORx under a FSOC channel state [48–50].

The received signal power at the ORx, $P_r(H)$ at a distance L with a transmitter signal power P_t may be expressed as follows:

$$P_r(H) = P_t \cdot \tau_{T_x} \cdot \tau_{R_x} \cdot \left(\frac{c}{4 \cdot \pi \cdot L \cdot f}\right)^2 \cdot G_{T_x} \cdot G_{R_x} \cdot L_{T_x} \cdot L_{R_x} \cdot H. \quad (22)$$

In equation (22), the parameters c, f, L and P_t are defined in the previous subsection, τ_{T_x} refers the optical transmitter efficiency, τ_{R_x} refers the optical receiver efficiency, G_{T_x} characterizes the transmitter telescope gain, G_{R_x} typifies the receiver telescope gain, L_{T_x} illustrates the transmitter pointing loss factor, L_{R_x} illustrates the receiver pointing loss factor, and H refers to the channel state for FSOC link [17, 18, 48–52].

Although many FSOC systems employ a laser transmitter with a small beam divergence angle and a receiver with a small field of view, a small pointing error can cause a loss of signal. The estimated pointing loss factor for the transmitter can be determined by

$$L_{T_x} = e^{\left(-G_{T_x} \cdot \theta_{T_x}^2\right)}. \quad (23)$$

However, the estimated pointing loss factor for the receiver can be determined by

$$L_{R_x} = e^{\left(-G_{R_x} \cdot \theta_{R_x}^2\right)}. \quad (24)$$

In equations (23) and (24), the parameters θ_{T_x} and θ_{R_x} are, respectively, the transmitter azimuth pointing error angle (or TAPEA) and the receiver azimuth pointing error angle (or RAPEA). In this paper, the RAPEA is considered to be ideal (i.e., $0 \, \mu$rad) [17, 18, 48–52].

The FSOC channel state H can be written as the optical intensity fluctuations caused by the atmospheric attenuation $\alpha_{AA_{tt}}$ and the atmospheric turbulence α_{AT} [17, 18, 48–52], which is expressed as follows:

$$H = \alpha_{AA_{tt}} \cdot \alpha_{AT}. \quad (25)$$

However, when the atmospheric turbulence α_{AT} is present, one can evaluate the probability of error P_e for electrical signal-coded optical data, detected with an APD, by the following formula:

$$P_e = Q\left(\frac{1}{2} \cdot \sqrt{\text{ESNR}}\right). \quad (26)$$

Finally, the BER for a direct detection FSOC system estimated by averaging the conditional error probability P_e across the probability distribution function (or PDF) under AWGN which is

(1) For the log-normal turbulence model,

$$\text{BER} = \int_0^\infty P_e \cdot F_I(x) \cdot dx. \quad (27)$$

(2) For the gamma-gamma turbulence model,

$$\text{BER} = \int_0^\infty P_e \cdot F(II) \cdot dI \, I. \quad (28)$$

The following section focuses on describing the configuration of the basic FSOC system proposed in this paper.

5. Simulation Design

The simulation configuration of a simple high-speed P2P-OL under a FSOC-SISO channel is depicted in Figure 5. Inside the FSOC-SISO channel, the optical transceivers communicate through the air to form a direct P2P-OL. The optical transmitter (OTx) is responsible for converting the electrical signal into an optical signal and sending
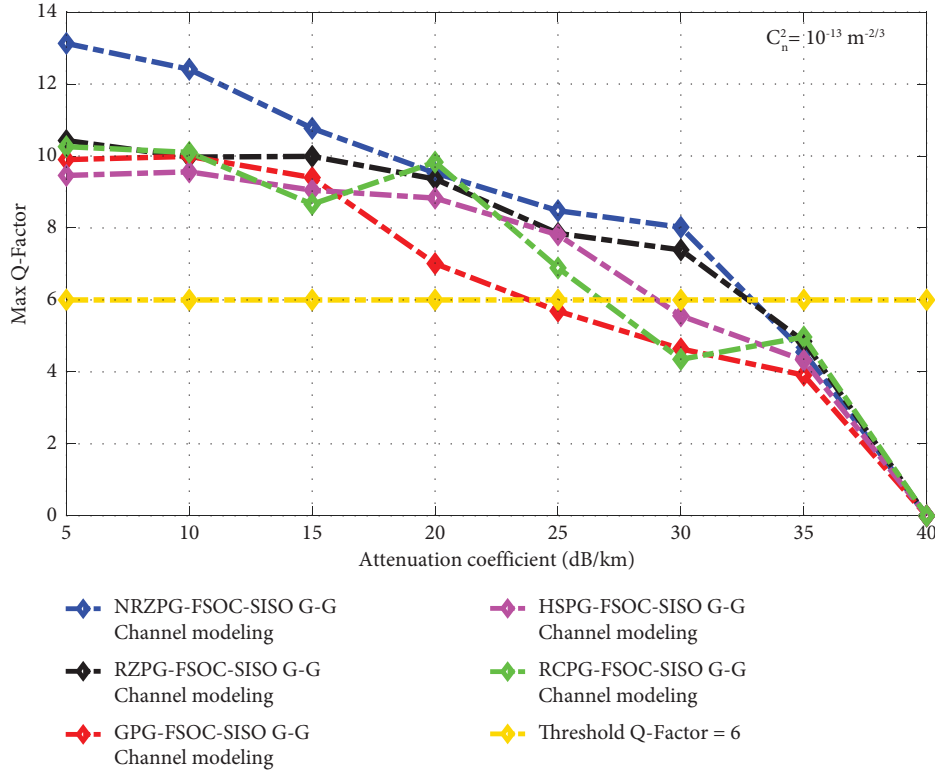
Figure 26: Max Q-factor vs. attenuation coefficient (dB/km) with strong AT using DOM for EPG formats under various G-G FSOC-SISO channel states without PE.

Table 5: Acceptable performances of min BER, max Q-factor, and max OSNR vs. attenuation coefficient (dB/km) using DOM for EPG formats under a G-G FSOC-SISO channel with $C_n^2 = 10^{-13}$ m$^{-2/3}$ without PE.

Attenuation (dB/km)	33.39 (NRZPG) $\implies$	33.12 (RZPG) $\implies$	29.24 (HSPG) $\implies$	27.12 (GPG) $\implies$	24.07 (RZPG) $\implies$
Min BER	$1.000e - 09$	$1.000e - 09$	$1.000e - 09$	$1.000e - 9$	$1.000e - 09$
Max Q-factor	6	6	6	6	6
Max OSNR (dB)	25.03	23.06	25.53	27.07	19.09

it through the atmosphere environment (or free space environment). Whereas, the optical receiver (or ORx) reconverts the optical signal into an electrical signal (consult Figure 5). The performance of a P2P-OL under a FSOC-SISO channel is estimated using three metrics: the bit error rate (or BER), the optical signal-to-noise ratio (or OSNR), and the Q-factor.

The OTx section includes a data generator (here, the pseudo-random bit sequence generator (or PRBS) is applied), an electrical pulse generator (or EPG), and an optical source (here, the continuous wave lasers (or CWL) is employed). The EPG provides a modulation format on the digital data that is attributed through a PRBS, in which the entire data rate is delivered in the digital format 0 and 1. The optical power of the CWL is 30 dBm with a wavelength of 1552.524 nm. Furthermore, the characteristics of the FSOC-SISO channel are recapitulated in Table 2. At the end of a P2P-OL under a FSOC-SISO channel, the ORx is present, which consists of a high-sensitivity detector designed to perform the reverse operation of the OTx (here, avalanche photo-diode (APD) is exploited). Then, a low-pass

Bessel filter is used to pass the wanted a low-frequency electrical signal with a cutoff frequency equal to $0.75 *$ symbol rate. After the filtering, the 3R regenerator performs reamplification, reshaping, and resynchronization of the received electrical signal with the original electrical signal to reduce the deterioration of the wanted electrical signal due to noise sources in the OTWNs.

Typically, the data are transmitted in the 0 and 1 digital domains which can be influenced by noise, and therefore intersymbol interference can occur. A BER analyzer is used to measure the transmission errors and the quality of the received optical signal, and to evaluate the OSNR performances, an electrical carrier analyzer is required [7, 53].

6. Results

6.1. Impact of Attenuation Coefficient Variation

6.1.1. Direct Optical Modulation (or DOM) with Different EPG Formats. In this subsection, the obtained results regarding the performances of the proposed system (see
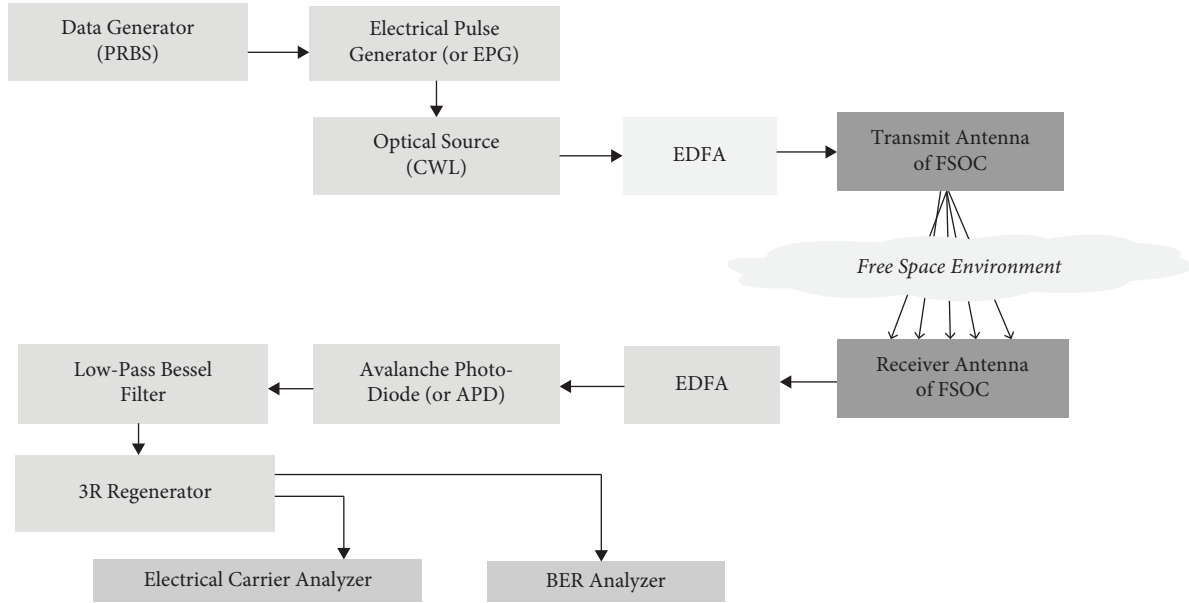
Figure 27: Configuration of a simple high-speed P2P-OL under a FSOC-SISO channel using DOM and EDFAs without PE.

Table 6: Comparison in terms of the performance of min BER, max Q-factor, and max OSNR vs. attenuation coefficient (dB/km) using DOM for EPG formats with and without the use of EDFAs.

RZPG no FSOC-SISO channel modeling			
Attenuation (dB/km)	32.63 without EDFAs	32.63 with EDFAs	70.55 with EDFAs
Min BER	$1.000e - 9$	0	$1.000e - 09$
Max Q-factor	6.00	100.67	6.00
Max OSNR (dB)	20.94	60.43	34.30
NRZPG no FSOC-SISO channel modeling			
Attenuation (dB/km)	32.83 without EDFAs	32.83 with EDFAs	63.96 with EDFAs
Min BER	$1.000e - 09$	0	$1.000e - 09$
Max Q-factor	6.00	156.04	6.00
Max OSNR (dB)	23.46	64.06	35.25
GPG no FSOC-SISO channel modeling			
Attenuation (dB/km)	32.3 without EDFAs	32.3 with EDFAs	69.74 with EDFAs
Min BER	$1.000e - 09$	0	$1.000e - 09$
Max Q-factor	6.00	61.64	6.00
Max OSNR (dB)	24.6	59.08	40.14
HSPG no FSOC-SISO channel modeling			
Attenuation (dB/km)	31.87 without EDFAs	31.87 with EDFAs	69.49 with EDFAs
Min BER	$1.000e - 09$	$45.87e - 312$	$1.000e - 09$
Max Q-factor	6.00	37.68	6.00
Max OSNR (dB)	25.77	74.26	37.18
RCPG no FSOC-SISO channel modeling			
Attenuation (dB/km)	31.97 without EDFAs	31.97 with EDFAs	70.35 with EDFAs
Min BER	$1.000e - 09$	0	$1.000e - 09$
Max Q-factor	6.00	61.56	6.00
Max OSNR (dB)	16.41	50.79	28.17

Figure 5) when the attenuation coefficient is varied to reach the optimal conditions for the FSOC-SISO channel under the AT are presented. The data transmission rate used under a FSOC-SISO channel has been selected at 1 Gbps, with a sequence size of 512 bits and the number of samples per bit being 64, which gives several samples of 32768. In addition, the range of the FSOC-SISO channel is chosen to be 1000 m.

In Figure 6, the relationship between the max OSNR and the varying attenuation of the transmitted signal under a FSOC-SISO channel is illustrated. Referring to the obtained results, one can observe that the increased attenuation coefficient of the transmitted signal under a FSOC-SISO channel (here, the channel is completely considered as an ideal which is not modeled) can affect the performance of the system in Figure 5. As an example, one can detect that within

TABLE 7: Comparison in terms of the performance of min BER, max Q-factor, and max OSNR vs. attenuation coefficient (dB/km) using DOM for EPG formats under a LNF FSOC-SISO channel with $C_n^2 = 10^{-13}$ m$^{-2/3}$ and with and without the use of EDFAs.

RZPG-LNF FSOC-SISO channel, $C_n^2 = 10^{-13}$ m$^{-2/3}$			
Attenuation (dB/km)	27.76 without EDFAs	27.76 with EDFAs	68.57 with EDFAs
Min BER	$1.000e-9$	0	$1.000e-09$
Max Q-factor	6.00	117.13	6.00
Max OSNR (dB)	21.91	70.55	33.51
NRZPG-LNF FSOC-SISO channel, $C_n^2 = 10^{-13}$ m$^{-2/3}$			
Attenuation (dB/km)	33.92 without EDFAs	33.92 with EDFAs	60.16 with EDFAs
Min BER	$1.000e-09$	0	$1.000e-09$
Max Q-factor	6.00	114.18	6.00
Max OSNR (dB)	26.90	70.46	37.12
GPG-LNF FSOC-SISO channel, $C_n^2 = 10^{-13}$ m$^{-2/3}$			
Attenuation (dB/km)	29.48 without EDFAs	29.48 with EDFAs	69.14 with EDFAs
Min BER	$1.000e-09$	0	$1.000e-09$
Max Q-factor	6.00	71.45	6.00
Max OSNR (dB)	25.00	76.38	41.14
HSPG-LNF FSOC-SISO channel, $C_n^2 = 10^{-13}$ m$^{-2/3}$			
Attenuation (dB/km)	29.24 without EDFAs	29.24 with EDFAs	67.64 with EDFAs
Min BER	$1.000e-09$	$5.94e-270$	$1.000e-09$
Max Q-factor	6.00	35.08	6.00
Max OSNR (dB)	21.75	70.67	35.51
RCPG-LNF FSOC-SISO channel, $C_n^2 = 10^{-13}$ m$^{-2/3}$			
Attenuation (dB/km)	34.23 without EDFAs	34.23 with EDFAs	67.26 with EDFAs
Min BER	$1.000e-09$	0	$1.000e-09$
Max Q-factor	6.00	107.096	6.00
Max OSNR (dB)	15.96	62.08	22.89

TABLE 8: Comparison in terms of the performances of min BER, max Q-factor, and max OSNR vs. attenuation coefficient (dB/km) using DOM for EPG formats under a G-G FSOC-SISO channel with $C_n^2 = 10^{-13}$ m$^{-2/3}$ and with and without the use of EDFAs.

RZPG-G-G FSOC-SISO channel, $C_n^2 = 10^{-13}$ m$^{-2/3}$			
Attenuation (dB/km)	33.12 without EDFAs	33.12 with EDFAs	65.5 with EDFAs
Min BER	$1.000e-9$	0	$1.000e-09$
Max Q-factor	6.00	69.90	6.00
Max OSNR (dB)	23.06	72.44	39.23
NRZPG-G-G FSOC-SISO channel, $C_n^2 = 10^{-13}$ m$^{-2/3}$			
Attenuation (dB/km)	33.39 without EDFAs	33.39 with EDFAs	61.13 with EDFAs
Min BER	$1.000e-09$	0	$1.000e-09$
Max Q-factor	5.973	70.54	6.00
Max OSNR (dB)	25.03	62.22	38.12
GPG-G-G FSOC-SISO channel, $C_n^2 = 10^{-13}$ m$^{-2/3}$			
Attenuation (dB/km)	27.12 without EDFAs	27.12 with EDFAs	65.43 with EDFAs
Min BER	$1.000e-09$	0	$1.000e-09$
Max Q-factor	6.00	58.45	6.00
Max OSNR (dB)	27.07	71.41	37.45
HSPG-G-G FSOC-SISO channel, $C_n^2 = 10^{-13}$ m$^{-2/3}$			
Attenuation (dB/km)	29.24 without EDFAs	29.24 with EDFAs	64.30 with EDFAs
Min BER	$1.000e-09$	$19.46e-207$	$1.000e-09$
Max Q-factor	6.00	30.64	6.00
Max OSNR (dB)	25.53	80.41	42.87
RCPG-G-G FSOC-SISO channel, $C_n^2 = 10^{-13}$ m$^{-2/3}$			
Attenuation (dB/km)	24.07 without EDFAs	24.07 with EDFAs	65.55 with EDFAs
Min BER	$1.000e-09$	0	$1.000e-09$
Max Q-factor	6.00	68.41	6.00
Max OSNR (dB)	19.09	68.73	26.24
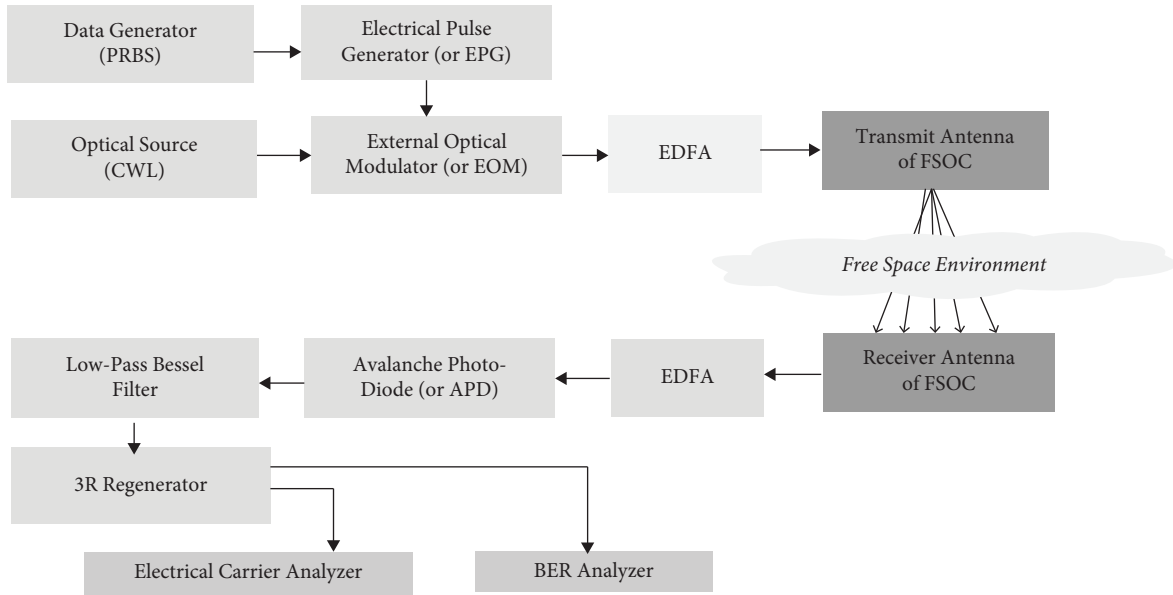
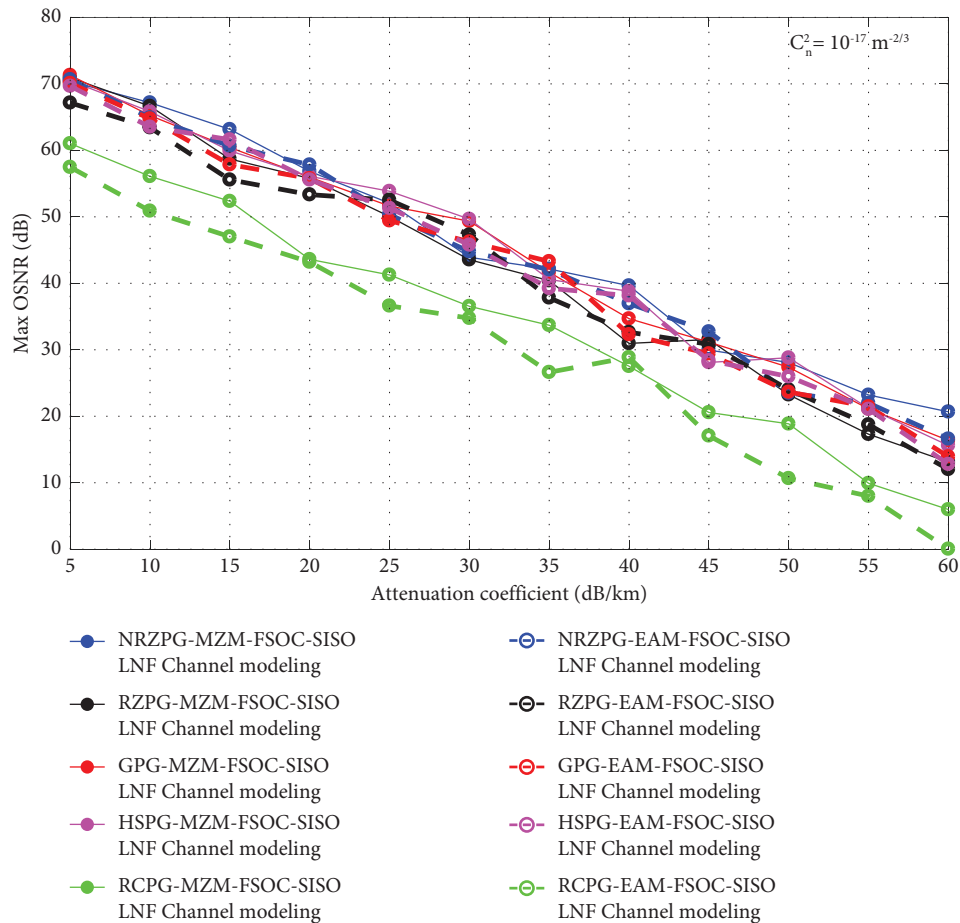FIGURE 28: Configuration of a simple high-speed P2P-OL under a FSOC-SISO channel using EOM without PE.

$C_n^2 = 10^{-17} \, m^{-2/3}$

- ●— NRZPG-MZM-FSOC-SISO
  LNF Channel modeling
- –◉– NRZPG-EAM-FSOC-SISO
  LNF Channel modeling
- ●— RZPG-MZM-FSOC-SISO
  LNF Channel modeling
- –◉– RZPG-EAM-FSOC-SISO
  LNF Channel modeling
- ●— GPG-MZM-FSOC-SISO
  LNF Channel modeling
- –◉– GPG-EAM-FSOC-SISO
  LNF Channel modeling
- ●— HSPG-MZM-FSOC-SISO
  LNF Channel modeling
- –◉– HSPG-EAM-FSOC-SISO
  LNF Channel modeling
- ●— RCPG-MZM-FSOC-SISO
  LNF Channel modeling
- –◉– RCPG-EAM-FSOC-SISO
  LNF Channel modeling

FIGURE 29: Max OSNR (dB) vs. attenuation coefficient (dB/km) with weak AT using EOM for EPG formats under various LNF FSOC-SISO channel states without PE.
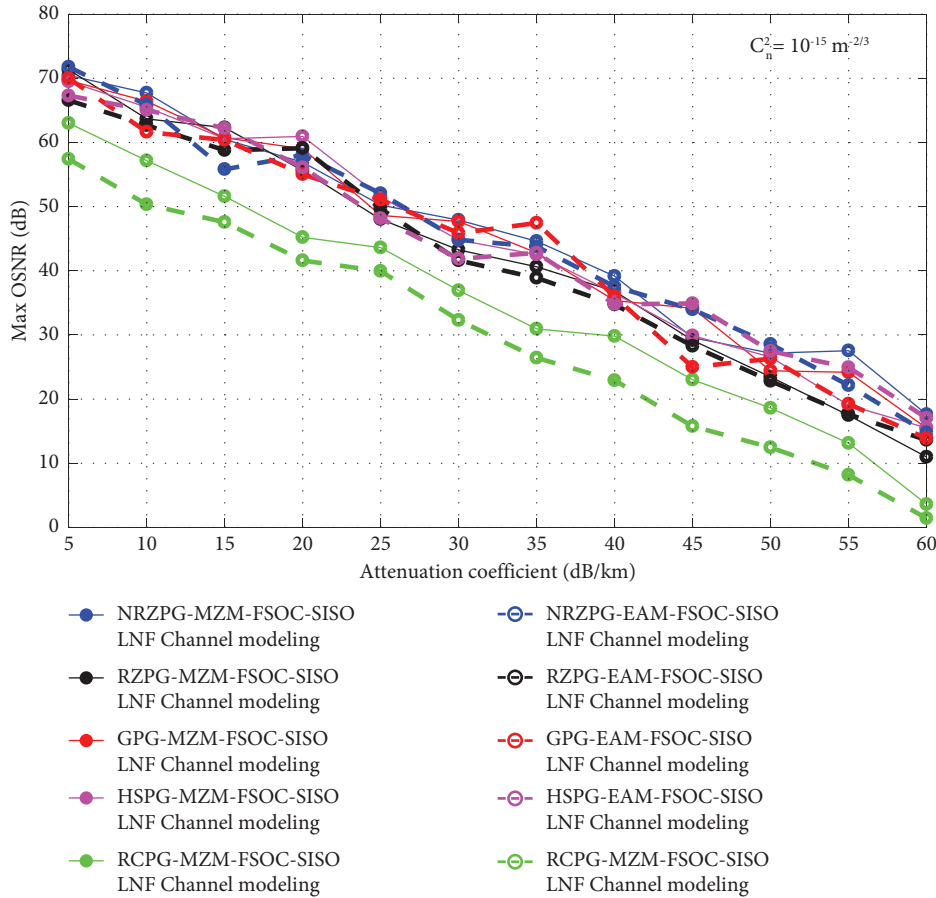
Figure 30: Max OSNR (dB) vs. attenuation coefficient (dB/km) with moderate AT using EOM for EPG formats under various LNF FSOC-SISO channel states without PE.

the range of attenuation values (5 dB/km to 32.32 dB/km), the simple high-speed P2P-OL under no FSOC-SISO channel modeling using DOM is in the optimal condition. On the other hand, beyond the 32.32 dB/km value, the system in Figure 5 is completely degraded. With the average acceptable attenuation value of the proposed FSOC-SISO channel (here, the channel is completely considered as an ideal which is not modeled) at 32.32 dB/km, the estimated average max OSNR value between the OTx antenna and ORx antenna under no FSOC-SISO channel modeling for the different EPG formats, namely, RZPG, NRZPG, GPG, HSPG, and RCPG, is equal to 22.24 dB.

However, if one wants to discuss how well the proposed system (see Figure 5) transmits data, one refers to the performances of the min BER and the max Q-factor. Figures 7 and 8 illustrate these performances. One can see that the min BER and the max Q-factor performances of the proposed system deteriorate when the attenuation coefficient of the FSOC-SISO channel (here, the channel is completely considered as an ideal which is not modeled) is increased. As an example, one can also observe that the quality of the setup (see Figure 5) always remains under optimal conditions within the range of attenuation values (5 dB/km to 32.32 dB/km). Considering the average acceptable attenuation value of the proposed FSOC-SISO channel (here, the channel is completely considered as an

ideal which is not modeled) which is 32.32 dB/km, the average min BER value is $1.000e - 09$ and the average max Q-factor value is 6 dB, and that is for the different EPG formats, namely, RZPG, NRZPG, GPG, HSPG, and RCPG.

In conclusion, one can record that when the EPG format, NRZPG type is employed, the simple high-speed P2P-OL under no FSOC-SISO channel modeling that is proposed in this subsection with DOM offers good performances compared to the other formats, namely, RZPG, GPG, HSGP, and RCGP. Table 3 summarizes the acceptable attenuation values for each EPG format in the order of highest priority.

However, the proposed system (see Figure 5) can be apparently more realistic when the FSOC-SISO channel is modeled in a more cluttered environment, whereby a log-normal fading (LNF) channel or gamma-gamma (G-G) channel is used here (see the previous sections). As an example, for the LNF channel, referring to the obtained results in Figures 9 to 17, one can observe that when the FSOC-SISO channel has exploited the log-normal fading (LNF) channel type with the change in index of refraction structure parameter (or IRSP), which is equal 10^{-17} m$^{-2/3}$ to 10^{-13} m$^{-2/3}$ (for the weak-to-strong turbulence regimes), the optimal conditions of the simple high-speed P2P-OL using DOM can obviously change and deteriorate a little bit.
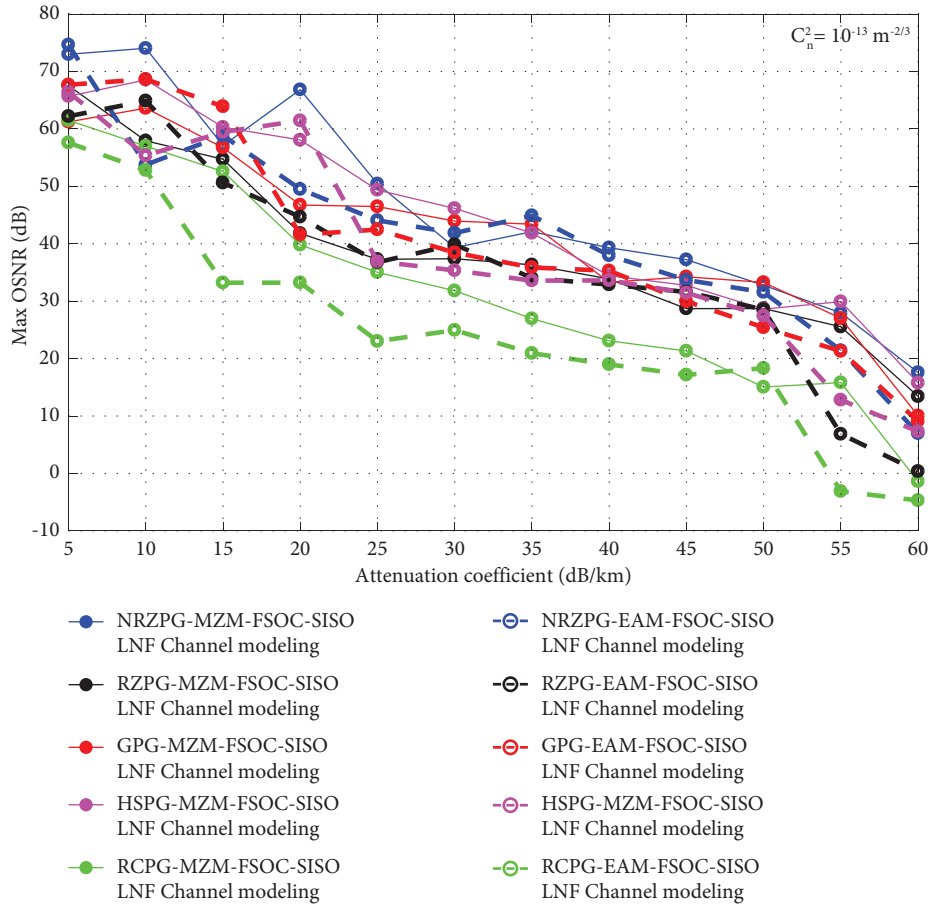
FIGURE 31: Max OSNR (dB) vs. attenuation coefficient (dB/km) with strong AT using EOM for EPG formats under various LNF FSOC-SISO channel states without PE.

Considering the obtained results in Figures 9 to 17, it is observed that the optimal conditions of the simple high-speed P2P-OL using DOM greatly decrease as AT gets stronger (it starts from the weak-to-strong turbulence regimes). It is also worth noting that the AT (when the IRSP is increased) incurs a greater loss with an attenuation coefficient at high values than at low values. For instance, one can find that within the range of attenuation values (5 dB/km to 31.00 dB/km), the performances of the suggested simple high-speed P2P-OL under a LNF FSOC-SISO channel (when the IRSP is equal to 10^{-13} $m^{-2/3}$) using DOM are in the optimal conditions. On the other side, beyond the 31.00 dB/km value, the proposed system in Figure 5 has totally deteriorated. With the average acceptable attenuation value of the recommended LNF FSOC-SISO channel with $C_n^2 = 10^{-13}$ $m^{-2/3}$ at 31.00 dB/km, the estimated average max OSNR value between the OTx antenna and ORx antenna of the LNF FSOC-SISO channel with $C_n^2 = 10^{-13}$ $m^{-2/3}$ for the different EPG formats, namely, RZPG, NRZPG, GPG, HSPG, and RCPG, is equal to 22.30 dB. Simultaneously, the average min BER value is equal to $1.000e - 09$ and the average max Q-factor value is equal to 6, and that is also true for the different EPG formats, namely, RZPG, NRZPG, GPG, HSPG, and RCPG.

In conclusion, one can record that when the RCPG format is used, the recommended simple high-speed P2P-OL under a LNF FSOC-SISO channel (when the IRSP is equal to 10^{-13} $m^{-2/3}$) employing DOM performs well compared to the other formats, namely, NRZPG, HSPG, GPG, and RZPG. Table 4 recapitulates the acceptable attenuation values for each EPG format in the order of highest priority.

On the flip side, for the G-G FSOC-SISO channel, referring to the obtained results in Figures 18 to 26, one can also observe that when the FSOC-SISO channel has exploited the gamma-gamma (or G-G) channel type with the change in the index of refraction structure parameter (or IRSP), which is equal to 10^{-17} $m^{-2/3}$ to 10^{-13} $m^{-2/3}$ (for the weak-to-strong turbulence regimes), the optimal conditions of the simple high-speed P2P-OL using DOM can obviously change and deteriorate a little bit more than when the LNF channel is exploited. For instance, one can find that within the range of attenuation values (5 dB/km to 29.39 dB/km), the performances of the proposed simple high-speed P2P-OL under a G-G FSOC-SISO channel (when the IRSP is equal to 10^{-13} $m^{-2/3}$) using DOM in the optimal conditions. On the other side, beyond the 29.39 dB/km value, the system in Figure 5 has totally deteriorated. With the average acceptable attenuation value of the
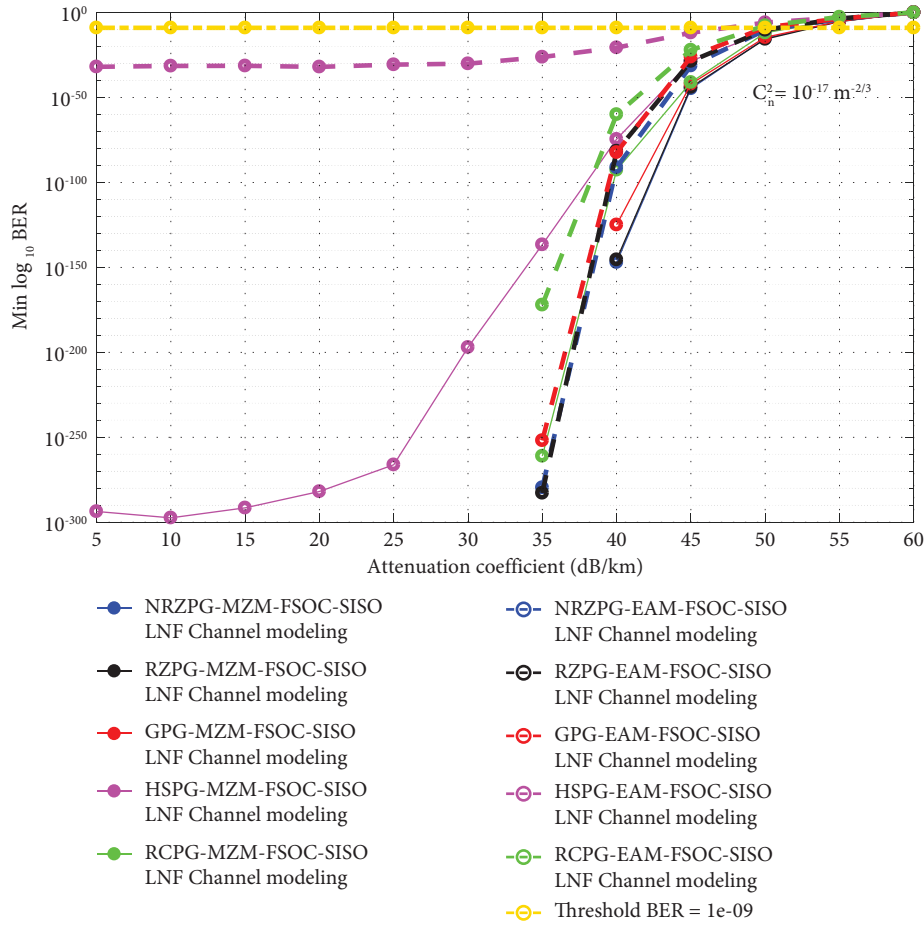
FIGURE 32: Min BER vs. attenuation coefficient (dB/km) with weak AT using EOM for EPG formats under various LNF FSOC-SISO channel states without PE.

recommended G-G FSOC-SISO channel with $C_n^2 = 10^{-13}$ $m^{-2/3}$ at 29.39 dB/km, the estimated average max OSNR value between the OTx antenna and ORx antenna of the G-G FSOC-SISO channel with $C_n^2 = 10^{-13}$ $m^{-2/3}$ for the different EPG formats, namely, RZPG, NRZPG, GPG, HSPG, and RCPG, is equal to 23.96 dB. Simultaneously, the average min BER value is equal to $1.000e - 09$ and the average max Q-factor value is equal to 6, and that is also for the different EPG formats, namely, RZPG, NRZPG, GPG, HSPG, and RCPG.

In conclusion, one can record that when the NRZPG format is used, the proposed simple high-speed P2P-OL under a G-G FSOC-SISO channel (when the IRSP is equal to 10^{-13} $m^{-2/3}$) employing DOM performs well compared to the other formats, namely, RZPG, HSPG, RCPG, and GPG. Table 5 recapitulates the acceptable attenuation values for each EPG format in the order of highest priority.

During the optical signal propagation under a FSOC-SISO channel, its attenuation poses a major challenge in the context of high-speed OTWNs owing to the metrological conditions. Consequently, we proposed to add an EDFA, in upstream (gain: 16 dB, and noise figure: 6 dB) and downstream (gain: 32 dB, and noise figure: 4.5 dB) of the FSOC-SISO channel that

is shown in Figure 5. For more details, the new configuration is depicted in Figure 27 [54–58].

As communication throughput increases, great importance is attached to optical amplifiers such as EDFAs (erbium-doped fiber amplifiers) which can directly amplify optical signals with no conversion to electrical signals and have been largely deployed in conventional OTWNs. The EDFA amplifier allows us to apply it as a booster and preamplifier in the proposed system (see Figure 27). The EDFAs are the most commonly applied amplifiers due to their many advantages, such as their low noise level, very low connection losses to other opto-electronic components, low sensitivity to light polarization, and very low saturation power. This successful amplification technology is applied to a next-generation solution for amplifying free space laser communication signals for FSOC networks. The optical amplifiers are principally evaluated by power gain and noise figure. The output gain measures the ratio between the output power P_{out} and the input power P_{in} injected into the amplifier; it is expressed in dB and defined by [54–58]:

$$G_{[\text{dB}]} = 10 \cdot \log\left(\frac{P_{\text{out}}}{P_{\text{in}}}\right). \tag{29}$$
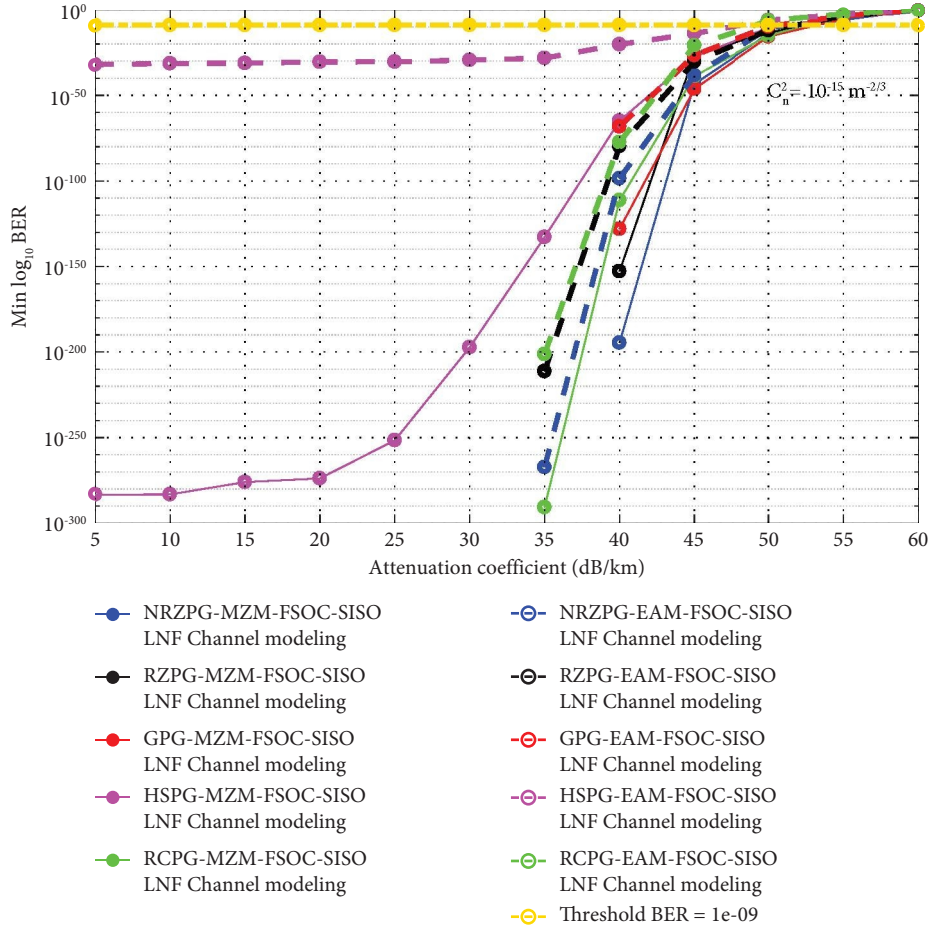
FIGURE 33: Min BER vs. attenuation coefficient (dB/km) with moderate AT using EOM for EPG formats under various LNF FSOC-SISO channel states without PE.

However, the amplified spontaneous emission (or ASE) noise which is generated through the amplification process gets mixed into the signal, resulting in a lower optical signal-to-noise ratio (or OSNR) at the amplifier's output.

The reduction ratio OSNR from the input to the output at the amplifier is set as the noise figure (or NF). It is expressed by

$$NF = \frac{SNR_{in}}{SNR_{out}}, \tag{30}$$

where $OSNR_{in}$ is the optical signal-to-noise ratio when no amplifier is present, and $OSNR_{out}$ is the optical signal-to-noise ratio expressed higher. An EDFA's noise figure changes linearly with the ASE power and vice versa with the amplifier's gain; hence, the NF of an EDFA may be reduced to a minimum level by increasing the gain [54–58].

When both the proposed configurations in terms of optical amplification have been applied, the performances of the system (see Figure 27) in terms of min BER, max Q-factor, and max OSNR are improved. This finding has been successfully observed for all the employed EPG formats. As an example, with the average acceptable attenuation value of the proposed FSOC-SISO channel of 32.32 dB/km (here, the

channel is completely considered as an ideal which is not modeled) which has been estimated with the previous system (see Figure 5); the system using the EDFAs (see Figure 27) gives the following results: the average min BER value is equal to $9.17e - 312$, the average max Q-factor value is equal to 83.52, and the estimated average max OSNR value between OTx and ORx is equal to 61.72 dB. On the other hand, when the proposed system in Figure 27 uses the LNF FSOC-SISO channel with $C_n^2 = 10^{-13}$ m$^{-2/3}$ at 31.00 dB/km (this value is estimated in the previous system without using the EDFAs), the estimated average max OSNR value between OTx and ORx is equal to 70.028 dB, the average min BER value is equal to $1.18e - 270$, and the average max Q-factor value is equal to 88.98. Thus, despite the AT getting strong under the LNF FSOC-SISO channel with $C_n^2 = 10^{-13}$ m$^{-2/3}$, except that the performances of the previous system in Figure 5 using the EDFAs (see Figure 27) are improved, this finding has been also successfully observed for all the employed EPG formats. In addition, when the G-G FSOC-SISO channel is used with $C_n^2 = 10^{-13}$ m$^{-2/3}$ at 29.39 dB/km (this value is estimated in the previous system without using the EDFAs) for the proposed system in Figure 27, the estimated average max OSNR value between OTx and ORx is equal to 71.04 dB, the average min BER
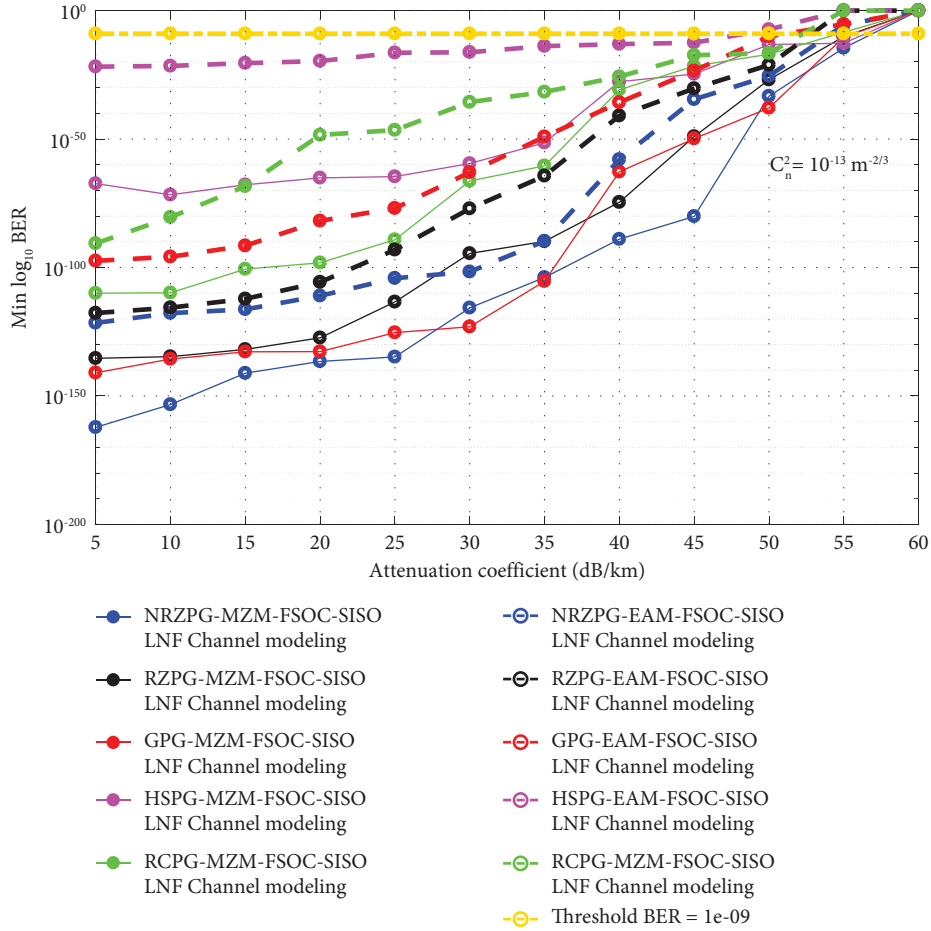
FIGURE 34: Min BER vs. attenuation coefficient (dB/km) with strong AT using EOM for EPG formats under various a LNF FSOC-SISO channel states without PE.

value is equal to $3.89e-207$, and the average max Q-factor value is equal to 59.60.

Furthermore, as an observational measure, it was found that the system in Figure 27 can achieve acceptable performance in terms of max OSNR, min BER, and max Q-factor when the average attenuation value is equal to 68.82 dB/km under no FSOC-SISO channel modeling. Conversely, for the system in Figure 27 under a LNF FSOC-SISO channel with $C_n^2 = 10^{-13}$ $m^{-2/3}$, it was found that the acceptable performance in terms of maxOSNR, min BER, and max Q-factor are achieved when the average attenuation value is equal to 66.60 dB/km. On the other hand, when the system in Figure 27 is under a G-G FSOC-SISO channel with $C_n^2 = 10^{-13}$ $m^{-2/3}$, it was found that the acceptable performances in terms of max OSNR, min BER, and max Q-factor are reached for the average attenuation value is equal to 64.38 dB/km. Finally, it has been noted that the best EPG format applied in the setup associated with the optical amplification (see Figure 27) under no FSOC-SISO channel modeling or under a LNF FSOC-SISO channel, or else, a G-G FSOC-SISO channel, with $C_n^2 = 10^{-13}$ $m^{-2/3}$ is RZPG format, and after that, the other formats are in the order RCPG, GPG, HSPG, and NRZPG (see Tables 6–8).

6.1.2. External Optical Modulation with All EPG Formats.
In this subsection, we analyze the performances of the proposed setup in Figure 28 using an external optical modulation (or EOM), such as a Mach-Zehnder modulator (or MZM) and an electro-absorption modulator (or EAM), where we have selected all EPG formats, which have been reviewed and evaluated in the previous case. In addition, the parameters of the OTx, ORx, and FSOC-SISO channel sections of the new design remain (see Figure 28) the same as before, with the exception that there will be a change in the optical modulation type, see Figures 27 and 28.

However, in the present study, Figures 29 to 46 present a comparison between two EOMs (MZM and EAM) in terms of the performance of maxOSNR, min BER, and max Q-factor, respectively, when all EPG formats are employed under a LNF FSOC-SISO channel modeling or, under a G-G FSOC-SISO channel. Depending on the obtained results in Figures 29 to 46, one can generally see that the performance of the setup in Figure 28 are robust when the EOM, MZM type is applied under a LNF FSOC-SISO channel modeling or under a G-G FSOC-SISO channel, especially when the NRZPG format is realized. This remark is concluded for the average attenuation values between 5 dB/km to 54.15 dB/km. Despite that, the associated EOM, EAM type with the
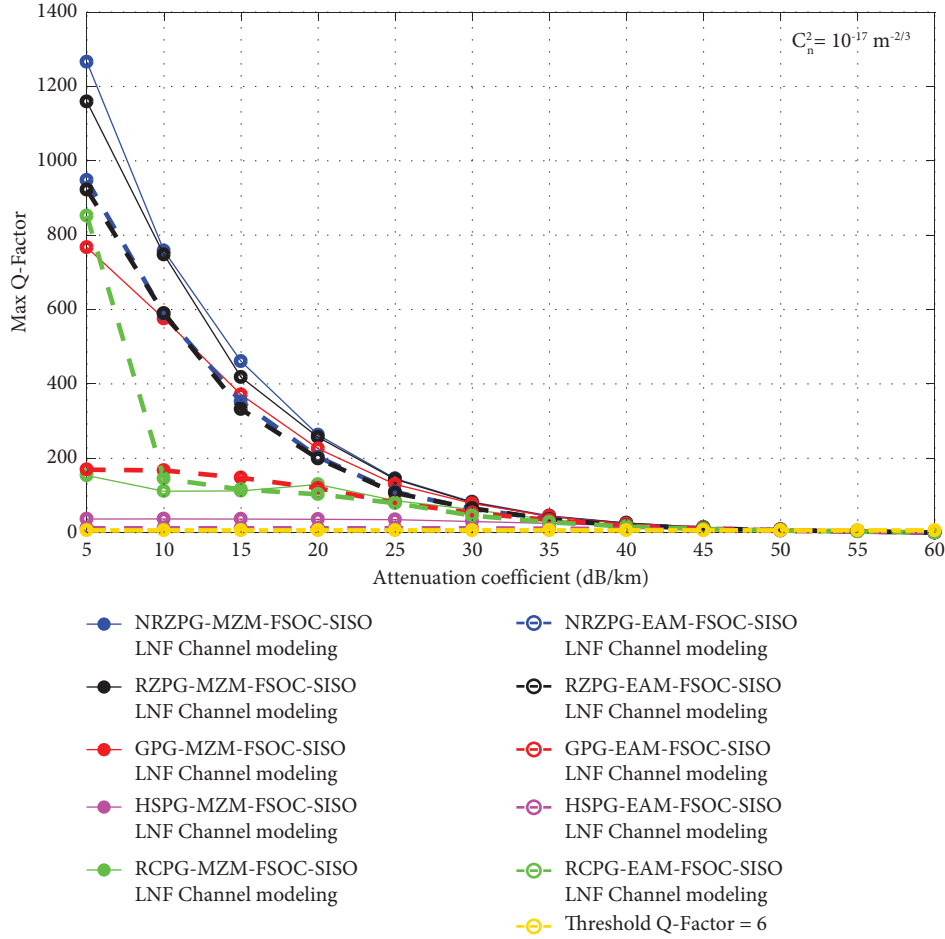
FIGURE 35: Max Q-factor vs. attenuation coefficient (dB/km) with weak AT using EOM for EPG formats under various LNF FSOC-SISO channel states without PE.

NRZPG format under a LNF FSOC-SISO channel modeling or under a G-G FSOC-SISO channel, also gives better performance for the proposed setup in Figure 28. On the other hand, despite the AT getting strong under a G-G FSOC-SISO channel with $C_n^2 = 10^{-13}$ m$^{-2/3}$, except that the associated EOM, MZM type with the NRZPG format under this channel type gives the better performances compared to the other configurations (see Figures 29 to 46). This remark is concluded for the attenuation values between 5 dB/km and 55.13 dB/km. Last remark is that, the lowest level performances of the proposed setup in Figure 28 are obtained with the associated EOM, EAM type with the HSPG format under a G-G FSOC-SISO channel with $C_n^2 = 10^{-13}$ m$^{-2/3}$ (see Figures 29 to 46); this remark is estimated for the attenuation values between 5 dB/km and 32.69 dB/km. As an example, for an attenuation value of 32.69 dB/km obtained at the lowest level performance when the EAM is associated with HSPG, we have summarized in Table 9 some results around the attenuation value of 32.69 dB/km for judging the performances of the proposed setup (see Figure 28) in terms of max OSNR, min BER, and max Q-factor for all proposed configurations. The max OSNR, min BER, and max Q-factor performances in Table 9 are significantly higher than the acceptable performance levels. So, we must

still try to estimate the acceptable performance levels for the setup in Figure 28. Table 10 summarizes some of the obtained results of the estimated attenuation values for the acceptable performance levels, in the order of highest priority.

6.2. Performance Improvement of the Simple High-Speed P2P-OL under a FSOC-SISO Channel

6.2.1. High-Speed P2P-OL under a FSOC-MIMO Channel Using NRZPG-MZM without Pointing Errors. Regarding the achieved results in the previous subsections, the setup in Figure 28 suffers some limitations related to the performances of min BER, max Q-factor, and max OSNR as the attenuation values increase. Consequently, to surmount these limitations, we will multiplicate the number of OTx and ORx antennas under a FSOC channel, as illustrated in Figure 47, especially when the channel is modeled as a G-G distribution with $C_n^2 = 10^{-13}$ m$^{-2/3}$. In this subsection, we will compare the performances of a P2P-OL under a FSOC-2×2 channel using NRZPG-MZM with the proposed setup in Figure 28 (when the FSOC-1×1 channel is used, either under a LNF FSOC-SISO channel modeling or under a G-G
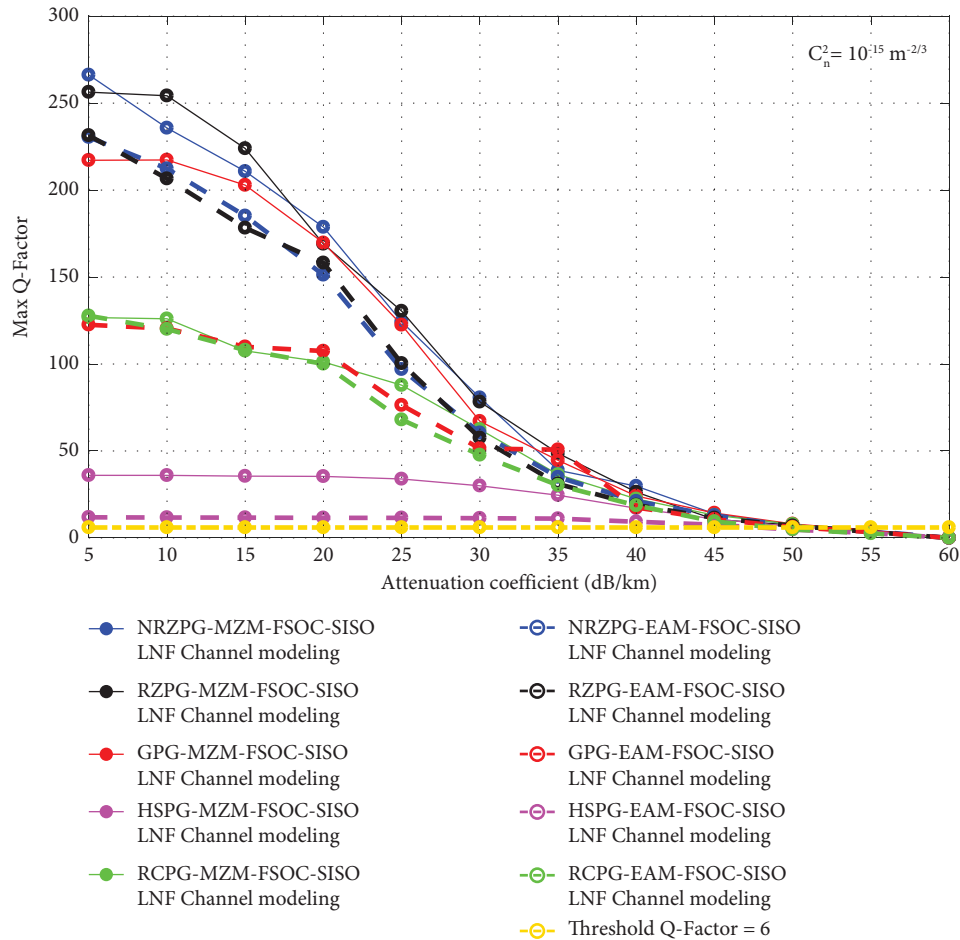
FIGURE 36: Max Q-factor vs. attenuation coefficient (dB/km) with moderate AT: using EOM for EPG formats under various LNF FSOC-SISO channel states without PE.

FSOC-SISO channel with $C_n^2 = 10^{-13}$ m$^{-2/3}$). This is done using the same configuration as in Figure 28 with the same FSOC-SISO (or FSOC-1×1) channel parameters but increasing the number of OTx and ORx antennas over the FSOC-MIMO channel to 2×2 (or FSOC-2×2). To evaluate the performance of the proposed configuration (see Figure 47), the attenuation coefficient variation is within this range (55.12 dB/km to 60 dB/km) with a step size of 0.976 dB/km. This variation corresponds to the critical situation part when the EOM, MZM type associated with the NRZPG format, is used in the proposed system (see Figure 28).

The obtained results in Figures 48–50 clearly illustrate that the P2P-OL under a FSOC-2×2 channel (for LNF channel modeling or for G-G channel modeling, with $C_n^2 = 10^{-13}$ m$^{-2/3}$.) has better performances than the P2P-OL under a FSOC-1×1 channel (for LNF channel modeling or for G-G channel modeling, with $C_n^2 = 10^{-13}$ m$^{-2/3}$). However, one can note that when two antennas are used for transmitting and receiving over a FSOC-MIMO channel, the max Q-factor and max OSNR have increased, and the min BER has decreased, although the beam-forming gain of the FSOC-2×2 channel (for LNF channel modeling or for G-G channel modeling, with

$C_n^2 = 10^{-13}$ m$^{-2/3}$.) is low. The beam forming gain of the FSOC-2×2 channel (for LNF channel modeling or for G-G channel modeling, with $C_n^2 = 10^{-13}$ m$^{-2/3}$) in this case is equal to 4. As an example, for the attenuation of 55.12 dB/km under a G-G FSOC-1×1 channel modeling with $C_n^2 = 10^{-13}$ m$^{-2/3}$, the min BER is equal to 1.00e-09, the max OSNR is equal to 22.51 dB and the max Q-factor is about 6. On the other side, at the same attenuation value under a G-G FSOC-2×2 channel modeling with $C_n^2 = 10^{-13}$ m$^{-2/3}$, the min BER is equal to $5.24e - 15$, the max OSNR is equal to 27.16 dB, and the max Q-factor is about 7.66. As another example, when the setup in Figure 28 is under a FSOC-MIMO channel modeling, it is possible to obtain some other performances: for the attenuation of 55.12 dB/km under a LNF FSOC-1×1 channel modeling with $C_n^2 = 10^{-13}$ m$^{-2/3}$, the min BER is equal to $6.13e - 15$, the max OSNR is equal to 27.72 dB, and the max Q-factor is about 7.65. On a side note, at the same attenuation value under LNF FSOC-2×2 channel modeling with $C_n^2 = 10^{-13}$ m$^{-2/3}$, the min BER is equal to 1.37e-30, the max OSNR is equal to 29.30 dB, and the max Q-factor is about 11.38.

Alternatively, since the attenuation value of 55.12 dB/km under a G-G FSOC-2×2 channel modeling with $C_n^2 = 10^{-13}$
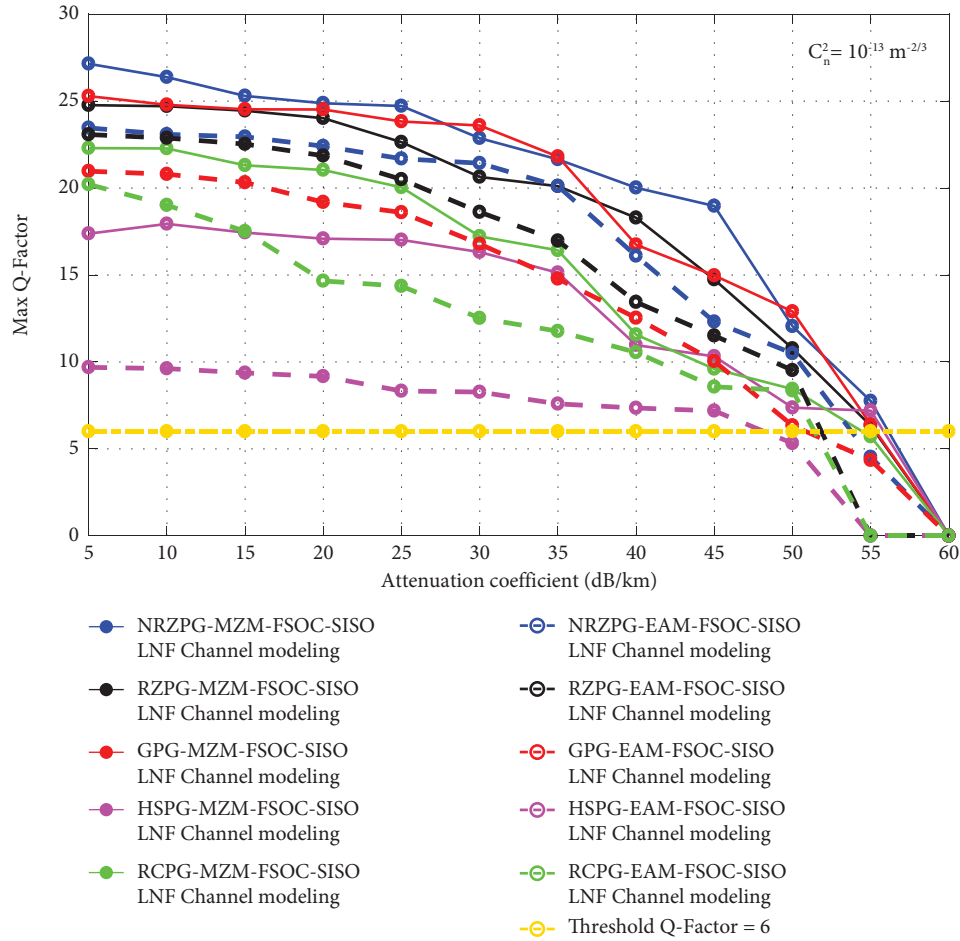
FIGURE 37: Max Q-factor vs. attenuation coefficient (dB/km) with strong AT using EOM for EPG formats under various LNF FSOC-SISO channel states, without PE.

$m^{-2/3}$ has substantial performance compared to the acceptable performance levels under a G-G FSOC-1×1 channel modeling with $C_n^2 = 10^{-13}$ $m^{-2/3}$ (at the attenuation value of 55.12 dB/km, max OSNR = 22.51 dB, min BER = $1.000e - 09$ and max Q-factor = 6), in this case, one has the opportunity to obtain the new attenuation value under a G-G FSOC-2×2 channel modeling with $C_n^2 = 10^{-13}$ $m^{-2/3}$, which has been estimated for previously acceptable performance levels that were chosen (i.e., Q-factor ≈ 6 and BER $\leq 1.00e - 09$).

For this purpose, it is again necessary to vary and increase the attenuation value from 55.12 dB/km until the new value is estimated. From the summarized results in Table 11, the attenuation value under G-G FSOC-2×2 channel modeling with $C_n^2 = 10^{-13}$ $m^{-2/3}$ which is estimated for the acceptable performance levels is equal to 56.5 dB/km.

One final note in this subsection is that, since the same attenuation value of 55.12 dB/km under LNF FSOC-2×2 channel modeling with $C_n^2 = 10^{-13}$ $m^{-2/3}$ has also substantial performances compared to the acceptable performance levels under a LNF FSOC-1×1 channel modeling with $C_n^2 = 10^{-13}$ $m^{-2/3}$ (at the attenuation value of 56.90 dB/km, max OSNR = 24.02 dB, min BER = $1.000e - 09$ and max Q-

factor = 6), in this case, one has the opportunity to obtain the new attenuation value under a LNF FSOC-2×2 channel modeling with $C_n^2 = 10^{-13}$ $m^{-2/3}$ which has been estimated for previously acceptable performance levels that were chosen (i.e. Q-factor ≈ 6 and BER $\leq 1.00e - 09$). For this purpose, it is again necessary to vary and increase the attenuation value from 55.12 dB/km until the new value is estimated. From the summarized results in Table 12, the attenuation value under a LNF FSOC-2×2 channel modeling with $C_n^2 = 10^{-13}$ $m^{-2/3}$ which is estimated for the acceptable performance levels is equal to 57.60 dB/km.

6.2.2. Effect of Beam Forming Gain over a FSOC-MIMO Channel.

The beam forming gain over a FSOC-MIMO channel is the multiplication between the number of OTx and ORx antennas. To clarify, the beam forming gain over a FSOC-2×2 channel is equal to 4. Consequently, based on what the previous subsection has demonstrated, if the beam forming gain over a FSOC-MIMO channel (for LNF channel modeling or for G-G channel modeling, with $C_n^2 = 10^{-13}$ $m^{-2/3}$) is set to 4 (i.e., FSOC-2×2 channel), the performances of a P2P-OL under a FSOC-MIMO channel (for LNF channel modeling or for G-G channel modeling,
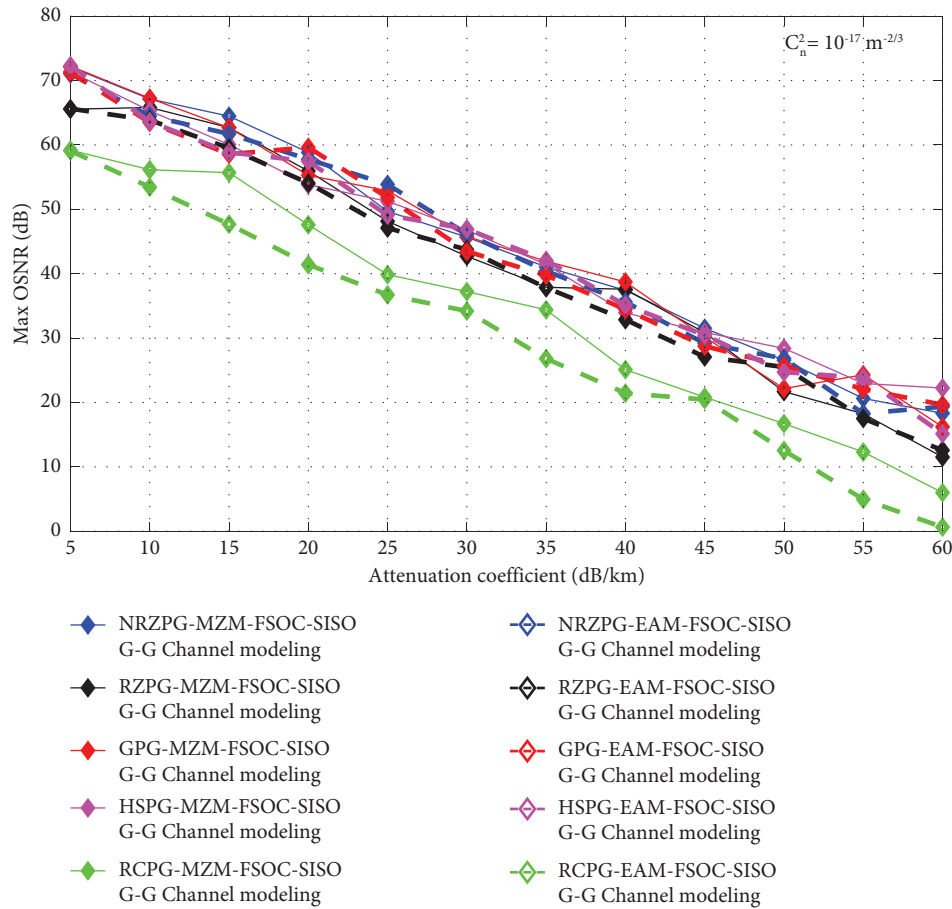
FIGURE 38: Max OSNR (dB) vs. attenuation coefficient (dB/km) with weak AT: using EOM for EPG formats under various G-G FSOC-SISO channel states without PE.

with $C_n^2 = 10^{-13}$ m$^{-2/3}$) can improve. So, this observation has motivated us to vary the beam forming gain over a FSOC-MIMO channel (for LNF channel modeling or for G-G channel modeling, with $C_n^2 = 10^{-13}$ m$^{-2/3}$) and see its influence on the performances of the proposed setup (see Figure 47). For this purpose, we keep the same parameters of the proposed setup in Figure 47 with an attenuation value of 56.5 dB/km, which corresponds to the evaluated attenuation value under G-G FSOC-2 × 2 channel modeling with $C_n^2 = 10^{-13}$ m$^{-2/3}$ for the acceptable performance levels, as shown in Table 13. However, the obtained new results for the setup performances in Figure 16 based on the beam forming gain number variation under a G-G FSOC-MIMO channel modeling with $C_n^2 = 10^{-13}$ m$^{-2/3}$ are shown in Table 11. In addition, for the obtained new results by the proposed setup in Figure 47 under a LNF FSOC-MIMO channel with $C_n^2 = 10^{-13}$ m$^{-2/3}$, the attenuation value of 57.60 dB/km, which corresponds to the evaluated attenuation value under LNF FSOC-2 × 2 channel modeling with $C_n^2 = 10^{-13}$ m$^{-2/3}$ for the acceptable performance levels, is displayed in Table 14.

After analyzing the results in Tables 13 and 14, one can notice that the P2P-OL under a FSOC-MIMO channel (for LNF channel modeling or for G-G channel modeling, with $C_n^2 = 10^{-13}$ m$^{-2/3}$) is more efficient when the beam forming

gain over a FSOC-MIMO channel (for LNF channel modeling or for G-G channel modeling, with $C_n^2 = 10^{-13}$ m$^{-2/3}$) increases and vice versa. For example, when the G-G FSOC-9 × 9 channel modeling with $C_n^2 = 10^{-13}$ m$^{-2/3}$ is exploited, the min BER is reduced to the value of $35.38e - 39$ and, consequently, the max Q-factor is increased to the value of 12.82, as well as the max OSNR is raised to the value of 30.22 dB. Another example of this is when the LNF FSOC-9 × 9 channel with $C_n^2 = 10^{-13}$ m$^{-2/3}$ is exploited, the min BER is reduced to the value of $1.43e - 36$ and, consequently, the max Q-factor is increased to the value of 12.53, as well as the max OSNR is raised to the value of 30.49 dB. In addition, the eye diagrams in Figures 51 to 58 also illustrate the robustness of the increased beam forming gain technique over a FSOC-MIMO channel (for LNF channel modeling or for G-G channel modeling, with $C_n^2 = 10^{-13}$ m$^{-2/3}$). It is evident that the most open-eye diagram is the FSOC-9 × 9 channel (i.e., 9-OTx antennas and 9-ORx antennas under a LNF channel modeling or under a G-G channel modeling, with $C_n^2 = 10^{-13}$ m$^{-2/3}$. Furthermore, as long as the attenuation coefficient value of 56.5 dB/km under a G-G FSOC-9 × 9 channel modeling with $C_n^2 = 10^{-13}$ m$^{-2/3}$ has appreciable performances compared to the acceptable performance levels under an G-G FSOC-1 × 1 channel modeling with $C_n^2 = 10^{-13}$ m$^{-2/3}$ (at the attenuation value of 55.12 dB/km,
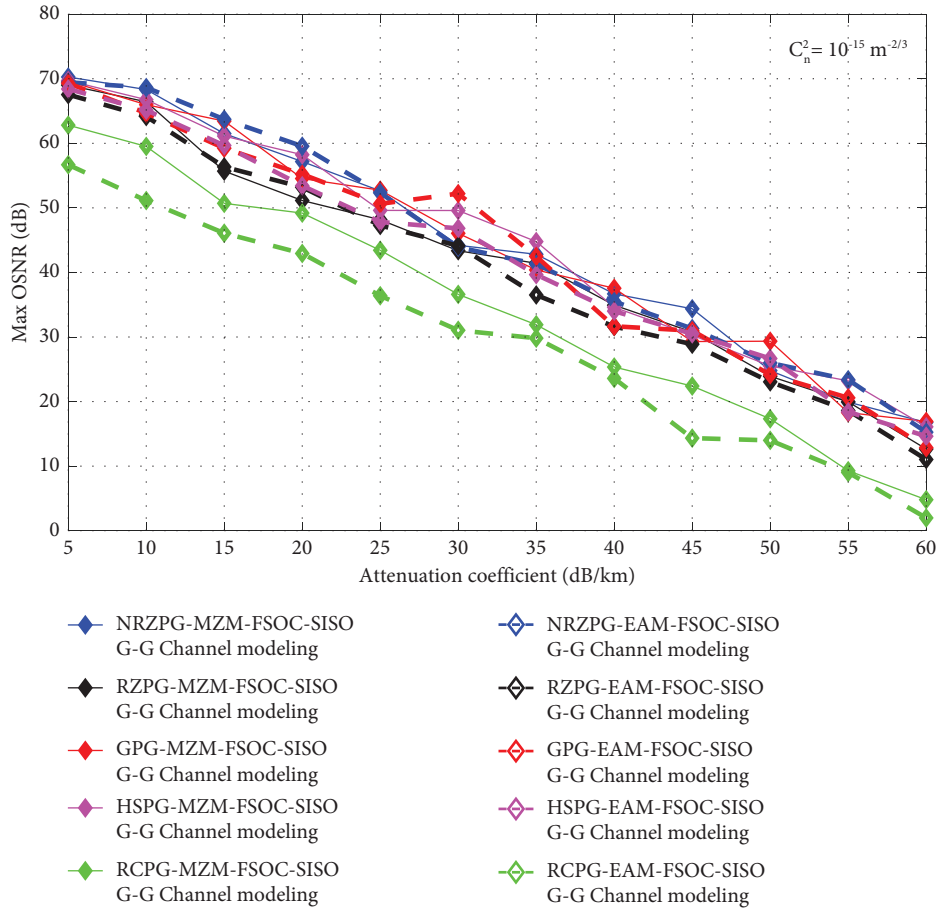
FIGURE 39: Max OSNR (dB) vs. attenuation coefficient (dB/km) with moderate AT using EOM for EPG formats under various G-G FSOC-SISO channel states without PE.

max OSNR = 22.51 dB, min BER = 1.000$e-09$ and max Q-factor = 6), the new estimated attenuation coefficient value after a few variations under a G-G FSOC-9 × 9 channel modeling with $C_n^2 = 10^{-13}$ m$^{-2/3}$ for the acceptable performance levels (i.e. max OSNR = 23.03 dB, min BER = 1.000$e-09$ and max Q-factor = 6) is therefore, equal to 61.45 dB/km. Last remark: as long as the attenuation coefficient value of 57.6 dB/km under a LNF FSOC-9 × 9 channel with $C_n^2 = 10^{-13}$ m$^{-2/3}$ has also appreciable performances compared to the acceptable performance levels under a LNF FSOC-1 × 1 channel modeling with $C_n^2 = 10^{-13}$ m$^{-2/3}$ (at the attenuation value of 56.9 dB/km, max OSNR = 24.02 dB, min BER = 1.000$e-09$ and max Q-factor = 6), the new estimated attenuation coefficient value after a few variations under a LNF FSOC-9 × 9 channel modeling with $C_n^2 = 10^{-13}$ m$^{-2/3}$ for the acceptable performance levels (i.e. max OSNR = 25.42 dB, min BER = 1.000$e-09$ and max Q-factor = 6) is therefore, equal to 62.60 dB/km.

In conclusion, we can say that there is a MIMO technique between the techniques that exist to solve the attenuation problem under the FSOC channel (for LNF channel modeling or for G-G channel modeling, with $C_n^2 = 10^{-13}$ m$^{-2/3}$). Despite its robustness, this technique is related to energy consumption. In fact, the higher the beam forming gain, the more energy is consumed by the OTx and ORx antennas of the FSOC-MIMO channel (for LNF channel modeling or for G-G channel modeling, with $C_n^2 = 10^{-13}$ m$^{-2/3}$).

6.2.3. High-Speed P2P-OL under a FSOC-9 × 9 Channel Using NRZPG-MZM with TAPEA.
Interfacing FSOC-MIMO communication is one of the revolutionary techniques that may be used to transmit the date at high speed. Nevertheless, the spatial turbulence such as transmitting pointing errors (TPE) plays an extensive role when designing the interfacing FSOC-MIMO communication systems. For this reason, we incorporate the transmitter azimuth pointing error angle (TAPEA) on the proposed previous system (see Figure 47) under a FSOC-9 × 9 channel using NRZPG-MZM and use that to determine other additional performances. For evaluating the performances of the proposed configuration (see Figure 47) with TAPEA, the variation of the attenuation coefficient in this range (50 dB/km to 65 dB/km) with a step of 2.5 dB/km is used, and it corresponds to the totality of the performances that have been analyzed in both subsections 6.2.1 and 6.2.2. However, in the present study, Figures 59 to 61 present the performances of max OSNR, min BER, and max Q-factor, as the
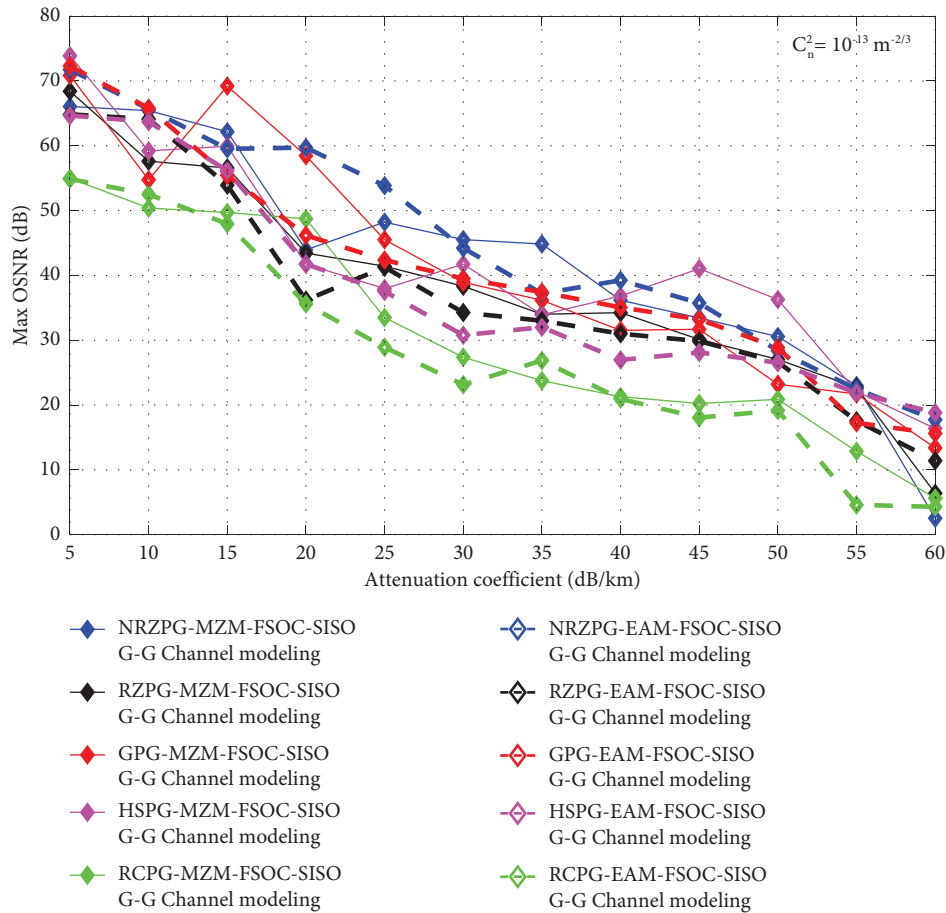
FIGURE 40: Max OSNR (dB) vs. attenuation coefficient (dB/km) with strong AT using EOM for EPG formats under various a G-G FSOC-SISO channel states without PE.

attenuation values increase from 50 dB/km to 65 dB/km and when one varies the TAPEA with the following constants: 0, 1, 3 and 5 μrad.

With respect to TAPEA, it is apparent from Figures 59 to 61 that the proposed system performance may degrade as the TAPEA value increases and vice versa. As an example, when the TAPEA value is equal to 0 μrad, the estimated attenuation coefficient value after a few variations under a G-G FSOC-9 × 9 channel modeling with $C_n^2 = 10^{-13}$ $m^{-2/3}$ for the acceptable performance levels (i.e., max OSNR = 23.03 dB, min BER = $1.000e-09$ and max Q-factor = 6) is therefore, equal to 61.45 dB/km. However, the TAPEA value is equal to 5 μrad, the new estimated attenuation coefficient value after a few variations under a G-G FSOC-9 × 9 channel modeling with $C_n^2 = 10^{-13}$ $m^{-2/3}$ for the acceptable performance levels (i.e., max OSNR = 24.67 dB, min BER = 1.000e-09, and max Q-factor = 6) is so equal to 58.55 dB/km. Similar is the case for the LNF FSOC-9 × 9 channel modeling with $C_n^2 = 10^{-13}$ $m^{-2/3}$. As an example, when the TAPEA value is equal to 0 μrad, the estimated attenuation coefficient value after a few variations under a LNF FSOC-9 × 9 channel modeling with $C_n^2 = 10^{-13}$ $m^{-2/3}$ for the acceptable performance levels (i.e., max OSNR = 25.42 dB, min BER = $1.000e-09$ and max Q-factor = 6) is therefore, equal to 62.60 dB/km. Whereas the

TAPEA value is equal to 5 μrad, the new estimated attenuation coefficient value after a few variations under LNF FSOC-9 × 9 channel modeling with $C_n^2 = 10^{-13}$ $m^{-2/3}$ for the acceptable performance levels (i.e., max OSNR = 24.9 dB, min BER = $1.000e-09$, and max Q-factor = 6) is so equal to 59.66 dB/km.

In conclusion, it is demonstrated that the proposed system under a FSOC-9 × 9 channel using NRZPG-MZM (for LNF channel modeling or for G-G channel modeling, with $C_n^2 = 10^{-13}$ $m^{-2/3}$) is more affected by the TAPEA when increased.

6.2.4. *High-Speed WDM-P2P-OL under a FSOC-9 × 9 Channel Using NRZPG-MZM with TAPEA.* In recent times, there has been a growing interest in the advanced bandwidth technologies for improving the bandwidth capacity for the future FSOC links. One of these technology types is WDM, which incorporates data from multiple sources into a single optical link while transporting its signals at different wavelengths. In a nutshell, WDM technology can enhance the bandwidth capacity of the suggested system in Figure 47. In this subsection, the proposed system (see Figure 62) includes 16 channels each of which has a variable bit rate from 5 Gbps to 10 Gbps, NRZPG-encoded
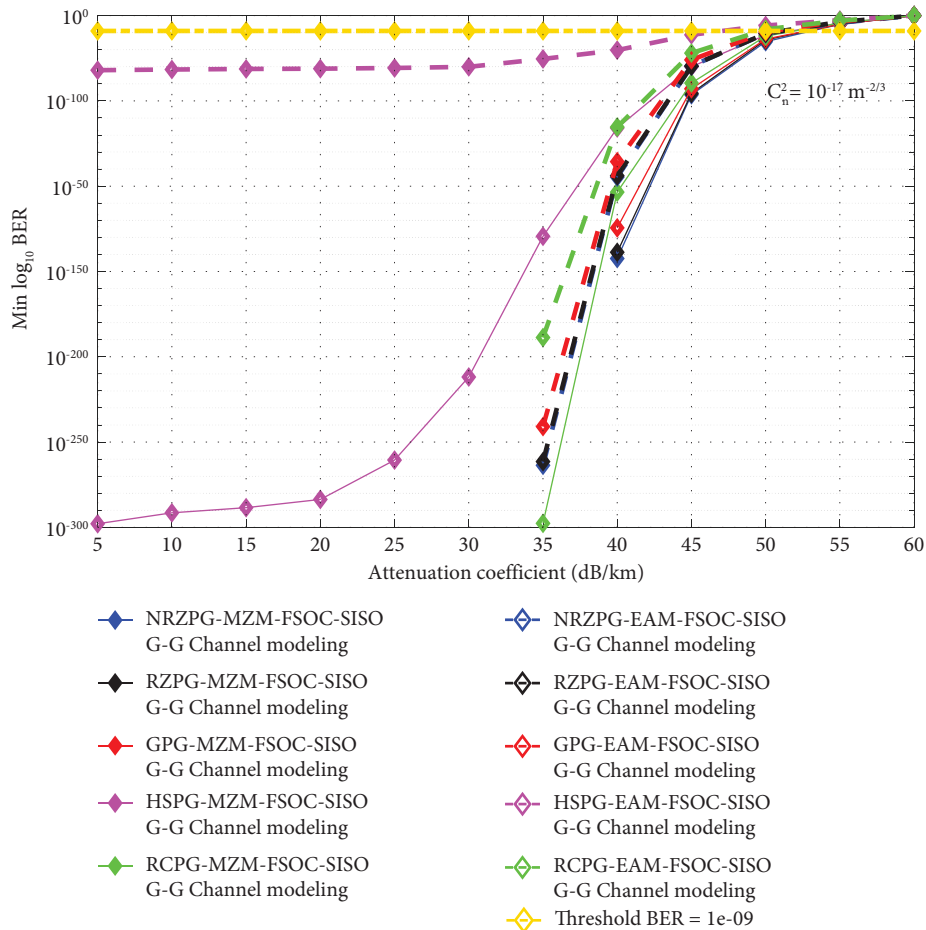
FIGURE 41: Min BER vs. attenuation coefficient (dB/km) with weak AT using EOM for EPG formats under various G-G FSOC-SISO channel states without PE.

information modulated by a MZM over light sources of 30 dBm operating at 1552.5244 nm and 0.8 nm spacing between 16 channels.

The objective of the present study is to estimate the transmission capacity (or TC) of the proposed system under a FSOC-9×9 channel (for LNF channel modeling or for G-G channel modeling, with $C_n^2 = 10^{-13}$ m$^{-2/3}$) using NRZPG-MZM at different rates of flow of each 16 users. However, the selected attenuation coefficient value of 57.39 dB/km for this section is based on the findings obtained in the previous subsection where the impact of TAPEA variation is studied. Therefore, the 57.39 dB/km value is an average value between the extreme value of 59.66 dB/km for the acceptable performance levels under a LNF FSOC-9×9 channel modeling with $C_n^2 = 10^{-13}$ m$^{-2/3}$ (here, TAPEA is equal to 5 μrad) and the lower value of 55.12 dB/km for the acceptable performance levels under a G-G FSOC-1×1 channel modeling with $C_n^2 = 10^{-13}$ m$^{-2/3}$ (here, TAPEA is equal to 0 μrad). After analyzing the obtained results in Figures 63 to 65, it has been observed that the performance of the proposed system may degrade whenever the bit rate per user increases. As a general rule, it is necessary to estimate the overall transmission capacity (or OTC) of the proposed system at the acceptable performance levels. Therefore, one can provide a few interesting results. As an example, we have selected the first user and the end user to provide feedback on the obtained results. So, under a G-G FSOC-9×9 channel modeling with $C_n^2 = 10^{-13}$ m$^{-2/3}$ (here, TAPEA is equal to 5 μrad), the estimated TC of user 1 for the acceptable performance levels (i.e., max OSNR = 54.61 dB, min BER = $1.000e - 09$ and max Q-factor = 6) is equal to 9.464 Gbps, whereas for the estimated TC of user 16 for the acceptable performance levels (i.e., max OSNR = 57.54 dB, min BER = $1.000e - 09$ and max Q-factor = 6) is equal to 9.482 Gbps, which is required that the OTC for 16 users for the acceptable performance levels (i.e., average max OSNR = 60.97 dB, average min BER = $1.000e - 09$ and average max Q-factor = 6) is equal to 150.72 Gbps. Similarly, under LNF FSOC-9×9 channel modeling with $C_n^2 = 10^{-13}$ m$^{-2/3}$ (here, TAPEA is equal to 5 μrad), the estimated TC of user 1 for the acceptable performance levels (i.e., max OSNR = 48.17 dB, min BER = $1.000e - 09$ and max Q-factor = 6) is equal to 9.413 Gbps, whereas the estimated TC of user 16 for the acceptable performance levels (i.e., max OSNR = 49.65 dB, min BER = $1.000e - 09$ and max Q-factor = 6) is equal to 9.440 Gbps, which is required that the OTC for 16 users for the acceptable performance levels (i.e.,
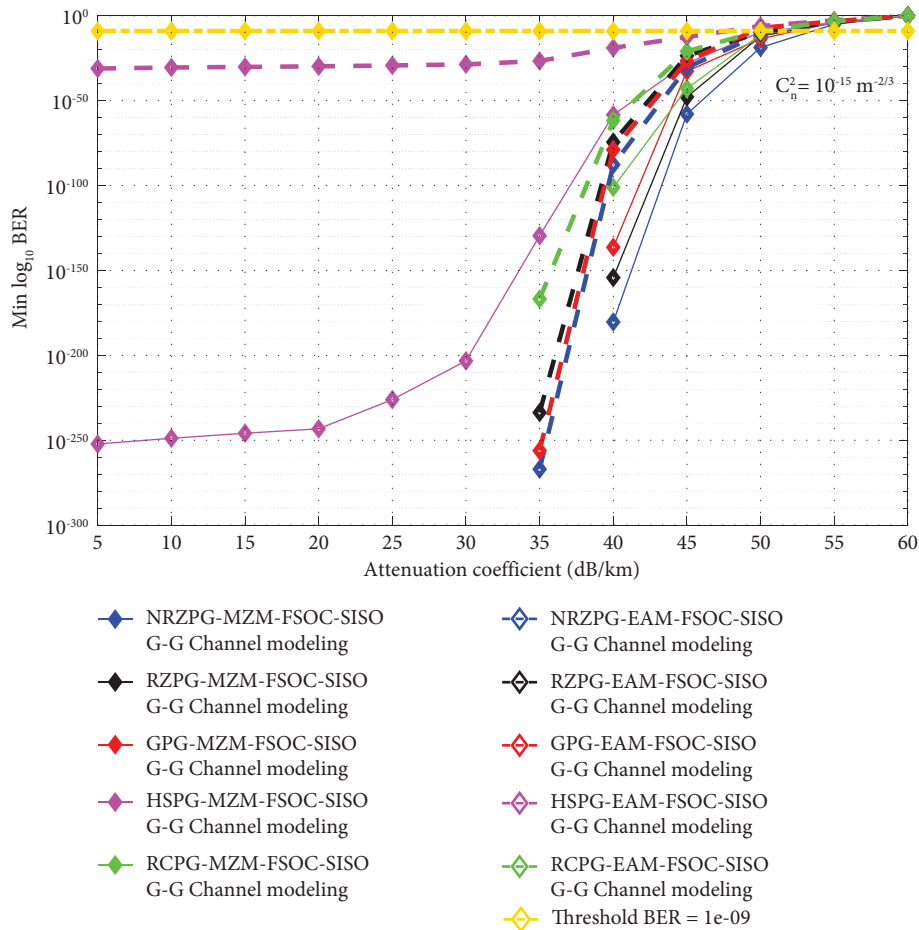
FIGURE 42: Min BER vs. attenuation coefficient (dB/km) with moderate AT using EOM for EPG formats under various G-G FSOC-SISO channel states without PE.
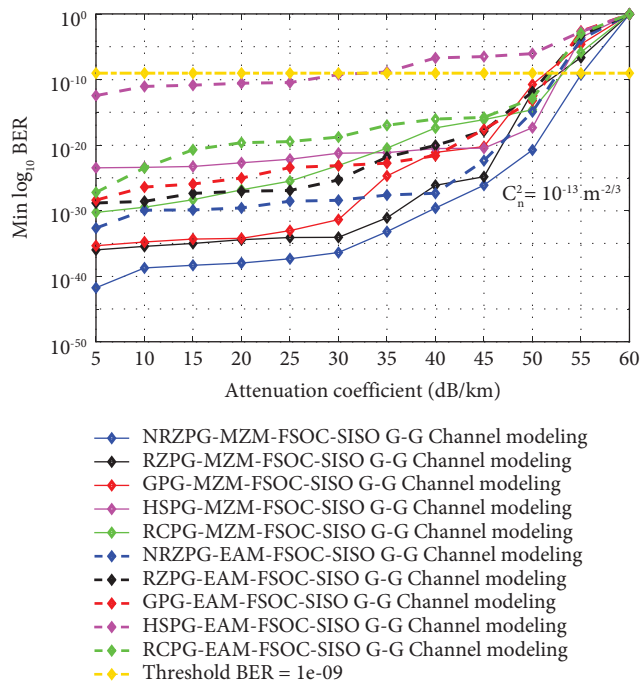

FIGURE 43: Min BER vs. attenuation coefficient (dB/km) with strong AT using EOM for EPG formats under various G-G FSOC-SISO channel states without PE.
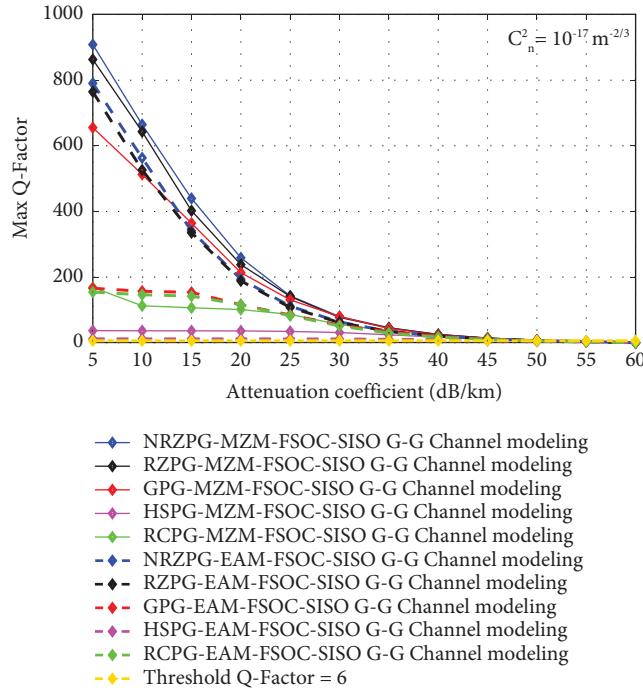
FIGURE 44: Max Q-factor vs. attenuation coefficient (dB/km) with weak AT using EOM for EPG formats under various G-G FSOC-SISO channel states without PE.
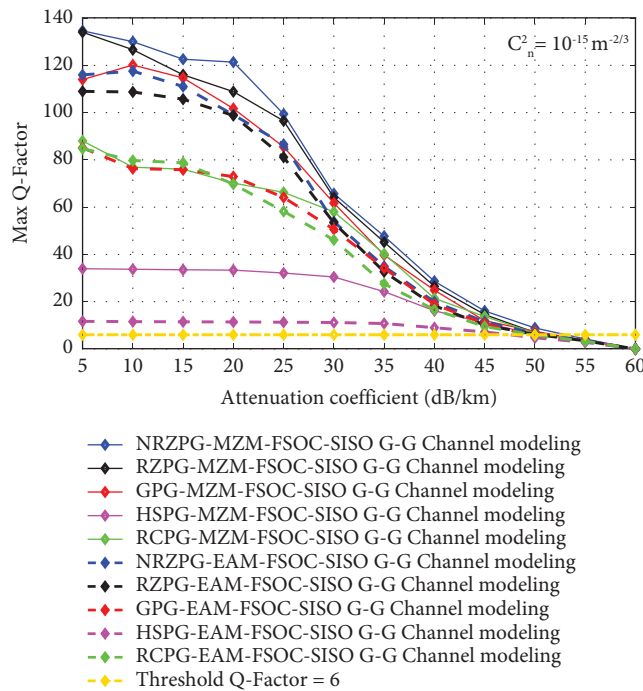

FIGURE 45: Max Q-factor vs. attenuation coefficient (dB/km) with moderate AT using EOM for EPG formats under various a G-G FSOC-SISO channel states, without PE.
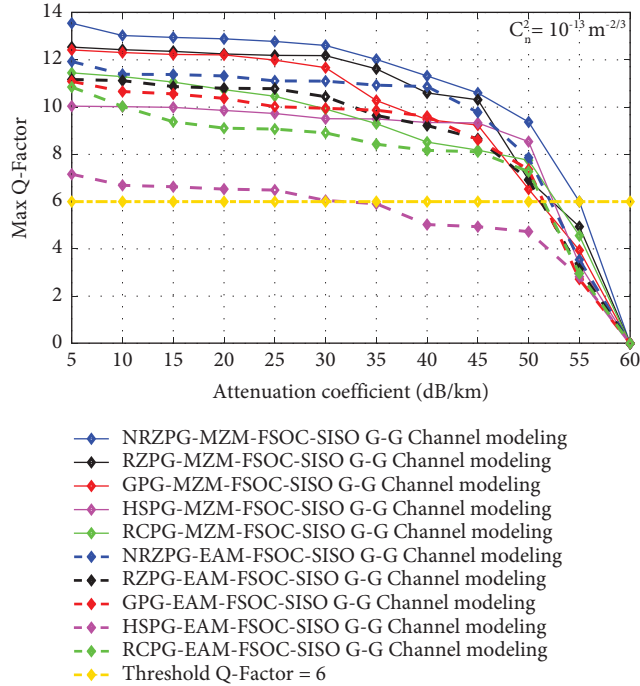
FIGURE 46: Max Q-factor vs. attenuation coefficient (dB/km) with strong AT: using EOM for EPG formats under various G-G FSOC-SISO channel states without PE.

TABLE 9: Comparison in terms of the performances of max OSNR, min BER, and max Q-factor at 32.69 dB/km using EOMs for EPG formats, with $C_n^2 = 10^{-13}$ m$^{-2/3}$ without PE.

LNF FSOC-SISO channel modeling	NRZPG-MZM	RZPG-MZM	GPG-MZM	HSPG-MZM	RCPG-MZM
Min BER	$4.533e - 110$	$9.611e - 93$	$2.858e - 114$	$6.777e - 56$	$5.541e - 64$
Max Q-factor	22.21	20.35	22.64	15.68	16.79
Max OSNR (dB)	40.82	36.82	43.66	43.85	29.20
LNF FSOC-SISO channel modeling	NRZPG-EAM	RZPG-EAM	GPG-EAM	HSPG-EAM	RCPG-EAM
Min BER	$5.517e - 96$	$5.803e - 71$	$3.052e - 56$	$1.181e - 09$	$3.21e - 34$
Max Q-factor	20.72	17.73	15.70	7.904	12.12
Max OSNR (dB)	43.50	36.72	37.06	34.40	22.79
G-G FSOC-SISO channel modeling	NRZPG-MZM	RZPG-MZM	GPG-MZM	HSPG-MZM	RCPG-MZM
Min BER	$2.284e - 35$	$3.701e - 33$	$1.792e - 28$	$6.916e - 22$	$2.175e - 22$
Max Q-factor	12.29	11.88	10.92	9.505	9.586
Max OSNR (dB)	45.15	36.01	37.45	37.54	25.43
G-G FSOC-SISO channel modeling	NRZPG-EAM	RZPG-EAM	GPG-EAM	HSPG-EAM	RCPG-EAM
Min BER	$1.105e - 028$	$3.936e - 24$	$1.261e - 23$	$1.000e - 09$	$1.649e - 18$
Max Q-factor	11.01	10.01	9.907	6.00	8.652
Max OSNR (dB)	40.45	33.59	38.38	31.44	25.15

Table 10: Comparison in terms of the acceptable performance levels of max OSNR, min BER, and max Q-factor vs. estimated attenuation values (dB/km) using EOMs for EPG formats with $C_n^2 = 10^{-13}$ m$^{-2/3}$ without PE.

| LNF FSOC-SISO channel modeling	NRZPG-MZM	HSPG-MZM	GPG-MZM	RZPG-MZM	RCPG-MZM
	Att = 56.90	Att = 56.46	Att = 55.66	Att = 55.53	Att = 54.65
Min BER	$1.000e-09$	$1.000e-09$	$1.000e-09$	$1.000e-09$	$1.000e-09$
Max Q-factor	6.00	6.00	6.00	6.00	6.00
Max OSNR (dB)	24.02	25.78	24.78	24.25	15.77
LNF FSOC-SISO channel modeling	NRZPG-EAM	RZPG-EAM	RCPG-EAM	GPG-EAM	HSPG-EAM
	Att = 54.13	Att = 52.86	Att = 52.27	Att = 51.07	Att = 48.37
Min BER	$1.000e-09$	$1.000e-09$	$1.000e-09$	$1.000e-09$	$1.000e-09$
Max Q-factor	6.00	6.00	6.00	6.00	6.00
Max OSNR (dB)	23.17	16.12	8.59	24.54	28.75
G-G FSOC-SISO channel modeling	NRZPG-MZM	RCPG-MZM	HSPG-MZM	RZPG-MZM	GPG-MZM
	Att = 55.12	Att = 53.17	Att = 53.02	Att = 52.73	Att = 51.39
Min BER	$1.000e-09$	$1.000e-09$	$1.000e-09$	$1.000e-09$	$1.000e-09$
Max Q-factor	6.00	6.00	6.00	6.00	6.00
Max OSNR (dB)	22.51	27.30	22.30	24.67	22.79
G-G FSOC-SISO channel modeling	NRZPG-EAM	GPG-EAM	RCPG-EAM	RZPG-EAM	HSPG-EAM
	Att = 52.66	Att = 51.97	Att = 51.95	Att = 51.64	Att = 32.69
Min BER	$1.000e-09$	$1.000e-09$	$1.000e-09$	$1.000e-09$	$1.000e-09$
Max Q-factor	6.00	6.00	6.00	6.00	6.00
Max OSNR (dB)	24.05	24.28	13.49	23.66	31.44
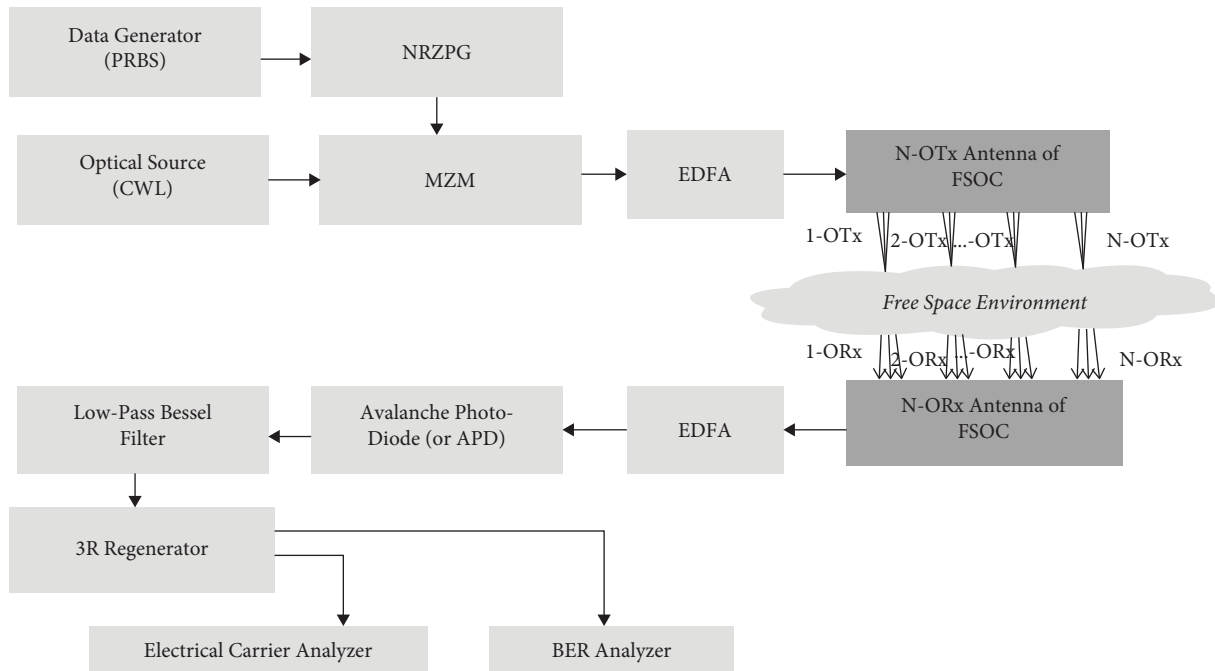
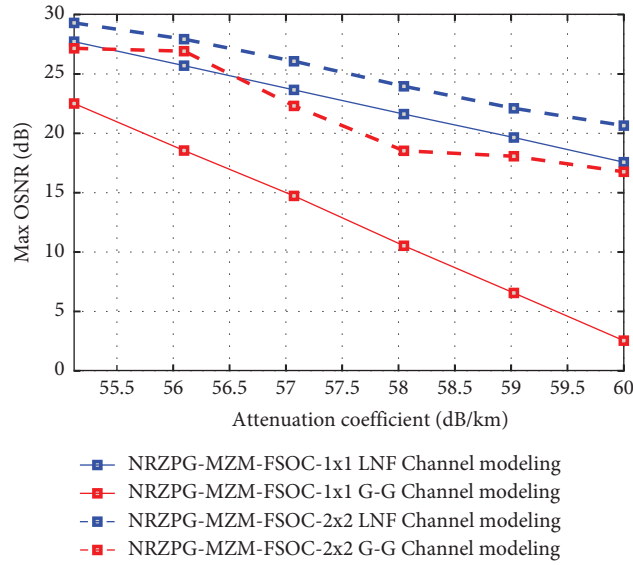Figure 47: Setup of a high-speed P2P-OL under a FSOC-MIMO channel using NRZPG-MZM.

FIGURE 48: Max OSNR (dB) vs. attenuation coefficient (dB/km): comparison between the FSOC-1×1 channel and FSOC-2×2 channel without PE.
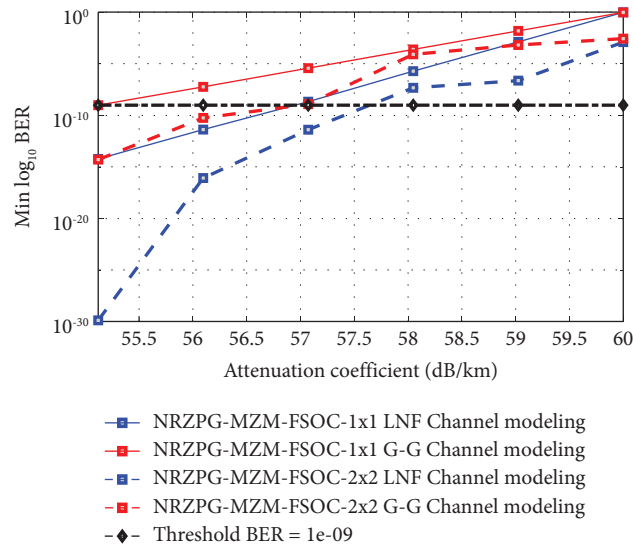

FIGURE 49: Min BER vs. attenuation coefficient (dB/km): comparison between the FSOC-1×1 channel and FSOC-2×2 channel without PE.
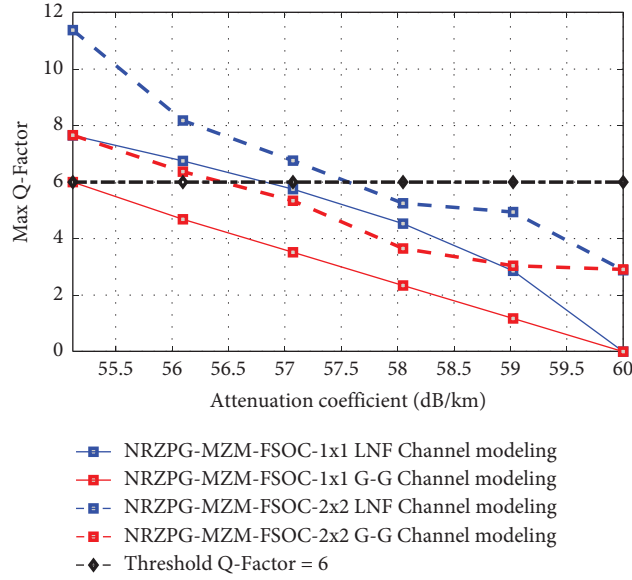
FIGURE 50: Max Q-factor vs. attenuation coefficient (dB/km): comparison between the FSOC-1×1 channel and FSOC-2×2 channel without PE.

TABLE 11: Estimated attenuation value for the acceptable performance levels under G-G FSOC-2×2 channel modeling with $C_n^2 = 10^{-13}$ m$^{-2/3}$, without PE.

Attenuation	55.12 dB/km (NRZPG-MZM)	55.5 dB/km (NRZPG-MZM)	. . .	56.5 dB/km (NRZPG-MZM)
Min BER	$5.240e - 15$	$2.033e - 13$	. . .	$1.000e - 09$
Max Q-factor	7.66	7.16	. . .	6
Max OSNR (dB)	27.16	27.07	. . .	25.02

TABLE 12: Estimated attenuation value for the acceptable performance levels under LNF FSOC-2×2 channel modeling with $C_n^2 = 10^{-13}$ m$^{-2/3}$, without PE.

Attenuation	55.12 dB/km (NRZPG-MZM)	55.5 dB/km (NRZPG-MZM)	. . .	57.60 dB/km (NRZPG-MZM)
Min BER	$1.37e - 30$	$3.469e - 25$	. . .	$1.000e - 09$
Max Q-factor	11.38	10.14	. . .	6
Max OSNR (dB)	29.30	28.76	. . .	24.92

TABLE 13: Performances of beam forming gain variation under G-G FSOC-MIMO channel modeling with $C_n^2 = 10^{-13}$ m$^{-2/3}$, when the attenuation value of 56.50 dB/km without PE.

Beam forming gain	4 (FSOC-2×2)	16 (FSOC-4×4)	. . .	49 (FSOC-7×7)	81 (FSOC-9×9)
Min BER	$1.000e - 09$	$0.13e - 15$	. . .	$0.25e - 30$	$35.38e - 39$
Max Q-factor	6	8.13	. . .	11.53	12.82
Max OSNR (dB)	25.02	28.67	. . .	29.91	30.22

TABLE 14: Performances of beam forming gain variation under LNF FSOC-MIMO channel modeling with $C_n^2 = 10^{-13}$ m$^{-2/3}$, when the attenuation value of 57.60 dB/km without PE.

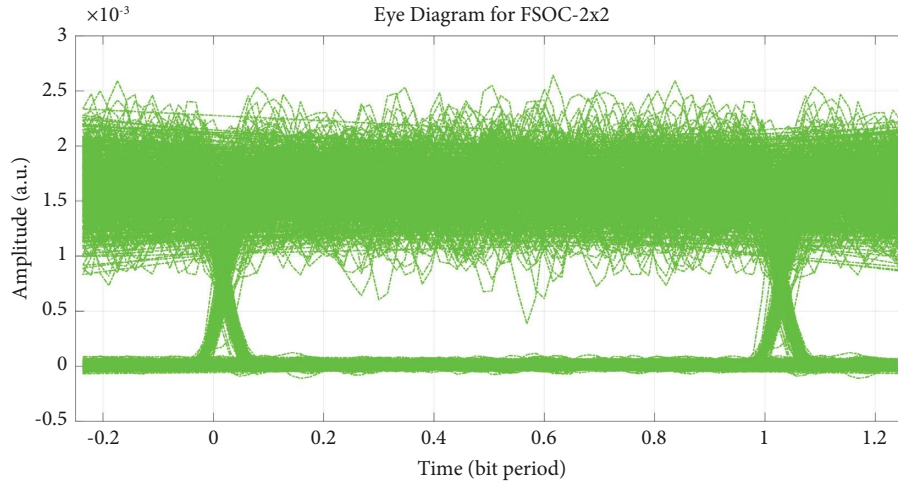| Beam forming gain	4 (FSOC-2×2)	16 (FSOC-4×4)	. . .	49 (FSOC-7×7)	81 (FSOC-9×9)
Min BER	$1.000e - 09$	$0.16e - 15$	. . .	$2.85e - 33$	$1.43e - 36$
Max Q-factor	6	8.10	. . .	11.911	12.53
Max OSNR (dB)	24.92	28.20	. . .	28.95	30.49

FIGURE 51: Eye diagrams under a LNF FSOC-2×2 channel modeling with $C_n^2 = 10^{-13}$ m$^{-2/3}$.
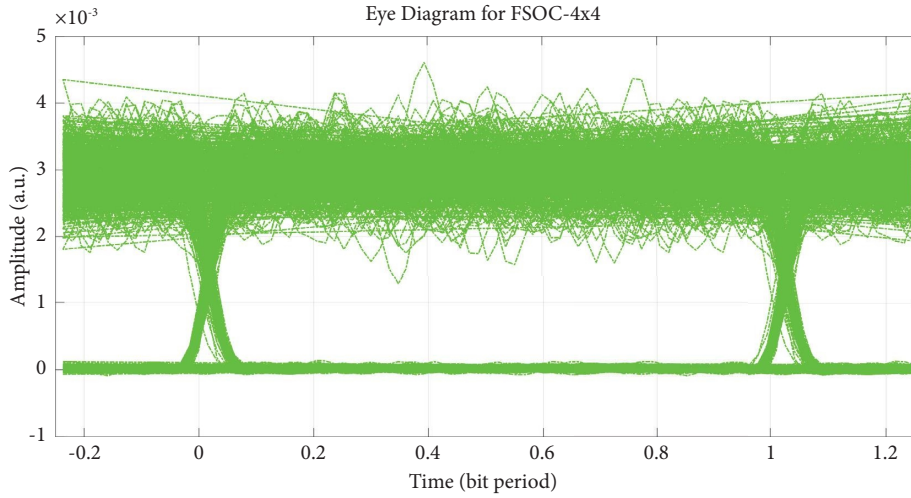

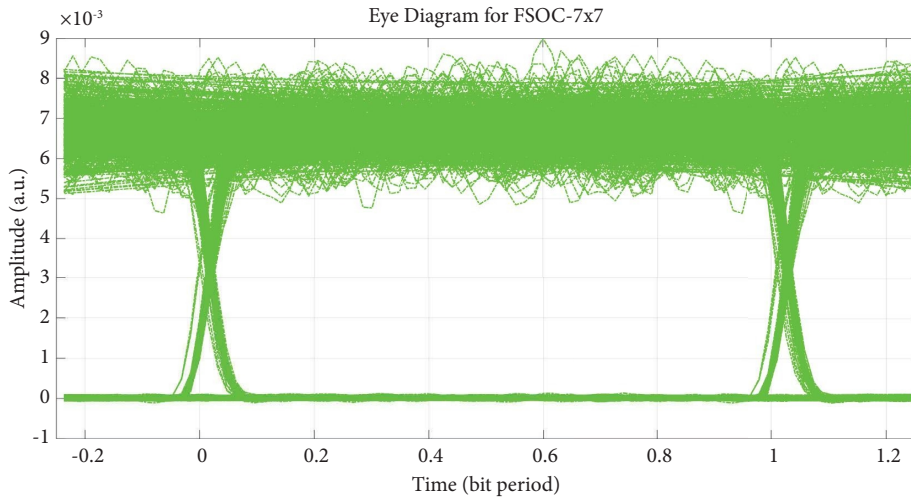FIGURE 52: Eye diagrams under a LNF FSOC-4×4 channel modeling with $C_n^2 = 10^{-13}$ m$^{-2/3}$.

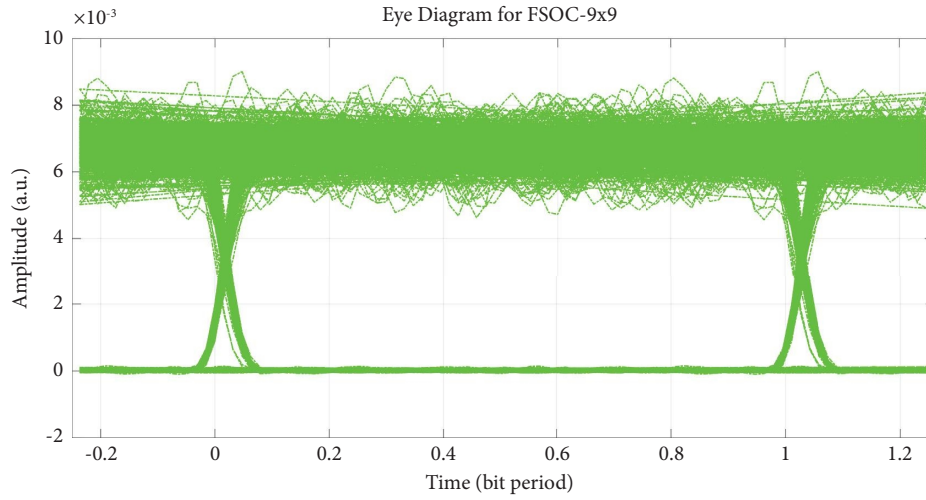FIGURE 53: Eye diagrams under a LNF FSOC-7×7 channel modeling with $C_n^2 = 10^{-13}$ m$^{-2/3}$.

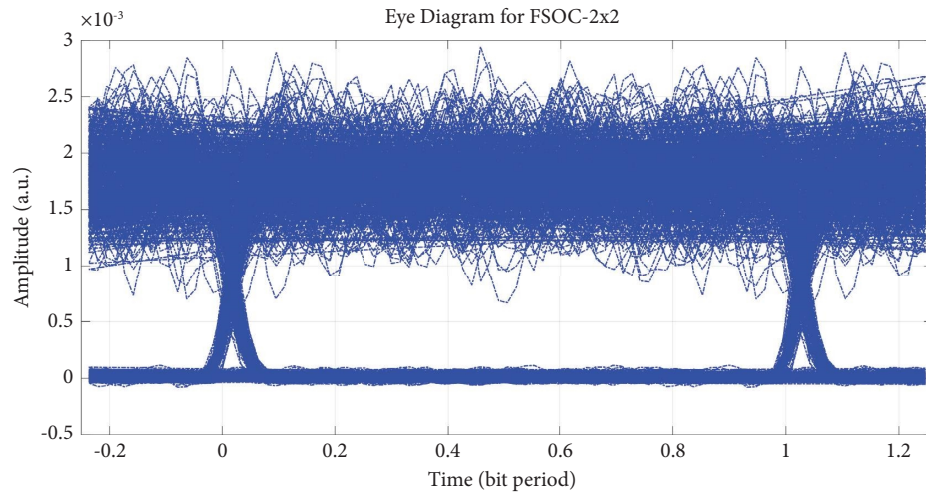FIGURE 54: Eye diagrams under a LNF FSOC-9×9 channel modeling with $C_n^2 = 10^{-13}$ m$^{-2/3}$.

FIGURE 55: Eye diagrams under a G-G FSOC-2×2 channel modeling with $C_n^2 = 10^{-13}$ m$^{-2/3}$.

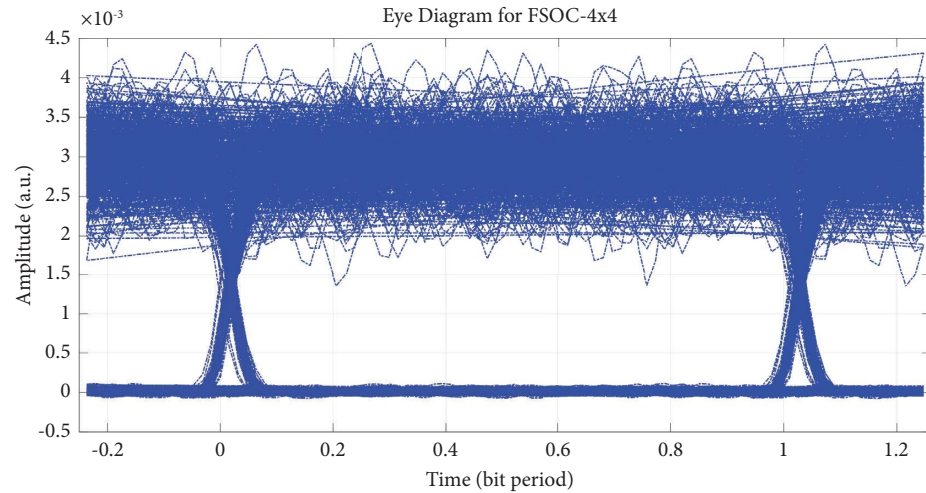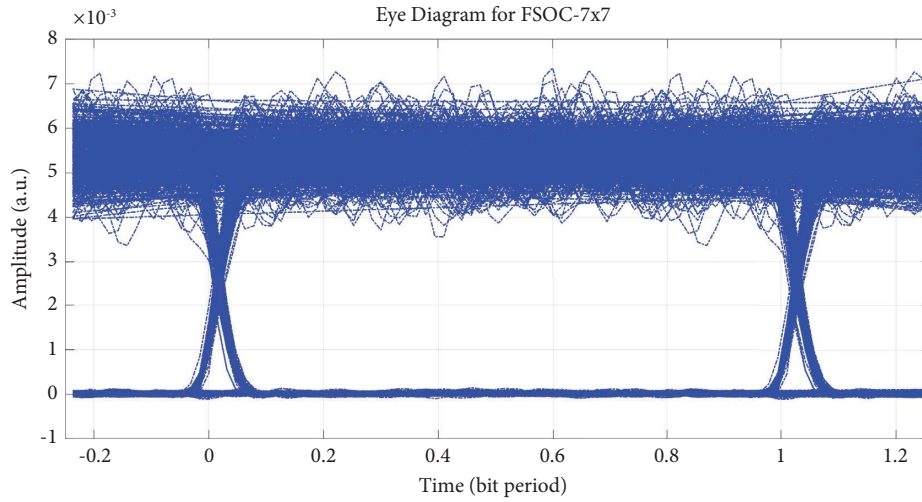FIGURE 56: Eye diagrams under a G-G FSOC-4×4 channel modeling with $C_n^2 = 10^{-13}$ m$^{-2/3}$.

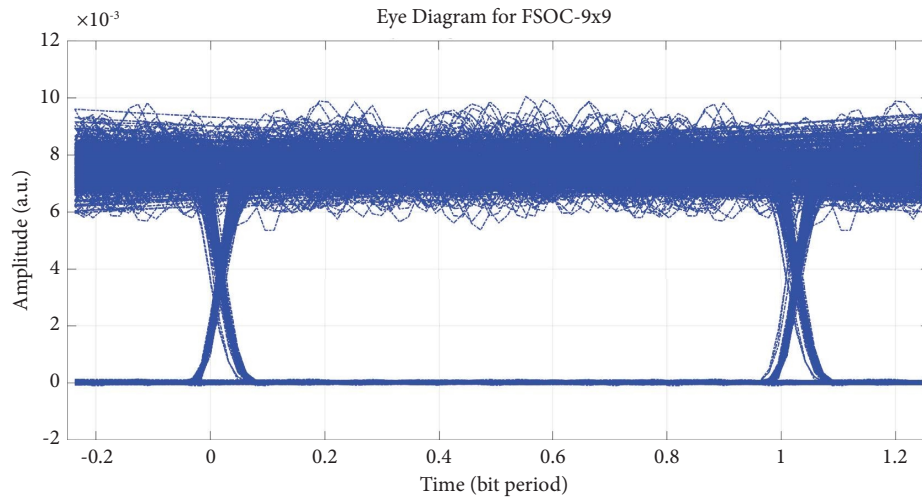FIGURE 57: Eye diagrams under a G-G FSOC-7$\times$7 channel modeling with $C_n^2 = 10^{-13}$ m$^{-2/3}$.

FIGURE 58: Eye diagrams under a G-G FSOC-9$\times$9 channel modeling with $C_n^2 = 10^{-13}$ m$^{-2/3}$.
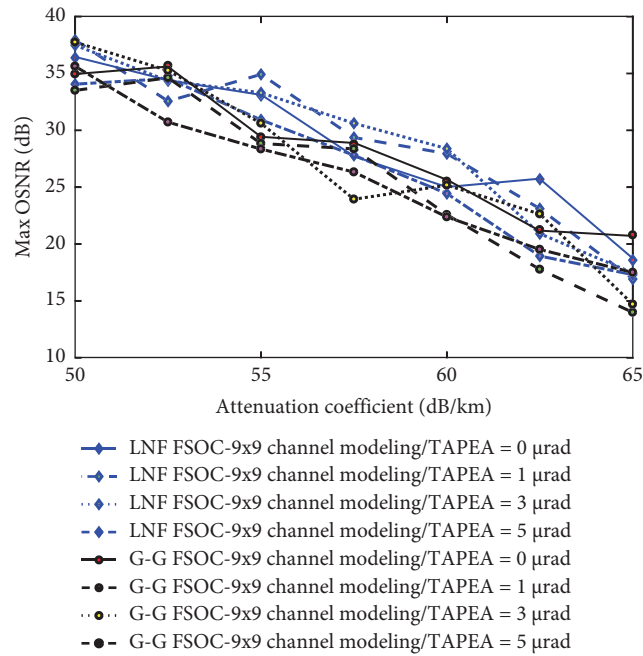
FIGURE 59: Max OSNR (dB) vs. attenuation coefficient (dB/km) under a LNF FSOC-9 × 9 channel and G-G FSOC-9 × 9 channel states with TAPEA.
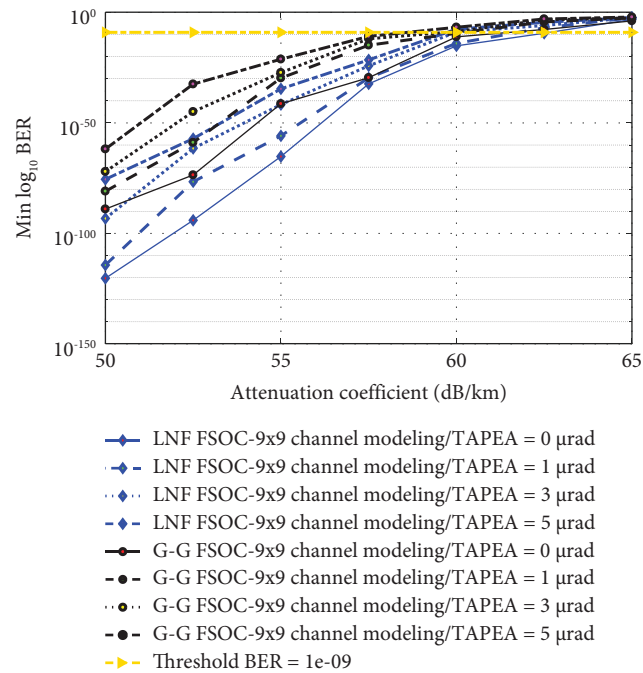

FIGURE 60: Min BER vs. attenuation coefficient (dB/km) under a LNF FSOC-9 × 9 channel and G-G FSOC-9 × 9 channel states with TAPEA.
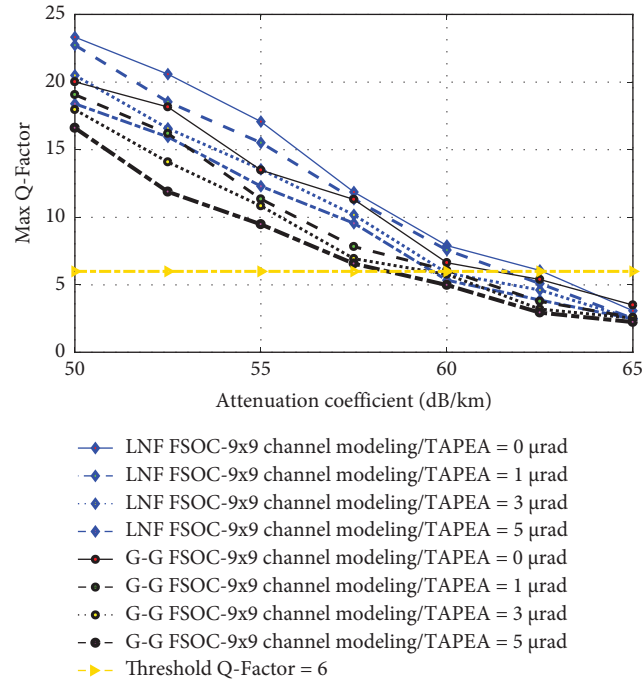
Figure 61: Max Q-factor vs. attenuation coefficient (dB/km) under a LNF FSOC-9 × 9 channel and G-G FSOC-9 × 9 channel states with TAPEA.
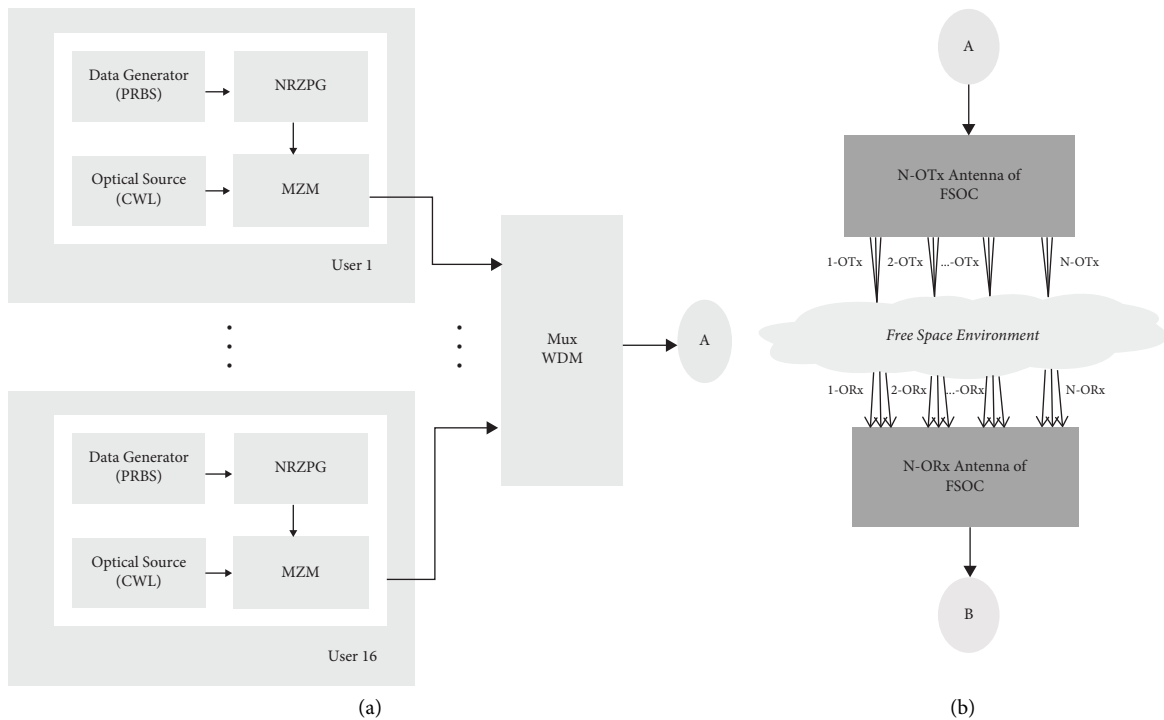

(a)

(b)

Figure 62: Continued.

(c)
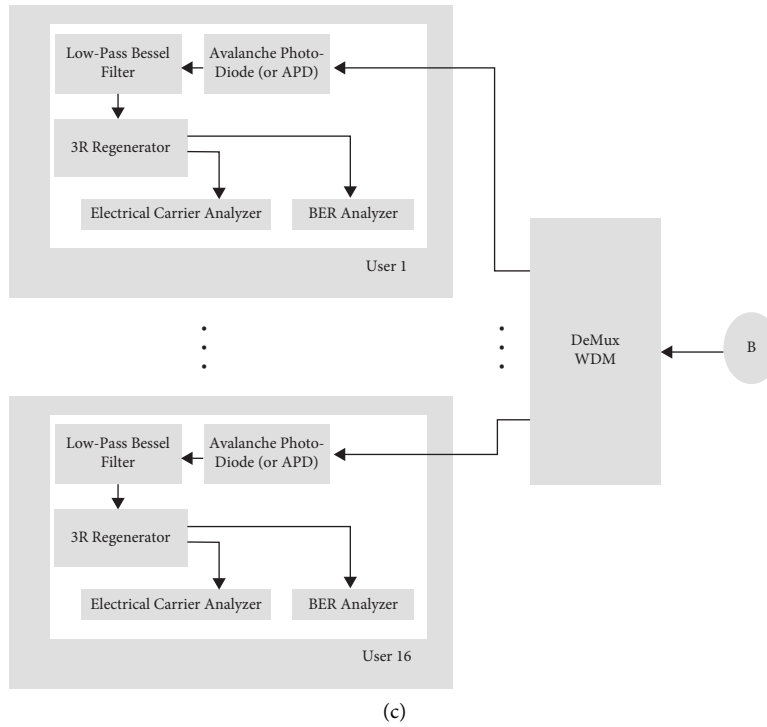
FIGURE 62: Setup component of a high-speed WDM-P2P-OL under a FSOC-MIMO channel using NRZPG- MZM with TAPEA. (a) WDM transmitter for 16 channels. (b) FSOC-MIMO channel. (c) WDM receiver for 16 channels.

-•- G-G FSOC-9x9 channel modeling with
    TAPEA = 5 μrad/User 1
-○- G-G FSOC-9x9 channel modeling with
    TAPEA = 5 μrad/User 16
-◆- LNF FSOC-9x9 channel modeling with
    TAPEA = 5 μrad/User 1
-◇- LNF FSOC-9x9 channel modeling with
    TAPEA = 5 μrad/User 16

FIGURE 63: Max OSNR (dB) vs. bit rate per user (Gbps) under a LNF FSOC-9×9 channel and G-G FSOC-9×9 channel states with TAPEA = 5 μrad.

FIGURE 64: Min BER vs. bit rate per user (Gbps) under a LNF FSOC-9 × 9 channel and G-G FSOC-9 × 9 channel states with TAPEA = 5 μrad.

FIGURE 65: Max Q-factor vs. bit rate per user (Gbps) under a LNF FSOC-9 × 9 channel and G-G FSOC-9 × 9 channel states with TAPEA = 5 μrad.
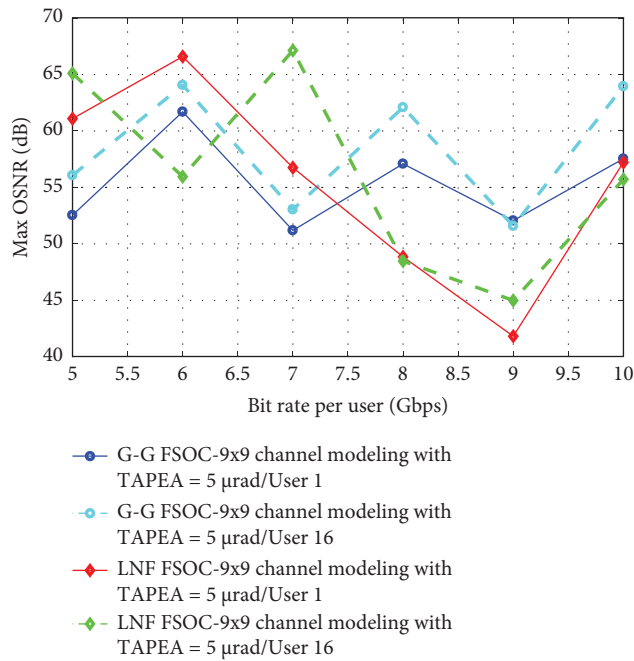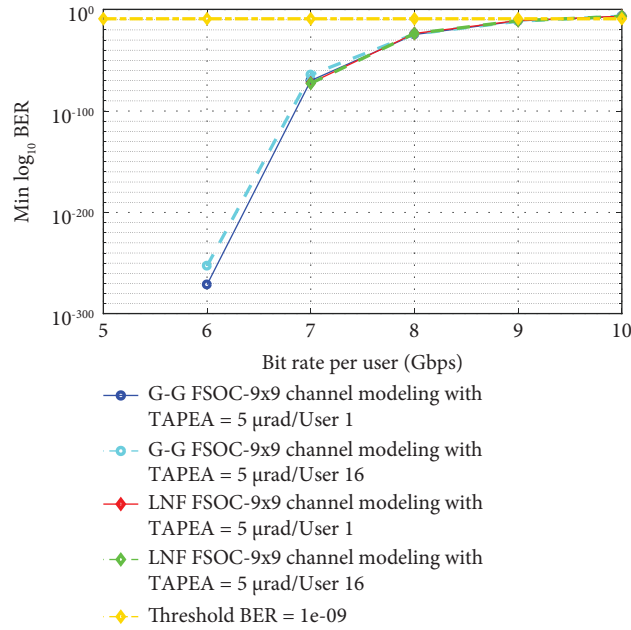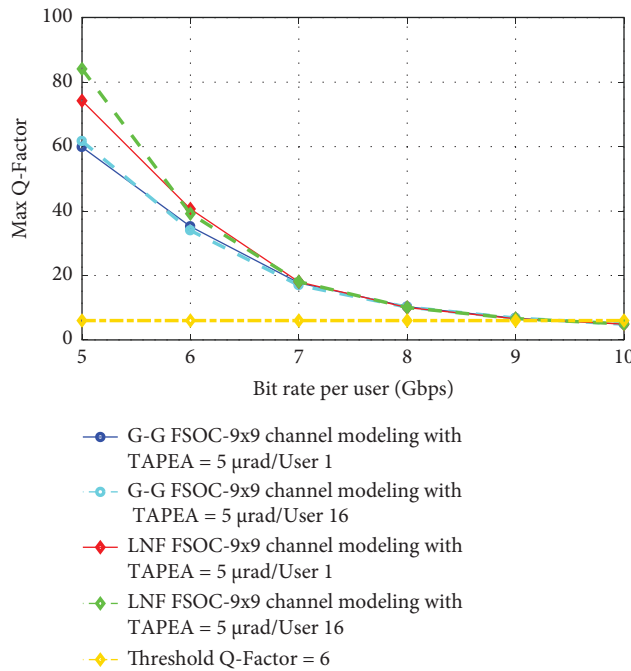
average max OSNR = 49.30 dB, average min BER = 1.000e − 09 and average max Q-factor = 6) is equal to 150.53 Gbps.

7. Conclusions and Suggested Future Work

In this work, the EOM technique, MZM type, coupled with the EPG format, NRZPG type in a high-speed P2P-OL system under a LNF/G-G FSOC-MIMO channel modeling provides better performances compared to the use of a LNF/G-G FSOC-SISO channel modeling, and this was validated for a dust-fog meteorological environment with strong, moderate, and weak AT. However, the simulation results with no application of TAPEA successfully show that the high-speed P2P-OL system under a G-G FSOC-1 × 1 channel modeling with strong AT can tolerate an attenuation up to 55.12 dB/km for a transmission distance of 1 km with the given set of parameters, whereas the high-speed P2P-OL

system under a G-G FSOC-9 × 9 channel modeling with strong AT can ensure, at best, approximately 61.45 dB/km for the same transmission distance and the same parameters used. In addition, the high-speed P2P-OL system can also tolerate an attenuation of up to 56.9 dB/km when it is exploited under a LNF FSOC-1 × 1 channel with strong AT for a transmission distance of 1 km with the given set of parameters. Furthermore, over the same LNF channel with strong AT under the variation of the beam forming gain number equal to 81, the high-speed P2P-OL system can ensure the best performance at an attenuation value of up to 62.60 dB/km for the same transmission distance and the same parameters used. On the other hand, when the TAPEA is equal to 5 μrad, the high-speed P2P-OL system can ensure the best performances with tolerate an attenuation up to 59.66 dB/km and 58.55 dB/km, respectively, under LNF FSOC-9 × 9 channel modeling with strong AT and a G-G FSOC-9 × 9 channel modeling with strong AT. Finally, for the high-speed WDM-P2P-OL system under a FSOC-9 × 9 channel, the conducted results show that the estimated OTC for 16 users with acceptable performance levels are, respectively, under LNF FSOC-9 × 9 channel modeling with strong AT is equal to 150.53 Gbps and under a G-G FSOC-9 × 9 channel modeling with strong AT is equal to 150.72 Gbps. For future work, the energy consumption management for the OTx and ORx antennas of the FSOC-MIMO channel is a hot subject.

Data Availability

The data used in this work are available in this article.

Conflicts of Interest

The authors declare that there are no conflicts of interest.

References

[1] A. M. M. Abdalmajeed, M. Mahmoud, A. ER. A. El-Fikky, H. A. Fayed, and M. H. Aly, "Improved indoor visible light positioning system using machine learning," *Optical and Quantum Electronics*, vol. 55, no. 3, p. 209, 2023.

[2] A. A. Ibrahim, S. Özgür- Ata, and L. Durak-Ata, "Performance analysis of FSO systems over imperfect málaga atmospheric turbulence channels with pointing errors," in *Proceedings of the 2020 12th International Symposium on Communication Systems, Networks and Digital Signal Processing (CSNDSP)*, pp. 1–5, Porto, Portugal, July 2020.

[3] H. Khallaf, A. El-Fikky, M. Elwekeil, A. Elfiqi, E. Mohamed, and H. Shalaby, "Efficiency analysis of cellular/LiFi traffic offloading," *Applied Optics*, vol. 60, no. 15, pp. 4291–4298, 2021.

[4] E. E. Elsayed, B. B. Yousif, and M. Singh, "Performance enhancement of hybrid fiber wavelength division multiplexing passive optical network FSO systems using M-ary DPPM techniques under interchannel crosstalk and atmospheric turbulence," *Optical and Quantum Electronics*, vol. 54, no. 2, p. 116, 2022.

[5] M. Singh, J. Malhotra, M. Mani Rajan, V. Dhasarathan, and M. H. Aly, "Performance evaluation of 6.4 Tbps dual polarization quadrature phase shift keying Nyquist-WDM superchannel FSO transmission link: impact of different weather conditions," *Alexandria Engineering Journal*, vol. 59, no. 2, pp. 977–986, 2020.

[6] K. Singh, S. Chebaane, S. Ben Khalifa et al., "Investigations on mode-division multiplexed free-space optical transmission for inter-satellite communication link," *Wireless Networks*, vol. 28, no. 3, pp. 1003–1016, 2022.

[7] A. El-Fikky, A. Ghazy, H. Khallaf, E. Mahmoud Mohamed, H. Shalaby, and M. Aly, "On the performance of adaptive hybrid MQAM–MPPM scheme over Nakagami and log-normal dynamic visible light communication channels," *Applied Optics*, vol. 59, no. 7, pp. 1896–1906, 2020.

[8] S. Boobalan, S. A. Prakash, M. Angurala, J. Malhotra, and M. Singh, "Performance enhancement of 3 × 20 Gbit/s MDM-based OFDM-FSO system," *Wireless Personal Communications*, vol. 122, no. 4, pp. 3137–3165, 2022.

[9] V. S. Pandi, M. Singh, J. Malhotra, and A. Grover, "A spectral-efficient 1 Tbps terrestrial free-space optics link based on super-channel transmission," *Optical and Quantum Electronics*, vol. 53, no. 5, p. 252, 2021.

[10] P. K. Sahoo, "Error rate analysis of phase sampled RZ-GMSK over turbulent FSO channel," *Journal of Optical Communications*, vol. 43, no. 1, pp. 125–127, 2022.

[11] J. Ma, Y. Jiang, S. Yu, L. Tan, and W. Du, "Packet error rate analysis of OOK, DPIM and PPM modulation schemes for ground to satellite optical communications," *Optics Communications*, vol. 283, no. 2, pp. 237–242, 2010.

[12] H. Liu, R. Liao, Z. Wei, Z. Hou, and Y. Qiao, "BER analysis of a hybrid modulation scheme based on PPM and MSK subcarrier intensity modulation," *IEEE Photonics Journal*, vol. 7, no. 4, pp. 1–10, 2015.

[13] S. H. Alnajjar, M. H. Ali, and A. K. Abass, "Enhancing performance of hybrid FSO/fiber optic communication link utilizing multi-channel configuration," *Journal of Optical Communications*, vol. 43, no. 1, pp. 165–170, 2022.

[14] K. S. Anuranjana and R. Goyal, "Characterization of terrestrial FSO link performance for 850 and 1310 nm transmission wavelengths," *Journal of Optical Communications*, pp. 1–6, 2021.

[15] G. Soni, S. Gupta, and A. Vaish, "Performance investigation of diffractive optical elements effect and rain attenuation on BER of an optical free space communication based system," *Journal of Optics*, vol. 50, no. 4, pp. 606–610, 2021.

[16] S. Kumar and Payal, "Design of multi-beam free space optical communication system for mitigation of atmospheric and geometric nonlinearities," *Journal of Optics*, vol. 50, no. 4, pp. 664–670, 2021.

[17] M. Al-Nahhal and T. Ismail, "Enhancing spectral efficiency of FSO system using adaptive SIM/M-PSK and SIMO in the presence of atmospheric turbulence and pointing errors," *International Journal of Communication Systems*, vol. 32, no. 9, 2019.

[18] T. Ismail, E. Leitgeb, Z. Ghassemlooy, and M. Al-Nahhal, "Performance improvement of FSO system using multi-pulse pulse position modulation and SIMO under atmospheric turbulence conditions and with pointing errors," *IET Networks*, vol. 7, no. 4, pp. 165–172, 2018.

[19] E. E. Elsayed and B. B. Yousif, "Performance enhancement of M-ary pulse-position modulation for a wavelength division multiplexing free-space optical systems impaired by interchannel crosstalk, pointing error, and ASE noise," *Optics Communications*, vol. 475, Article ID 126219, 2020.

[20] E. E. Elsayed and B. B. Yousif, "Performance enhancement of the average spectral efficiency using an aperture averaging and

spatial-coherence diversity based on the modified-PPM modulation for MISO FSO links," *Optics Communications*, vol. 463, Article ID 125463, 2020.

[21] B. B. Yousif, E. E. Elsayed, and M. M. Alzalabani, "Atmospheric turbulence mitigation using spatial mode multiplexing and modified pulse position modulation in hybrid RF/FSO orbital-angular-momentum multiplexed based on MIMO wireless communications system," *Optics Communications*, vol. 436, pp. 197–208, 2019.

[22] H. Liang, C. Gao, Y. Li, M. Miao, and X. Li, "Analysis of selection combining scheme for hybrid FSO/RF transmission considering misalignment," *Optics Communications*, vol. 435, pp. 399–404, 2018.

[23] M. A. Amirabadi and V. Tatataba Vakili, "Performance of a relay-assisted hybrid FSO/RF communication system," *Physical Communication*, vol. 35, Article ID 100729, 2019.

[24] N. Nikbakht-Sardari, M. Ghiamy, M. E. Akbari, and A. Charmin, "Novel adaptive hard-switching based hybrid RF-FSO system architecture using two threshold values in the presence of atmospheric turbulence and pointing error," *Results in Engineering*, vol. 17, Article ID 100813, 2023.

[25] L. Nadeem, M. Saadullah Qazi, and A. Hassam, "Performance of FSO links using CSRZ, RZ, and NRZ and effects of atmospheric turbulence," *Journal of Optical Communications*, vol. 39, no. 2, pp. 191–197, 2018.

[26] L. Jing and M. Uysal, "Optical wireless communications: system model, capacity and coding," in *Proceedings of the 2003 IEEE 58th Vehicular Technology Conference VTC 2003-Fall (IEEE Cat. No.03CH37484)*, vol. 1, pp. 168–172, Orlando, FL, USA, October 2003.

[27] J. Li and M. Uysal, "Achievable information rate for outdoor free space optical communication with intensity modulation and direct detection," in *Proceedings of the GLOBECOM '03. IEEE Global Telecommunications Conference (IEEE Cat. No.03CH37489)*, vol. 5, pp. 2654–2658, San Francisco, CA, USA, December 2003.

[28] G. Aarthi, K. Prabu, and G. R. Reddy, "Aperture averaging effects on the average spectral efficiency of FSO links over turbulence channel with pointing errors," *Optics Communications*, vol. 385, pp. 136–142, 2017.

[29] M. Safari, M. Rad, and M. Uysal, "Multi-hop relaying over the atmospheric Poisson channel: outage analysis and optimization," *IEEE Transactions on Communications*, vol. 60, no. 3, pp. 817–829, 2012.

[30] D. J. T. Heatley, D. R. Wisely, I. Neild, and P. Cochrane, "Optical wireless: the story so far," *IEEE Communications Magazine*, vol. 36, no. 12, 1998.

[31] A. Malik and P. Singh, "Free space optics: current applications and future challenges," *International Journal of Optics*, vol. 2015, Article ID 945483, pp. 1–7, 2015.

[32] A. Harris, J. J. Sluss, H. H. Refai, and P. G. LoPresti, "Alignment and tracking of a free-space optical communications link to a UAV," in *Proceedings of the 24th Digital Avionics Systems Conference*, vol. 1, Washington, DC, USA, October 2005.

[33] A. Ishimaru, *Wave Propagation and Scattering in Random Media*, Academic Press, New York, NY, USA, 1978.

[34] S. Karp, R. Gagliardi, S. E. Moran, and L. B. Stotts, *Optical Channels*, Plenum Press, New York, NY, USA, 1988.

[35] X. Zhu and J. M. Kahn, "Free-space optical communication through atmospheric turbulence channels," *IEEE Transactions on Communications*, vol. 50, no. 8, pp. 1293–1300, 2002.

[36] M. Al-Nahhal, T. Ismail, H. Selmy, and M. M. Elmesalawy, "BPSK based SIM-FSO communication system with SIMO over log-normal atmospheric turbulence with pointing errors," in *Proceedings of the 2017 19th International Conference on Transparent Optical Networks (ICTON)*, pp. 1–4, Girona, Spain, July 2017.

[37] M. Al-Nahhal, H. M. Kasem, T. Ismail, and M. E. Nasr, "FSO-SIMO system with SIM-DPSK over log-normal atmospheric turbulence and misalignment," in *Proceedings of the 2017 19th International Conference on Transparent Optical Networks (ICTON)*, pp. 1–4, Girona, July 2017.

[38] A. Sangeetha, N. Sharma, and I. Deb, "Feasibility evaluation of MIMO based FSO links," *Journal of Communications*, vol. 14, no. 3, pp. 187–193, 2019.

[39] M. Ijaz, Z. Ghassemlooy, J. Perez, V. Brazda, and O. Fiser, "Enhancing the atmospheric visibility and fog attenuation using a controlled FSO channel," *IEEE Photonics Technology Letters*, vol. 25, no. 13, pp. 1262–1265, 2013.

[40] H. Samimi and F. Akhavan, "FSO communication with EGC diversity receiver over double generalised gamma turbulence channel," *IET Optoelectronics*, vol. 11, no. 6, pp. 253–258, 2017.

[41] Z. Ghassemlooy, W. Popoola, and S. Rajbhandari, *Optical Wireless Communications: System and Channel Modelling with Matlab®*, CRC Press, Boca Raton, FL, USA, 2012.

[42] A. G. Alkholidi and K. S. Altowij, *Contemporary Issues in Wireless Communications*, IntechOpen, London, UK, 2014.

[43] P. Kaur, V. K. Jain, and S. Kar, "Effect of atmospheric conditions and aperture averaging on capacity of free space optical links," *Optical and Quantum Electronics*, vol. 46, no. 9, pp. 1139–1148, 2014.

[44] A. Mukherjee, S. Kar, and V. Kumar Jain, "Analysis of beam wander effect in high turbulence for FSO communication link," *IET Communications*, vol. 12, no. 20, pp. 2533–2537, 2018.

[45] M. A. Esmail, H. Fathallah, and M. S. Alouini, "On the performance of optical wireless links over random foggy channels," *IEEE Access*, vol. 5, pp. 2894–2903, 2017.

[46] Z. Ghassemlooy and W. Popoola, *In Mobile and Wireless Communications Network Layer and Circuit Level Design*, IntechOpen, London, UK, 2010.

[47] J. B. Padhy and B. Patnaik, "Link performance evaluation of terrestrial FSO model for predictive deployment in Bhubaneswar smart city under various weather conditions of tropical climate," *Optical and Quantum Electronics*, vol. 53, no. 2, p. 82, 2021.

[48] L. C. Andrews and R. L. Phillips, *Laser Beam Propagation through Random Media*, SPIE Press, Washington, DC, USA, 2nd edition, 2005.

[49] J. M. Senior and M. Y. Jamro, *Optical Fiber Communications: Principles and Practice*, Pearson Education Ltd, London, UK, 3rd edition, 2009.

[50] P. Kumar, "Comparative analysis of ber performance for direct detection and coherent detection fso communication systems," in *Proceedings of the 2015 Fifth International Conference on Communication Systems and Network Technologies*, pp. 369–374, Gwalior, India, April 2015.

[51] A. A. Shatnawi, M. N. Bin Mohd Warip, A. M. Safar, and A. M. Safar, "Influence of transmitting pointing errors on high

speed WDM-AMI-is-OWC transmission system," *Journal of Optical Communications*, vol. 39, no. 1, pp. 123–128, 2017.

[52] L. Bouanane, F. M. Abbou, F. Abdi, F. Chaatit, and A. Abid, "The effect of weak atmospheric turbulence and fog on OOK-FSO communication system," in *Innovations in Smart Cities Applications Edition 2. SCA 2018. Lecture Notes in Intelligent Transportation and Infrastructure*, M. Ben Ahmed, A. Boudhir, and A. Younes, Eds., Springer, Berlin, Germany, 2019.

[53] S. Parkash, A. Sharma, H. Singh, and H. P. Singh, "Performance investigation of 40 GB/s DWDM over free space optical communication system using RZ modulation format," *Advances in Optical Technologies*, vol. 2016, pp. 1–8, 2016.

[54] L. Pierre, *Télécoms sur fibres optiques*, vol. 366, Lavoisier, Rue Lavoisier, Paris, 2008.

[55] M. Jean-Pierre, *Télécoms optiques, composants à fibres, systèmes de transmission*, vol. 239, Lavoisier, Rue Lavoisier, Paris, 2003.

[56] B. O. Rashid and P. M. Jaff, "Gain and noise figure performance of erbium-doped fiber amplifiers," *Kirkuk University Journal - Scientific Studies*, vol. 3, no. 2, pp. 60–69, 2008.

[57] T. Zéno, *Optoélectronique, Composants photoniques et fibres optiques*, Edition Ellipse, Île-de-France, France, 2001.

[58] Anritsu, "Optical amplifier (edfa) characteristics evaluation," 2011, https://dl.cdn-anritsu.com/en-au/test-measurement/files/Application-Notes/Application-Note/MS9740A_EF1100.pdf.